# INFORMATION TO USERS

This manuscript has been reproduced from the microfilm master. UMI films the text directly from the original or copy submitted. Thus, some thesis and dissertation copies are in typewriter face, while others may be from any type of computer printer.

**The quality of this reproduction is dependent upon the quality of the copy submitted.** Broken or indistinct print, colored or poor quality illustrations and photographs, print bleedthrough, substandard margins, and improper alignment can adversely affect reproduction.

In the unlikely event that the author did not send UMI a complete manuscript and there are missing pages, these will be noted. Also, if unauthorized copyright material had to be removed, a note will indicate the deletion.

Oversize materials (e.g., maps, drawings, charts) are reproduced by sectioning the original, beginning at the upper left-hand corner and continuing from left to right in equal sections with small overlaps.

Photographs included in the original manuscript have been reproduced xerographically in this copy. Higher quality 6" x 9" black and white photographic prints are available for any photographs or illustrations appearing in this copy for an additional charge. Contact UMI directly to order.

Bell & Howell Information and Learning
300 North Zeeb Road, Ann Arbor, MI 48106-1346 USA
800-521-0600

# Aspects of Boreal Forest Hydrology: From Stand to Watershed

Bart Nijssen

A dissertation submitted in partial fulfillment

of the requirements for the degree of

Doctor of Philosophy

University of Washington

2000

Program Authorized to Offer Degree: Civil and Environmental Engineering

UMI Number: 9995417

UMI Microform 9995417



Bell & Howell Information and Learning Company
300 North Zeeb Road
P.O. Box 1346
Ann Arbor, MI 48106-1346

In presenting this dissertation in partial fulfillment of the requirements for the Doctoral degree at the University of Washington, I agree that the Library shall make its copies freely available for inspection. I further agree that extensive copying of this dissertation is allowable only for scholarly purposes, consistent with "fair use" as prescribed in the U.S. Copyright Law. Requests for copying or reproduction of this dissertation may be referred to Bell and Howell Information and Learning, 300 North Zeeb Road, Ann Arbor, MI 48106-1346, to whom the author has granted "the right to reproduce and sell (a) copies of the manuscript in microform and/or (b) printed copies of the manuscript made from microform."

Signature B Nyssen

Date October 26, 2000

University of Washington

Graduate School

This is to certify that I have examined this copy of a doctoral dissertation by

Bart Nijssen

and have found that it is complete and satisfactory in all respects,
and that any and all revisions required by the final
examining committee have been made.

Chairperson of the Supervisory Committee:

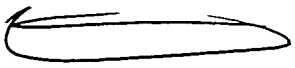

Dennis P. Lettenmaier

Reading Committee:

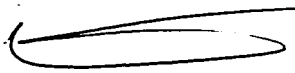

Dennis P. Lettenmaier

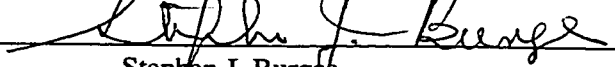

Stephen J. Burges

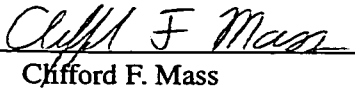

Clifford F. Mass

Date: October 26, 2000

University of Washington

Abstract

# Aspects of Boreal Forest Hydrology: From Stand to Watershed

Bart Nijssen

Chairperson of the Supervisory Committee:

Professor Dennis P. Lettenmaier
Department of Civil and Environmental Engineering

This dissertation evaluates land surface hydrologic processes in the boreal forest using observations collected as part of the Boreal Ecosystem Atmosphere Study (BOREAS). Three separate studies, two of which have appeared as journal publications, and one of which has been submitted for publication, are included. The first study describes the application of a spatially-distributed hydrologic model, originally developed for mid-latitude forested environments, to selected BOREAS flux measurement sites. Compared to point observations at the flux towers, the model represented energy and moisture fluxes reasonably well, but shortcomings were identified in the soil thermal submodel and the partitioning of evapotranspiration into canopy and subcanopy components. As a first step towards improving this partitioning, a new parameterization for transmission of shortwave radiation through boreal forest canopies was developed in the second study. The new model accounts for the transmission of diffuse and direct shortwave radiation, multiple scattering in the canopy, and multiple reflections between the canopy layers. Simulated sub-canopy radiation compared well with observations at a mature jack pine site, but errors were larger at a mature black spruce site. Absolute model errors were small in all cases compared to above-canopy radiation. The final study evaluates the origin of apparent water balance anomalies in the White Gull Creek Basin in the BOREAS southern study area during the 1994–1996 period, with particular empha-

sis on the fate of precipitation that occurred during an unusually wet period during July, 1994. Although precipitation was balanced by evapotranspiration and runoff in 1995 and 1996, it exceeded the sum of the latter two terms by 89 mm in 1994. Because field observations did not suggest increased storage at the end of the 1994 growing season, it seems likely that most of the excess precipitation evaporated when the basin was extremely wet after the heavy precipitation in July 1994. This suggests that the evaporative fluxes measured at the BOREAS flux towers under-represented the flux from the larger area during periods when the basin was very wet.

# TABLE OF CONTENTS

# LIST OF FIGURES

## LIST OF TABLES

## ACKNOWLEDGMENTS

I wish to thank the members of my committee, and in particular my advisor Dennis P. Lettenmaier, for their support and guidance. I also wish to thank all past and present members of our research group for the stimulating environment they helped create.

The field data used in this study were collected by a large number of people. J.-L. Roujean of Centre National de la Recherche Scientifique, Toulouse, France provided the below-canopy PAR[1] data sets for summer 1994 used in Chapter 4. W. Ni[2] of Raytheon STX, Lanham, Maryland provided the GORT results shown in Figure 4.2. Streamflow and precipitation data used in Chapters 3 and 5 were collected by R. Soulis and N. Kouwen from the Department of Civil Engineering, University of Waterloo, Ontario, Canada. The southern study area snow course data used in Chapter 5 were collected by M. Dalman, P. Pacholek, and V. Heap for Atmospheric Environment Service, Canada. R. E. Davis and J. P. Hardy from the Cold Regions Research Engineering Laboratory, U. S. Army Corps of Engineers, Hanover, New Hampshire provided the below-canopy radiation data sets for winters 1994 and 1996 used in Chapter 4, as well as snow data used in Chapter 5. Meteorological measurements collected by the Saskatchewan Research Council were used throughout the study. Mature black spruce tower flux data used in Chapters 3 and 5 were collected by P. G. Jarvis, J. M. Massheder, J. B. Moncrieff, M. B. Rayment, S. Hale, and S. Scott of the Institute of Ecology and Resource Management, Edinburgh University, Scotland. Mature black spruce flux data in the northern study area (Chapter 3) were collected by S. C. Wofsy, J. W. Munger, B. C. Daube, M. L. Goulden, K. A. Boering, and J. D. Burley from the Division of Engineering and Applied Sciences, Harvard University, Cambridge, Massachussetts. Mature aspen

---

[1] PAR - photosynthetically active radiation

[2] Now at: Department of Geography, University of Maryland, College Park, Maryland

flux data (Chapter 5) were collected and processed in 1994 by G. den Hartog and H. H. Neumann of Atmospheric Environment Service, Canada, and in 1996 by T. A. Black and Z. Nesic of the University of British Columbia, Canada. Mature jack pine flux measurements (Chapters 3 and 5) were obtained and prepared by D. Baldocchi and C. Vogel of the Atmospheric Turbulence and Diffusion Division, NOAA, Oak Ridge, Tennessee. Flux data at the fen site (Chapter 5) were collected by S. B. Verma and his colleagues of the University of Nebraska-Lincoln. The young aspen data (Chapter 5) were collected by P. Bessemoulin, D. Puech, G. Bouhours, G. Lachaud, E. Gizard and J. Marcel of the Centre National de Recherches Meteorologiques, Toulouse, France. Flux data at the young jack pine site (Chapter 5) were collected and processed by D. Anderson, R. Striegl, and K. Wickland of the United States Geological Survey. The efforts of the NASA/GSFC staff in processing and archiving the data were greatly appreciated.

This work was supported in part by the United States National Aeronautics and Space Administration under grants NASA/NAG-5-2294 and NASA/NAG-5-7300 to the University of Washington.

Last but not least a word of thanks to friends and family, especially my wife Mary Catlin, for giving me a life outside of graduate school.

## DEDICATION

This work is dedicated to my parents, J. M. Nijssen and M. G. C. Nijssen-Hermans, who never failed to encourage me.

# Chapter 1

# INTRODUCTION

This dissertation presents three studies of hydrological processes in the boreal forest, the circumpolar belt of high-latitude forest in Eurasia and North America that generally lies between 50°N and 70°N. Interest in the relationship between the boreal forest and the global climate system has heightened in recent years because the predicted amount of global warming is generally greater in this region than elsewhere globally, and because the region plays an important role in the global carbon cycle. The Boreal Ecosystem Atmosphere Study (BOREAS) was initiated in 1992 to study the interaction between the boreal forest and the global climate system. Data collection for this experiment took place from 1993–1996 at two sites in the boreal forest of Central Canada, resulting in a large, coherent data set of atmosphere, vegetation, and soil characteristics. The BOREAS project, the physical and hydrologic characteristics of the boreal forest, and the interaction between the boreal forest and the climate system are the topic of Chapter 2.

One of the main objectives of the BOREAS project was to collect observations that would support development and testing of process models that describe the exchanges of radiative energy, water, heat, carbon, and trace constituents between the boreal forest and the atmosphere [*Sellers et al.*, 1995]. The original intent of the reported research was to adapt a spatially-distributed, physically-based hydrological model for application in the boreal forest. Chapter 3 describes the application of the distributed hydrology-soil-vegetation model (DHSVM) [*Wigmosta et al.*, 1994] to specific locations in the BOREAS area, in order to identify the strengths and weaknesses of this model. Applied as a point model, DHSVM demonstrated considerable skill in simulating the observed energy and mositure fluxes, although shortcomings were identified in the soil thermal

submodel and the partitioning of evapotranspiration into its canopy and subcanopy components. This chapter was published in 1997 as B. Nijssen, I. Haddeland, and D. P. Lettenmaier, Point evaluation of a surface hydrology model for BOREAS, *J. Geophys. Res.*, *102*, 29,367–29,378, 1997.

As a first step towards improvement of both the soil thermal model and the division of evapotranspiration between the soil and vegetation layers, a better representation of the transmission of shortwave radiation through the boreal forest canopy was developed. Simultaneous above and below canopy radiation measurements are only rarely made, largely because the subcanopy radiation environment is usually highly variable, both in space and time. The availability of such measurements as part of the BOREAS project allowed the development of a simple radiation transmission model, which accounts for canopy geometry and solar zenith angle. The development of this model and the evaluation of its performance for two different boreal forest types are the subject of Chapter 4. This chapter was published in 1999 as B. Nijssen and D. P. Lettenmaier, A simplified approach for predicting shortwave radiation transfer through boreal forest canopies, *J. Geophys. Res.*, *104*, 27,859–27,868, 1999.

Early application of DHSVM in a spatially-distributed mode over the White Gull Creek basin in the BOREAS southern study area for the 1994 growing season showed that the main model response to a large rainfall event in July 1994 consisted of a greatly overestimated runoff peak [*Nijssen et al.*, 1996]. Whereas peak runoff of 25.4 $m^3/s$ was observed on July 21, 1994 following heavy precipitation on July 18–19, modeled discharge reached a peak as high as 76.4 $m^3/s$ on July 23. Not only was the runoff peak overestimated, but the total amount of runoff during and following the heavy precipitation in July 1994 was overpredicted as well. During the period from July 13–August 5, 1994 128.3 mm of precipitation fell on the White Gull Creek basin. While the observed areal average runoff for this same period was 35.6 mm, the predicted runoff was 76.8 mm, even though DHSVM modeled the evapotranspiration at the towers to within 10% when run at the flux tower sites. The discrepancy between these two results is an important issue in scaling the results from the flux towers to the watershed and beyond. If the precipitation did not

result in additional runoff or evapotranspiration, then where was it stored? *Suyker et al.* [1997] reported that the water level in a wetland in the southern study area rose by 10 cm following the storm of July 18–19, but dropped to pre-storm levels by August 5. The same rise and fall was observed in the streamflow hydrographs. To explore what happened to this "missing" water, it was decided that rather than attempting further model refinements, a better understanding of catchment scale processes would result from a careful analysis of the water balance of the White Gull Creek basin for the 1994–1996 observation period. This water balance study is the topic of Chapter 5.

The results from the three studies are summarized in Chapter 6. This last chapter also presents the conclusions and some recommendations for further research.

# Chapter 2

# BOREAS AND THE BOREAL FOREST

## *2.1 The Boreal Ecosystem-Atmosphere Study*

### *2.1.1 Large-Scale Field Experiments*

The Boreal Ecosystem Atmosphere Study (BOREAS) was initiated in 1992 as part of the International Satellite Land Surface Climatology Project (ISLSCP), which in turn is sponsored by the World Climate Research Program - Global Energy and Water Cycle Experiment (WCRP-GEWEX). BOREAS was a large-scale international research program, designed to improve understanding of the exchange of energy, moisture and trace gases, between the boreal forest and the atmosphere. BOREAS initially included 85 science teams, mostly from the United States and Canada. Funding for most American investigators was provided by the National Aeronautics and Space Administration (NASA), with participation from the National Oceanographic and Atmospheric Administration (NOAA), the National Science Foundation (NSF), the United States Geological Survey (USGS), and the Environmental Protection Agency (EPA). Participating Canadian agencies included the Canada Centre for Remote Sensing (CCRS), Environment Canada, the Natural Sciences and Engineering Research Council (NSERC), Agriculture Canada, the National Research Council (NRC), Heritage Canada (Parks), the Canadian Forest Service, the Institute for Space and Terrestrial Science, and the Royal Society of Canada. Although some activities started in 1993, the main BOREAS field activities took place in 1994 and in 1996. Some monitoring activities were continued in 1995. *Sellers et al.* [1995] provide a good overview of the BOREAS project.

One of the main obstacles to the improvement of land-surface parameterizations and the evaluation of land-surface models is a lack of appropriate observations [*Gates et al.*, 1996]. To address

this issue a number of large-scale field experiments have been executed in different climatic regions around the globe. The first of these experiments was HAPEX-MOBILHY (Hydrologic Atmospheric Pilot Experiment - Modelisation du Bilan Hydrique) which was conducted in a 100×100 km mixed forest and cropland site in southwestern France from 1985 till 1987 under the auspices of the WCRP [*André et al.*, 1986]. This experiment was conducted to provide [*André et al.*, 1986]

> "a data base of hydrological, pedological, surface, and atmospheric parameters against which it will be possible to test and develop parameterization schemes of hydrological budget and evaporation flux to be implemented in atmospheric GCMs".

The International Satellite Land Surface Climatology Project organized a similar experiment in a 15×15 km prairie grassland site near Manhattan, Kansas, with field phases in 1987 and 1989 [*Sellers et al.*, 1992]. The main objectives of the First ISLSCP Field Experiment (FIFE) were to gain a better understanding of the biologic controls on land surface-atmosphere interactions, and to investigate the use of satellites observations for inferring climatologically significant land surface parameters [*Sellers et al.*, 1992]. This project was followed by the European Field Experiment in Desertification-Threatened Areas (EFEDA) in Central Spain in 1991 [*Bolle*, 1993], the HAPEX-Sahel project in Northern Africa in 1993 [*Goutorbe et al.*, 1997], the Northern Hemisphere Climate Processes Land-Surface Experiment (NOPEX) in Central Sweden [*Haldinn et al.*, 1998], BOREAS [*Sellers et al.*, 1995], and the Large Scale Biosphere-Atmosphere Experiment in Amazonia (LBA) in Brazil with the main field phase from 1998 till 2000 [*LBA Science Planning Group*, 1996].

Although each of these projects focused on a different geographical region, and consequently addressed somewhat different research questions, they all were designed to:

1. Gain a better understanding of the role of land surface processes in the climate system.

2. Develop parameterizations of the important land surface processes at the scale at which climate and weather models are applied (on the order of $10^3$–$10^4$ km$^2$).

3. Develop methods to infer climatologically important land surface parameters from remote sensing observations.

The research reported here was conducted as part of BOREAS, for which the central scientific issues were defined as:

1. The sensitivity of the boreal forest biome to changes in the physical climate system.

2. The carbon cycle and biogeochemistry in the boreal forest.

3. Biophysical feedbacks between the boreal forest and the physical climate system.

The limited field observation period of BOREAS made it impossible to measure the ongoing effects of climate change on the boreal forest ecosystem directly. Instead, the experiment focused on data collection that would allow the development and testing of process models that in turn could be applied to evaluate the effect of global change on the boreal forest. Thus the experimental objectives of BOREAS were described as [*Sellers et al.*, 1995]:

1. Improve the process models that describe the exchanges of radiative energy, water, heat, carbon, and trace constituents between the boreal forest and the atmosphere.

2. Develop methods for applying the process models over larger areas using remote sensing and other integrative techniques.

### *2.1.2 Experimental Setup*

The experimental setup of BOREAS was geared towards measuring moisture, energy, and trace gas fluxes between the boreal forest and the atmosphere over a range of spatial and temporal scales. These measurements were carried out for the most representative vegetation types in the region. and under different climatic conditions. The measurement strategy was similar to the one developed for FIFE [*Sellers et al.*, 1992] and HAPEX-Sahel [*Goutorbe et al.*, 1997].

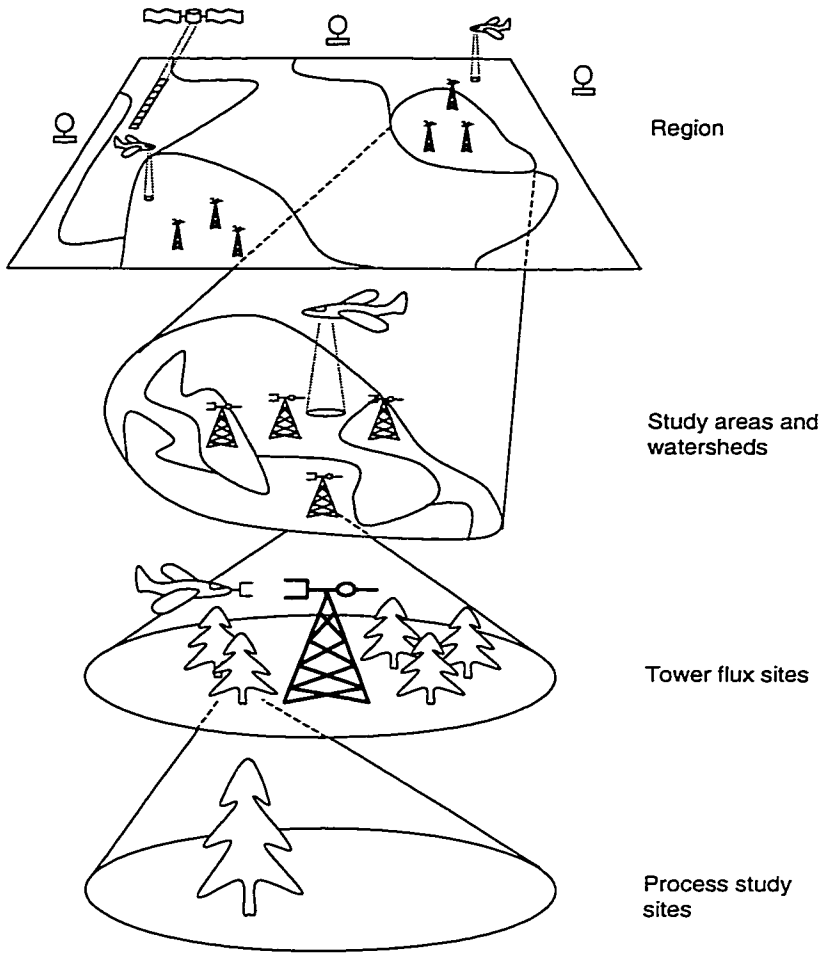


Figure 2.1: BOREAS scale domains.

A nested approach was used to integrate observations and models over a range of spatial scales. The scale domains were defined as illustrated in Figure 2.1:

**Region:** The region consisted of a roughly 1000 km×1000 km area in central Canada (Figure 2.2), covering 18 degrees of longitude (94°W to 111°W) and 9 degrees of latitude (51°N to 60°N). This area covered most of the central and northern parts of Saskatchewan and Manitoba. The region was the domain for satellite remote sensing, meteorological data

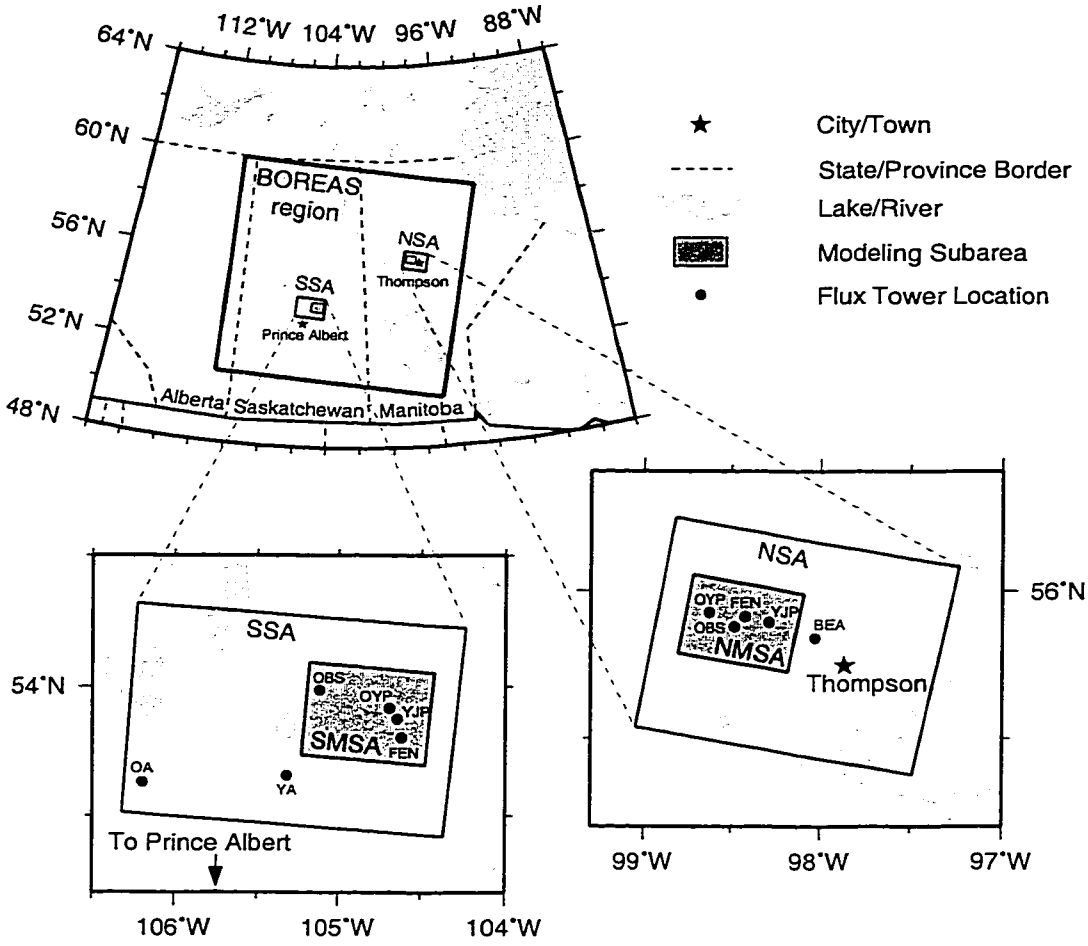


Figure 2.2: BOREAS region and study areas in Central Canada. SSA: southern study area, NSA: northern study area, SMSA: southern modeling subarea, NMSA: northern modeling subarea, OA: old (mature) aspen, YA: young aspen, OJP: old (mature) jack pine, YJP: young jack pine, FEN: fen, OBS: old (mature) black spruce, BEA: beaver pond.

acquisition, and large-scale modeling, and was large enough to occupy several GCM[1] grid cells.

**Study areas:** The study areas were located in the region (Figure 2.2), and were the focus of satellite and airborne remote sensing studies, airborne flux measurements, and meso-scale

[1]GCM: General Circulation Model

modeling. Two study areas were selected, one near the northern limit of the boreal forest near Thompson, Manitoba, and one near the southern limit of the boreal forest near Prince Albert, Saskatchewan. The northern study area (NSA) measured about 100 km×80 km (Figure 2.2), and the southern study area (SSA) measured about 130 km×90 km (Figure 2.2).

**Transect:** The transect was the area connecting and including the two study areas. This area received attention to study the gradients in vegetation types and climate.

**Modeling subareas:** Part of each of the study areas was designated as a modeling subarea. The northern modeling subarea (NMSA) was 40 km×30 km, while the southern modeling subarea (SMSA) was about 50 km×40 km. The subareas were the focus of modeling activities, and the development of gridded data products. To provide the necessary data for model development and application, these areas had the highest priority for airborne remote sensing studies and flux measurements.

**Tower flux sites:** Flux measurement towers were installed in each of the study areas to measure the energy, moisture and carbon fluxes between the boreal forest and the atmosphere. The flux towers were located in the center of areas of about 1 $km^2$ of homogeneous vegetation cover, and were expected to measure fluxes representative of this vegetation type. In the southern study area flux towers were installed in a mature aspen stand in Prince Albert National Park (Old Aspen – SSA-OA), a mature black spruce stand (Old Black Spruce – SSA-OBS), a mature jack pine stand (Old Jack Pine – SSA-OJP), a young aspen stand (Young Aspen – SSA-YA), a young jack pine stand (Young Jack Pine – SSA-YJP), and a fen site (SSA-FEN). All sites, except the mature aspen site, were located within the boundaries of the southern modeling subarea. In the northern study area flux towers were installed in a mature black spruce stand (NSA-OBS), a mature old jack pine stand (NSA-OJP), a young jack pine stand (NSA-YJP), and a fen site (NSA-FEN). In addition, a small tower was installed at a beaver pond site. All sites were within the boundaries of the northern

Table 2.1: BOREAS field campaigns.

| Field Campaign | Period | Duration (days) | Golden Days[a] SSA | Golden Days[a] NSA |
|---|---|---|---|---|
| 1993 | | | | |
| IFC-93 | 08/09/1993 – 08/29/1993 | 21 | | |
| 1994 | | | | |
| FFC-W | 02/02/1994 – 02/18/1994 | 17 | 02/05/1994 – 02/09/1994 | 02/05/1994 – 02/09/1994 |
| FFC-T | 04/12/1994 – 05/02/1994 | 21 | 04/17/1994 – 04/19/1994 | 04/17/1994 – 04/20/1994 |
| IFC-1 | 05/24/1994 – 06/16/1994 | 24 | 06/05/1994 – 06/09/1994 | 06/05/1994 – 06/12/1994 |
| IFC-2 | 07/19/1994 – 08/10/1994 | 23 | 07/21/1994 – 02/25/1994 | 08/03/1994 – 08/08/1994 |
| IFC-3 | 08/30/1994 – 09/19/1994 | 21 | 09/10/1994 – 09/17/1994 | 09/05/1994 – 09/10/1994, 09/17/1994 |
| 1996 | | | | |
| FFC-W | 02/27/1996 – 03/15/1996 | 18 | | |
| IFC-1 | 04/02/1996 – 04/28/1996 | 27 | | |
| IFC-2 | 07/09/1996 – 08/09/1996 | 32 | | |
| IFC-3 | 10/01/1996 – 10/20/1996 | 20 | | |

[a] For each IFC in 1994 the days that provided the best atmospheric conditions for remote sensing were designated "Golden Days". Remote sensing data acquired on these days received priority in processing.

modeling subarea.

**Auxiliary and process study sites:** About 80 auxiliary and process sites were used for investigator studies, mainly carbon cycle studies, or to provide ground observations to correlate with remote sensing measurements.

The BOREAS field period lasted from 1993 through 1996, with the majority of the field measurements taken during the focused and intensive field campaigns (FFCs and IFCs respectively) in 1994 and 1996 (Table 2.1). Only the mature aspen tower in the south and the mature black spruce tower in the north operated almost continuously during the entire BOREAS period. Routine

weather observations and the acquisition of images from satellite based remote sensing platforms also continued throughout most of the period. To coordinate efforts, the 85 BOREAS science teams were grouped into six disciplinary groups: airborne fluxes and meteorology (AFM), tower fluxes (TF), terrestrial ecology (TE), trace gas biochemistry (TGB), hydrology (HYD), and remote sensing science (RSS). In addition, BOREAS staff supported field operations, and implemented the BOREAS Information System (BORIS), which was used by all BOREAS investigators to store and exchange BOREAS data sets. Detailed information about the BOREAS experimental setup and field operations is provided in the BOREAS experiment plans [*BOREAS Science Team*, 1994, 1996].

## *2.2 The Boreal Forest*

### *2.2.1 Spatial Extent*

The boreal forest or taiga denotes the mixture of cool coniferous and deciduous forest in the high latitudes of the Northern Hemisphere. It forms a circumpolar belt through Canada, Scandinavia, and Siberia, which in places is up to 1000 km wide (Figure 2.3) [*Larsen*, 1980]. Estimates of the area occupied by the boreal forest vary depending on the definition [*Bonan and Shugart*, 1989; *Dixon et al.*, 1994; *Kirschbaum et al.*, 1996b]. *Goldammer and Furyaev* [1996] give an areal estimate of 12 million $km^2$, of which 9.2 million $km^2$ are closed forest. The latter number corresponds to about 29% of the global forested area, and 73% of the total coniferous area. More than 70% of the boreal forest lies in Eurasia.

Various climatological measures correlate with the location of the northern and southern limits of the boreal forest, especially summer air temperatures, and the location of arctic air masses [*Larsen*, 1980]. A good overview of the different indicators for the location of the transition zone between the boreal forest and the tundra is given by *Sirois* [1992]. The 10°C isotherm of mean monthly temperature during the warmest month is commonly used to indicate the position of the arctic tree line, and *Larsen* [1980] suggests the July 13°C isotherm for the northern limit of the boreal forest. Other measures for the transition zone between the boreal forest and the

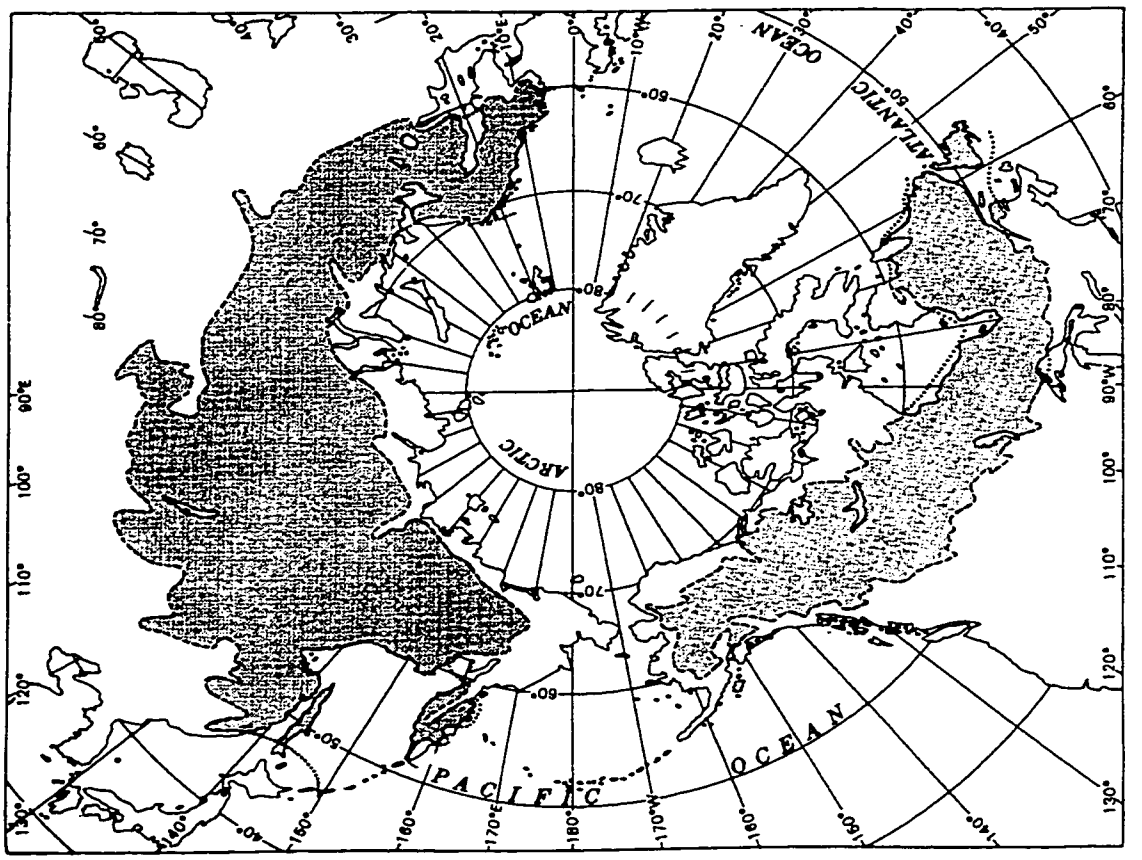


Figure 2.3: Extent of the boreal forest [*Larsen*, 1980].

tundra, or for the northern limit of the boreal forest, include the line where Thorntwaite's potential evapotranspiration is approximately 340–350 mm, the modal July position of the climatic frontal zone between the arctic air masses and the southern air masses, and various measures that use mean yearly or seasonal net radiation as a threshold.

*Pielke and Vidale* [1995] pose the hypothesis that it is not the position of the arctic front that establishes the northern limit of the boreal forest, but rather that the transition between the boreal forest and the tundra itself significantly influences the preferred position of the front. Because the albedo of the boreal forest is lower than the albedo of the tundra, a larger amount of the incoming energy is absorbed by the landscape. This increase in available energy is not accompanied by an

increase in evapotranspiration, because of cold soils and the strong control of the vegetation on the evapotranspiration. Consequently, most of this energy results in a heating of the vegetation and lower atmosphere. The resulting deep boundary layers and differential heating between the tundra and the boreal forest influence the location of the spring and summer position of the arctic front. In North America the arctic tree line coincides with the transition from discontinuous to continuous permafrost, but in parts of Siberia the continuous permafrost zone penetrates far into the boreal forest [*Sveinbjörnsson*, 1992]. Of course, most of these climatic measures are strongly correlated.

The southern border of the boreal forest is less well defined, because the boreal forest transitions to many different vegetation types, depending on the existing regional climate [*Larsen*, 1980], and because of encroachment of agricultural areas. A number of climatic measures correlate with the southern limit of the boreal forest. In eastern Canada the southern limit coincides more or less with the July 18°C isotherm, but as a result of drier conditions the forest boundary lies north of this line in the western provinces of Saskatchewan and Alberta [*Larsen*, 1980]. *Pastor and Mladenoff* [1992] quote a number of other degree-day and evapotranspiration-precipitation ratio thresholds that have been used in North America. Although climatological measures correlate with the forest boundaries, the specific biochemical and physiological plant processes that determine these boundaries are not clear [*Bonan and Shugart*, 1989; *Larsen*, 1980; *Sirois*, 1992; *Sveinbjörnsson*, 1992].

A better understanding of the processes that determine the limits of the boreal forest is needed to make meaningful estimates of changes in its range as a result of changes in climate. *Larsen* [1980] suggests that even though the limits appear to be thermally established, the main determinant of the northern limit might be the photosynthetic capacity of the trees. Warm-season temperature is linked to net radiation and thus the total energy available at the earth surface. *Bonan and Shugart* [1989] argue that in cold climates extreme or anomalous climatic fluctuations may be more limiting to plant processes than average weather patterns. *Sveinbjörnsson* [1992] identifies five different processes that contribute to reduced tree growth towards the tree line: insufficient

photosynthesis, insufficient or excessive respiration, reduced positive carbon balance, increased tissue loss, and (vaguely defined) soil processes. In the case of respiration, it is not clear whether trees near the tree line respire too much and thus limit growth, or whether they respire too little and fail to create enough energy for growth. Increased tissue loss is caused by snow and ice loads, and grazing by herbivores. Both soil temperature and nutrient availability influence tree growth.

*Bonan and Sirois* [1992] performed a model study to evaluate the effect of air temperature on individual tree growth and the northern and southern range limits of black spruce (*Picea mariana*), the most common tree species in most of the North American boreal forest. When only temperature was allowed to affect the carbon flux, they found that black spruce foliage could maintain a positive carbon balance over a wide temperature range. Black spruce could grow far south of its current range limit, but grew optimally at its southern range limit. They concluded that factors other than air temperature, such as reduced reproductive capability, and chilling requirements for bud burst, are responsible for the northern and southern limits of the boreal forest.

### *2.2.2 Physical Characteristics*

Large temperature and radiation gradients exist between the northern and southern limits of the boreal forest. Its climate is generally characterized by long, cold winters and short, moderately warm summers. Seasonal variations in mean monthly air temperature can be more than 56°C in eastern Siberia, while seasonal temperature extremes can differ by as much as 100°C [*Bonan and Shugart*, 1989]. The most widely used climate classification system is the one by Köppen [*Lamb*, 1972], which defines boreal forest and snow climates as those climates where the mean temperature of the warmest month is greater than 10°C and the mean temperature of the coldest month is less than -3°C. Most of the boreal forest is dominated by a continental climate and precipitation is generally light. In the North American boreal forest, the mean annual precipitation increases from less than 380 mm in the northwest, to almost 1000 mm in Eastern Canada. In Eurasia mean annual precipitation decreases from more than 510 mm west of the Ural Mountains to less than 250 mm in Eastern Siberia. In both North America and in Eurasia most of the precipitation tends

to fall during the summer [*Bonan and Shugart*, 1989].

Species diversity is low in the boreal forest. Fourteen tree species dominate the boreal zone in Scandinavia and Eurasia, and fifteen species dominate in North America [*Nikolov and Helmisaari*, 1992]. Interestingly, none of the boreal tree species has a circumpolar distribution, that is, all are restricted to either North America or Eurasia. In contrast, most moss and lichen species have a circumpolar distribution [*Larsen*, 1980]. The reasons for this are not clear.

Although there are no common tree species, the boreal forests in North America and Eurasia are virtually identical in structure, with a one layer canopy consisting mainly of evergreen coniferous trees, and a ground layer dominated by shrubs and some herbaceous plants. The ground surface is covered by a thick layer of moss and lichen [*Larsen*, 1980]. Outbreaks of insect pests and forest fires are common, and are important factors in shaping the boreal landscape. Lightning-induced fires are the most important natural factor controlling the age structure and species composition of boreal forest [*Goldammer and Furyaev*, 1996]. However, lightning-induced fires currently account for only 15% of recorded fires in the Russian Federation, with most of the remaining fires started by humans, either for agricultural and other land use purposes, or through negligence [*Korovin*, 1996]. Large, high-intensity forest fires lead to the replacement of entire forest stands by new successional species, while low-intensity surface fires favor selection of fire-tolerant trees. Forest fires immobilize carbon sequestered by plants through the formation of elemental or black carbon, which is unavailable to plants, and non-biodegradable. Since most boreal forest fires do not result in lower production of plant mass in the long term, *Goldammer and Furyaev* [1996] suggest that the formation of elemental carbon in forest fires acts as a sink for atmospheric carbon.

### *2.2.3 The Boreal Forest in the Climate System*

Interest in the role of the boreal forest in the climate system has increased for two reasons. First, the boreal forest plays an important role in global biogeochemical cycles, in particular the exchange of the radiatively active gases carbon dioxide ($CO_2$) and methane ($CH_4$). Second, the boreal forest influences the global climate through vegetation and albedo effects, and determines

the partitioning of available energy into latent and sensible heat over large areas in the northern hemisphere.

Seasonal oscillations in the atmospheric $CO_2$ concentration in the northern hemisphere are mainly caused by the seasonal dynamics of vegetation growth. Net photosynthesis, corresponding to an uptake of $CO_2$, occurs only during part of the growing season, while net respiration, corresponding to a release of $CO_2$ to the atmosphere, dominates during the remaining part of the year. *D'Arrigo et al.* [1987] modeled terrestrial based $CO_2$ production, using satellite-based NDVI[2] estimates, soil respiration data, and estimates of the net annual productivity for different vegetation types. The predicted $CO_2$ flux was then advected as an inert tracer using a three-dimensional atmospheric tracer transport model and GCM produced winds. They found that boreal forest photosynthesis and respiration could account for about 50% of the amplitude in the annual cycle of $CO_2$ concentration measured at Point Barrow, Alaska, and about 30% of the total amplitude at Mauna Loa, Hawaii. They suggested that an increased metabolic activity of land plants may be contributing to a positive trend in the annual amplitude of the $CO_2$ concentration. As further support for the connection between the annual variation in $CO_2$ concentration and tree growth, they showed that tree ring based estimates of $CO_2$ concentration were able to explain 64% of the variance in the annual amplitude observed at Point Barrow, Alaska.

*Bonan et al.* [1992] describe a model experiment which explores the effect of the albedo of the boreal forest on air temperature. Using a GCM based on the National Center for Atmospheric Research (NCAR) community climate model (CCM-1), they performed simulations with a boreal forest cover, and with the boreal forest replaced by bare ground. Although the magnitude of the temperature changes depended on the treatment of the oceans, global temperatures generally decreased under the bare soil scenario as a result of higher surface albedo. This effect was reinforced when the sea surface temperatures and sea ice were modeled interactively rather than being prescribed. Although results of these kinds of model sensitivity studies have to be treated with

---

[2]The Normalized Difference Vegetation Index or NDVI is a remote sensing based measure of the greenness of vegetation and is commonly used to derive vegetation parameters, see for example *Sellers et al.* [1994] or *DeFries and Townshend* [1994].

healthy skepticism given the current state of global climate models, they can give some insight into the effects of climate feedbacks.

In a more realistic model experiment, *Foley et al.* [1994] extended the boreal forest northward based on palaeobotanical data. They found that increased vegetation accounted for a 1.6°C increase in mean annual air temperature for land areas between 60°N and 90°N, with a maximum increase of about 4°C in March and April. These changes were the result of reduced snow cover, and a lower albedo associated with evergreen trees protruding above the snow cover instead of snow covered tundra.

### *2.2.4 Global Change*

A better understanding of the role of the boreal forest in global change processes is important, both because the boreal forest itself strongly affects the global climate, and because global warming is expected to manifest itself most strongly in mid to high northern latitudes. Important positive and negative feedback processes exist between changes in the boreal forest environment and changes in the global climate system. Many of these processes are only poorly understood, especially in a quantitative sense, making it difficult to provide realistic projections of the effects of global change on the boreal forest and of changes in the boreal forest on the global climate.

Observations show that maximum recent warming has occurred during the winter over the high mid-latitudes of the continents in the Northern Hemisphere [*Nicholls et al.*, 1996]. Most of the increase of the mean temperature has occurred as a result of increased daily minimum temperatures. Since 1950, the increase of land-surface minimum temperatures has been twice as large as the increase in maximum temperatures. Consequently, diurnal temperature ranges have decreased. This decrease in diurnal temperature range has been most pronounced over land areas in the Northern Hemisphere, particularly in the autumn. These changes have been found to correlate with increased cloud cover [*Nicholls et al.*, 1996].

Direct effects of increased temperatures and $CO_2$ concentrations on plant growth are reasonably well understood individually, but their combined outcome is unclear. As mentioned previ-

ously, extreme temperatures may be more limiting to plant processes than average temperatures. Consequently, decreased nighttime temperatures may allow plants to survive at higher altitudes and latitudes, and will lengthen the growing season for agricultural crops. However, premature budburst could lead to increased frost damage, and the chilling period could become too short for certain plant species to flower [*Kirschbaum et al.*, 1996a; *Melillo et al.*, 1996]. Higher temperatures could result in higher amounts of evapotranspiration, leading to water stress for plants. At the same time higher $CO_2$ concentrations may lead to an increased stomatal resistance, since plants will not have to open their stomata as much to exchange $CO_2$ with the atmosphere [*Melillo et al.*, 1996]. This effect would decrease the moisture stress to some extent, but could lead to higher leaf temperatures that can be detrimental to the plant [*Kirschbaum et al.*, 1996a].

Nutrient-limited environments such as the boreal forest are to some extent buffered against the effects of climate change. If the climate becomes less favorable for the current vegetation, nutrient availability will become less limiting, while if the climate becomes more favorable, the nutrient shortage will prevent the vegetation from taking advantage of the improved climate conditions.

*Kirschbaum et al.* [1996b] compare the results from model simulations using three different global vegetation models. Currently none of these models is able to simulate the transient behavior of forests in a changing climate, but instead they simulate the new vegetation-climate equilibrium under altered climate conditions. Because there is a good statistical agreement between the observed and predicted vegetation distributions, there is some measure of confidence in the vegetation distributions that they predict for different climate scenarios. For a $2\times CO_2$ equilibrium climate change scenario, two of the three models predict a large decrease in the extent of the boreal forest, despite a northwards migration of the arctic tree line. The third model predicts only a small decrease.

*Bonan and Sirois* [1992] show that these models may not always include appropriate sensitivities of plant growth to changes in environmental conditions, so care has to be taken when interpreting their results. Another reason to be careful is that although climate models are able to simulate many large scale climatic features reasonably well, simulation results for regional cli-

mate still leave much to be desired [*Kattenberg et al.*, 1996]. Regional biases in temperature and especially precipitation are large, which should have significant consequences for the equilibrium vegetation types predicted by the vegetation models.

*Wein and De Groot* [1996] suggest that fire may play an important role in vegetation succession in the boreal forest under a changed climate. Vegetation changes in the nutrient and energy- limited boreal forest are expected to be slow, but fire may literally clear the way for new, better-adapted species. In addition to clearing the forest, the fire also alters the nutrient availability and the energy balance at the surface. Increased temperatures and drier conditions are expected to increase the occurrence of forest fires.

## *2.3 Hydrological Perspective*

### *2.3.1 Land Surface–Atmosphere Interactions*

Most measurements of the interactions between the land surface and the atmosphere are point observations, which often have a high temporal resolution, but which represent only a small area. Consequently, they reveal little about the spatial variability of the observed process. For many applications, an insight in the spatial distribution of these land-atmosphere interactions is important, if only to determine the average quantity of mass, energy, or momentum exchanged over a certain area. Until recently, no measurement techniques existed that allowed routine observations of the spatial variability of exchange processes. This situation has changed somewhat with the advance of remote sensing techniques, although most of these techniques are still in an experimental stage.

Similarly, most surface-vegetation-atmosphere transfer schemes (SVATs) are very detailed in the vertical direction, with only a cursory treatment of the spatial variability of the modeled processes. One of the main challenges in research of land surface-atmosphere interactions is to integrate observations and understanding of processes at the point scale over larger areas in a rigorous and consistent manner. A better understanding of the hydrology of the boreal forest ecosystem is a prerequisite for integrating understanding of exchange processes at the plot and stand scale to the catchment scale, and eventually regional and continental scales. The availability of moisture,

modulated by plant-physiological controls, largely determines the partitioning of available energy in latent and sensible heat. The presence or absence of snow changes the albedo of the land surface and consequently the surface energy balance.

Water balance studies based on observed river discharge data in the BOREAS study areas can help to provide a reliable estimate of the areal average latent heat flux over these basins. Such an areal average flux will provide an important constraint for other aggregation schemes and larger-scale regional hydrologic and atmospheric models.

### *2.3.2 The Boreal Winter*

The hydrology of the boreal forest is largely characterized by the long, cold winter, which essentially stops vegetation growth for five to seven months of the year. *Harding and Pomeroy* [1996] describe a winter field experiment in which they compared the energy balance over a jack pine stand and a snow covered lake. The sensible heat fluxes above the snow free canopy and the snow covered lake showed opposite sign, with an upward flux over the canopy and a downward flux over the lake, largely because of the difference in albedo. However, when the canopy was snow covered, the sensible heat fluxes were of equal sign. In this case, the downward sensible heat flux above the canopy compensated for a large upward latent heat flux caused by sublimation of intercepted snow. As a result of interception and subsequent sublimation of snow in the canopy, snow accumulation under the canopy was 30% less than in adjacent clearings. Such large variations in the components of the energy balance over the different land surface types in the boreal forest complicate translation of understanding gained at the small (e.g. tower) scale to larger scales.

### *2.3.3 Evapotranspiration in the Boreal Forest*

One of the important early findings from BOREAS was that despite the abundance of water, evapotranspiration is limited, even on warm days with low humidity, suggesting a strong biophysical control [*Sellers et al.*, 1995]. According to *Sellers et al.* [1995], evapotranspiration rates were less than 2 mm/day over the season, while sensible heat fluxes were often high, resulting in Bowen

ratios[3] larger than one on many days. These high sensible heat fluxes lead to the development of deep convective boundary layers over the BOREAS region.

*Hogg and Hurdle* [1997] studied sap flow in trembling aspen, the most abundant deciduous tree in the North American boreal forest. One of their two study sites was the mature aspen site in the BOREAS southern study area, while the other site was located about 100 km further south. For both locations, they found that sap flow increased linearly for vapor pressure deficits (VPD) from 0 to 1 kPa, but that it remained constant for vapor pressure deficits greater than 1 kPa. Thus, an inverse relationship exists between the vapor pressure deficit and stomatal conductance for deficits above 1 kPa. Based on the sap flow measurements they estimated the maximum transpiration rates at the mature aspen sites at 0.4 mm/hr. One reason for the conservative water use by the aspen, might be the need to maintain a minimum water potential inside the leaves to prevent irreversible damage due to dehydration. In that case the resistance between the soil and the plant, and thus the rate at which water can be extracted from the ground, might determine the maximum transpiration rate [*Hogg and Hurdle*, 1997]. A similar response of stomatal resistance to vapor pressure deficits was found by *Saugier et al.* [1997], who studied transpiration at the branch, tree, and stand level at the mature jack pine site in the southern study area. Low transpiration rates were attributed to high stomatal resistances and low leaf area indices.

As part of the NOPEX project, *Grelle et al.* [1997] studied the evapotranspiration components in a mixed spruce (Norway spruce (*Picea abies*)) and pine (Scots pine (*Pinus silvestris*)) boreal forest in Sweden during the 1995 growing season. They found that although tree transpiration accounted for most of the total evaporation (65%), evaporation from interception storage (20%) and from the forest floor (15%) were important as well. Comparing their results to other evaporation experiments they concluded that the fraction of total evaporation that originates directly from the forest floor varies widely, but in all cases formed an important part of the forest water balance. They estimated the maximum interception storage for their site at 3.3 mm, for forests stands with leaf area index values between 3 and 5.

---

[3]The bowen ratio is the ratio of the sensible heat flux to the latent heat flux.

Figure 2.4: Root mass of a black spruce, demonstrating the small depth of the root zone.

### *2.3.4 The Organic Surface Layer*

Most of the forest floor in the boreal forest is covered by a moss and lichen layer. According to *Bonan and Shugart* [1989] 80–90% of the above-ground biomass in cold and wet black spruce stands may be contained in the moss layer. This organic layer influences both the moisture and thermal characteristics of the forest floor. Its presence increases soil moisture, decreases soil temperatures because of its high water content and low thermal conductivity, and reduces nutrient availability. Most of the roots of trees and shrubs (especially in the black spruce forests in the BOREAS region) are located in this organic/moss layer (Figure 2.4). Mosses lack roots and vascular systems and are dependent on moisture taken up directly through the leaf surfaces. In addition, moss leaves do not have stomata, and thus respond differently to moisture stress than do higher plants.

*Price et al.* [1997] describe a study of the water fluxes through the canopy and the moss layer at two sites near the northern limit of the boreal forest during summer 1994. One site was just outside

the BOREAS northern study area, while the other was near the mature black spruce flux tower site within the northern study area [see also *Haddeland and Lettenmaier*, 1995]. They found that about 23% of the total rainfall during their study was intercepted by the black spruce canopy, and evaporated directly from canopy storage. For individual storms the interception amount varied from about 60% for small events, to about 15-20% for large events with more than 30 mm of precipitation. Stemflow amounted to less than 1% of bulk precipitation, and could be neglected. About 21% of the throughfall was retained by the moss carpet, and subsequently evaporated. Maximum evaporation rates from the forest floor were more than 1 mm/day, with more typical rates about 0.5 mm/day. Water fluxes through the moss layer were large immediately after a storm event, but the amount of drainage between storm events was small. Canopy interception and moss evaporation accounted for about 41% of total precipitation during the measurement period.

The organic forest floor layer not only affects the hydrologic regime, but also plays an important role in the thermal balance of the surface and the underlying mineral soil [*Bonan and Van Cleve*, 1992]. Because of it low bulk density and the low thermal conductivity, the organic material acts as an effective insulator, resulting in lower soil temperatures and higher permafrost tables. The seasonal moisture regime of the organic layer aids in the formation and maintenance of permafrost. In the summer the surface layer dries out, and the low thermal conductivity of the organic material limits the amount of the warming of the soil. In the autumn and winter, decreased evapotranspiration leads to wetter conditions in the organic layer, resulting in a higher thermal conductivity, and consequently enhanced cooling of the underlying soil. As a result there is a net transport of heat from the soil to the atmosphere in the fall and winter, which is favorable for the formation of permafrost.

### *2.3.5 Carbon Exchange Between the Boreal Forest and the Atmosphere*

Water availability, soil moisture distribution, and soil temperature are also controlling factors in the exchange of $CO_2$, an important greenhouse gas, between the boreal forest and the atmosphere. *Frolking et al.* [1996] used a one-dimensional, daily time step carbon balance model to investigate

the temporal variability of carbon dynamics in a spruce/moss boreal forest environment. They showed that annual ecosystem productivity was particularly sensitive to the timing of the onset of spring, which is characterized by the disappearance of snow, and thawing of the soil layers. Model results indicated that ecosystem productivity tended to be highest in years with early springs and relatively wet summers and lowest in years with late springs and relatively dry summers.

Methane ($CH_4$), produced by anaerobic microbial decomposition of organic matter, is another important greenhouse gas whose emissions were monitored as part of the field phase of the BOREAS project. Methane emissions from a boreal fen in the southern study area showed a strong relationship with the temperature of the peat layers and the average height of the water table during the 1994 growing season [*Suyker et al.*, 1996]. For different parts of the growing season, peat temperature and water table height, either alone or in combination, were able to explain between 68% and 94% of the observed variation in methane emissions. Methane emission increased with increased peat temperature, both reaching their peak in early August. The relationship between the water table depth and methane emissions was more complicated, with abrupt changes in the water table followed by a more gradual change in methane emissions after a time lag of 12 days. Similar results have been reported by investigators in other boreal forest areas, for example *Kettunen et al.* [1996] in a study of boreal peatlands in Finland, and *Moosavi et al.* [1996] in a study of boreal peatlands in Alaska.

### *2.3.6 Drainage Network*

The limited topographical relief in most of the boreal forest area (Figure 2.5), combined with the geology and geomorphology of the landscape, leads to a complicated mosaic of lakes and wetlands (Figure 2.6). Many northern peatlands lack a clearly defined drainage network, and flow is often very diffuse. In the BOREAS area considerable effort was expended on defining the boundaries of the White Gull Creek Basin in the southern study area by R. Soulis and N. Kouwen from the University of Waterloo, Canada. This effort suggests that the boundary of the basin may well change with changes in local ground water table. Topographic gradients in the smaller NW2 and

Figure 2.5: View of the black spruce forest in the northern study area.

NW3 basins in the northern study area are steeper, and consequently these basins are somewhat better defined.

Hydrologic response of the White Gull Creek Basin is slow. During the period July 13–19, 1994, about 120 mm of precipitation fell on the White Gull Creek Basin, with most of that falling on July 18–19. However, the peak runoff measured at gauge SW1 (drainage area about 603 $km^2$), was only 25.4 $m^3/s$, measured on July 21, 1994. During the weeks following the storm, observed areal average runoff amounted to only 35.6 mm (July 13–August 5, 1994), while the total amount of precipitation during this period was 128.3 mm.

*Omernik and Bailey* [1997] argue that for areas where watersheds are difficult to define the basic unit for analysis, resource assessment, and management should not be the watershed, but the ecoregion. An ecoregion is a region within which the mosaic of ecosystem components is different from that of adjacent regions. In essence this is the approach followed in defining the

Figure 2.6: Lake and surrounding forest in the southern study area.

BOREAS region and study areas, whose boundaries do not coincide with watershed boundaries. However, in order to study the water balance of a region it is necessary to account for the fluxes across the boundary of the region. For water balance studies the watershed remains the analysis unit of choice, since fluxes across the boundary can be neglected.

### *2.3.7 White Gull Creek Basin*

The White Gull Creek basin upstream of Highway 106 formed the largest gauged area in the southern study area with an approximate drainage area of 603 $km^2$. The main stream gauge (SW1) was equipped with an all-season recorder, installed and operated by Environment Canada. White Gull Creek drains extensive wetland areas in a gently undulating to moderately rolling terrain east of Candle Lake, Saskatchewan. Three of the flux towers in the southern study area (mature black spruce, mature jack pine and young jack pine) were located within the boundaries of the White

Gull Creek basin, while a fourth (fen) was located just southeast of the watershed. The surface geology is characterized by Pleistocene and recent glacial deposits on top of Cretaceous bedrock. Vegetation consists mainly of black spruce in poorly drained areas, and jack pine on well-drained and sandy soils. Mixed stands of aspen and white spruce are common on well-drained glacial deposits.

## *2.4 Data Collection and Data Processing*

### *2.4.1 Hydrological Investigations*

The BOREAS hydrology group (HYD) consisted of eight science teams, who were responsible for snow and hydrology investigations. The science teams focused on soil moisture, snow processes and snow remote sensing, catchment hydrology, and hydrological modeling. The objectives of the hydrologic investigations were to characterize the storage of moisture, in both liquid and solid state, at and near the land surface, as well as the moisture fluxes to and from the land surface [*BOREAS Science Team*, 1994]. Five of the eight science groups focused on snow processes, three of which were mainly involved with the estimation of snow cover and snow depth from remote sensing observations. One science group focused on soil moisture, while the remaining two groups dealt with catchment hydrology, both from a modeling and data collection point of view.

Snow related measurements included field measurements of snow depth, snow water equivalence, profiles of density and temperature, and incident radiation on the snow pack. These measurements were only made during part of the FFCs. During the summer of 1994, soil moisture profiles were measured at selected flux tower sites, using neutron probe and TDR instruments. Streamflow measurements were made at year-round gauges operated by Water Survey of Canada (WSC) on White Gull Creek in the southern study area and the Sapochi River in the northern study area. Precipitation measurements were made using Belfort weighing gauges and tipping bucket gauges during the 1994–1996 growing seasons. In addition a rain radar was operated over the southern study area from May till September 1994 [*Schnur et al.*, 1997]. Moss gravimetric and canopy interception studies were performed near the mature black spruce site in the north.

Table 2.2: University of Washington participation in BOREAS field investigations

| Period and Participant | Location | Purpose | Activities |
|---|---|---|---|
| June 1994<br>Bart Nijssen | SMSA | Support HYD-9 in general hydrologic data collection | Stream gauging; monitoring of lake and groundwater levels; monitoring of rain gauges |
| August-September 1994<br>Ingjerd Haddeland[a] | NSA-OBS | Moss interception and evaporation measurements | Moss gravimetric studies; canopy interception |
| April 1995<br>Bart Nijssen | NSA-OBS | Support HYD-3 during snow studies. Work focused on attenuation of shortwave radiation by the tree canopy | Measurements of radiation, snow depth, snow density, and biophysical characteristics such as stem density, stem diameter, and needle density |
| February 1996<br>Bart Nijssen | SSA-OBS<br>SSA-OA | Support HYD-3 during snow studies. Work focused on attenuation of shortwave radiation by the tree canopy | Measurements of radiation, snow depth, snow density, and biophysical characteristics such as stem density, stem diameter, and needle density |
| August 1996<br>Bart Nijssen | SSA-OBS | Support HYD-8 during studies of the moss water balance | Moss gravimetric studies; monitoring of rain gauges |

[a] see *Haddeland and Lettenmaier* [1995]

The hydrological measurement program during 1996 was more limited. Although no precipitation radar was operated, soil moisture profiles were again measured at a number of tower sites and the precipitation gauge network were re-activated. Additional moss evaporation studies were performed near the mature black spruce site in the south. The water balance study in Chapter 5 combines data from a large number of BOREAS science teams to investigate the hydrological behavior of the White Gull Creek basin. University of Washington participation in BOREAS hydrological fieldwork is documented in Table 2.2.

Chapter 3

# POINT EVALUATION OF A SURFACE HYDROLOGY MODEL FOR BOREAS

This chapter has appeared as B. Nijssen, I. Haddeland, and D. P. Lettenmaier, Point evaluation of a surface hydrology model for BOREAS, *J. Geophys. Res.*, *102*, 29,367–29,378, 1997.

## *3.1 Introduction*

One of the main objectives of the Boreal Ecosystem-Atmosphere Study (BOREAS) is "to improve the process models that describe the exchanges of radiative energy, water, heat, carbon, and trace constituents between the boreal forest and the atmosphere" [*Sellers et al.*, 1995]. This paper describes the application and evaluation of one such process model which simulates the surface water and energy fluxes. The data gathered by BOREAS investigators offer a unique opportunity to evaluate model performance, to examine which processes are important, and whether they are adequately represented by process models.

The Distributed Hydrology-Soil-Vegetation Model (DHSVM) is a surface hydrology model developed to infer the spatial distribution of runoff generation, and moisture and energy fluxes at spatial scales on the order of 100 m to 1 km and a sub-daily time scale. This is accomplished by simulating a detailed water and energy balance at each node in a digital elevation model (DEM), and predicting lateral redistribution of water in the subsurface zone. DHSVM was originally developed for areas with complex terrain, and has been applied successfully in mountainous regions in the western United States [*Arola and Lettenmaier*, 1996; *Storck et al.*, 1995; *Wigmosta et al.*, 1994]. In all of these applications the model has been employed as a fully distributed hydrological model, although *Arola and Lettenmaier* [1996] examined the effects of varying spatial resolution on total regional energy and moisture fluxes. Our ultimate purpose in the BOREAS

context is to use DHSVM in distributed mode to analyze the spatial distribution of surface moisture and energy fluxes, and runoff generation in the BOREAS modeling subareas. To this end we will combine spatially distributed land surface characteristics such as vegetation and soil type, with spatially distributed meteorological forcings derived from interpolated point measurements and remote sensing observations. However, eliminating the complexity resulting from the spatial variability in surface characteristics and meteorological forcings facilitates testing of the model's ability to reproduce important hydrologic processes, and allows evaluation of the model structure. Once it can be shown that DHSVM is able to reproduce observed surface and energy fluxes at the point scale, e.g. tower flux site, the next step will be application of the model to the modeling subareas.

Application of DHSVM in the boreal forest area provides a number of modeling challenges. The model was originally developed for application in mountainous areas where topographic gradients are steep. Consequently catchment boundaries are well defined. The steep gradients also justify the approximation that the slope of the groundwater table is identical to the slope of the ground surface. In the BOREAS area, which has only modest topographic relief, considerable effort has been expended on defining the boundaries of the White Gull Creek Basin in the southern modeling subarea (SMSA). This effort suggests that the boundary of the basin may well change with changes in local ground water table. This uncertainty in catchment size makes comparison of measured and modeled stream discharge problematic. As for the lateral redistribution of subsurface water, the hydraulic gradient clearly depends on the slope of the water table. At the point scale the main challenges are an adequate representation of the soil thermal regime, and the influence of the organic soils that are present in much of the area on the moisture and energy balance. According to *Bonan and Shugart* [1989] 80-90% of the above-ground biomass may be contained in the moss layer in cold and wet black spruce stands. The presence of this organic/moss layer increases soil moisture, decreases soil temperatures because of its high water content and low thermal conductivity, and reduces nutrient availability. Most of the roots of trees and shrubs (especially in the dominant black spruce forests in the BOREAS region) are located in this organic/moss layer.

Early results from the summer 1994 Intensive Field Campaigns (IFCs) show that transpiration from the coniferous vegetation in the boreal forest is lower than expected, especially on clear dry days when there is no soil moisture stress. Evapotranspiration rates were less than 2 mm/day over the season, while sensible heat fluxes were often high, resulting in Bowen ratios larger than one on many days [*Sellers et al.*, 1995].

### *3.2 Model Description*

The model description given in this section is, of necessity, brief; for more details, the reader is referred to *Wigmosta et al.* [1994] and *Arola and Lettenmaier* [1996]. DHSVM simulates a water and energy balance for each surface element (pixel) at the scale dictated by a digital elevation model or DEM (Figure 3.1). This procedure accounts explicitly for the spatial variation of land surface processes. Because DHSVM maintains information about the physical location of surface hydrologic processes, it is ideally suited to deal with spatially distributed land surface characteristics and meteorological forcings. The time step of the model is typically less than a day which allows it to capture the diurnal variations in the energy and moisture fluxes. As a compromise between temporal resolution and computational requirements, a time step of three hours is typically selected.

For each pixel the model represents the soil and vegetation as a three layer soil column, and a vegetation canopy with a maximum of two layers (understory and overstory). Transpiration from the canopy is modeled using the Penman-Monteith approach, with evaporation from interception storage allowed at the potential rate. Soil evaporation is calculated as the minimum of atmospheric demand and soil desorption, which is defined as the amount of water the soil can deliver to the atmosphere during a time step. The evapotranspiration is calculated for each vegetation layer and the soil separately. However, actual transpiration/evaporation from the upper vegetation layers is subtracted from the potential evapotranspiration of the overstory, and subsequently, soil, to prevent the total evaporative flux from exceeding the atmospheric demand. For example, in case of a two layer canopy, the transpiration from the top layer is calculated, followed by the transpiration of the

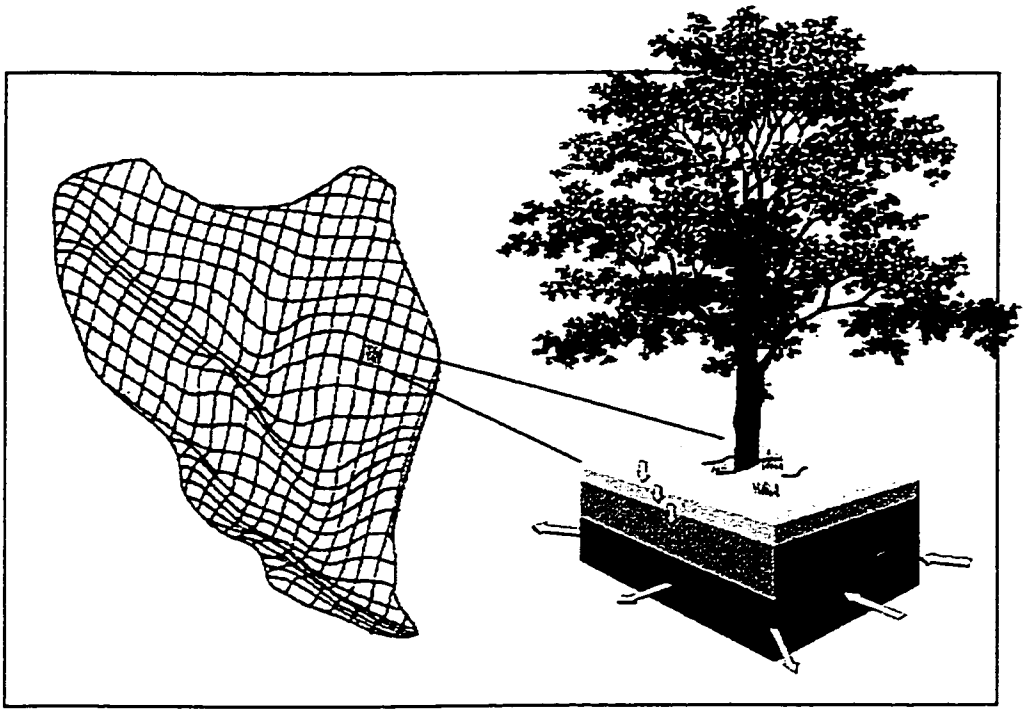

Figure 3.1: DHSVM model structure (adapted from *Wigmosta et al.* [1994])

understory, and finally direct evaporation from the soil. To calculate the evapotranspiration for the understory, the potential evapotranspiration is first adjusted by the actual evapotranspiration from the overstory.

All water that is not intercepted by one of the canopy layers is assumed to enter the soil column as long as the soil is not saturated. When the soil column is entirely saturated, saturation excess overland flow occurs. This flow is then routed to the basin outlet using the unit hydrograph formulation of *Maidment et al.* [1996].

Drainage from one soil layer to the next is represented by a Darcy equation assuming unit hydraulic gradient. The unsaturated hydraulic conductivity is calculated as a function of volumetric soil moisture content, porosity, and pore size distribution index [*Brooks and Corey*, 1964]. Saturated subsurface flow is routed from pixel to pixel using Darcy's equation based on the local water

table gradient.

Separate shortwave and longwave radiation budgets are calculated for the different canopy layers and the soil surface. The model assumes that the fraction of transmitted radiation decreases exponentially with increasing LAI. An effective surface temperature is calculated iteratively for each surface element, without adjusting the evaporative flux. Although a more exact approach would solve both the surface temperature and the evaporative flux iteratively, the approach used is computationally much more efficient. Currently DHSVM contains only a rudimentary ground heat flux mechanism. The temperature for the top layer of the soil is assumed to be equal to the surface temperature, while temperatures for deeper ground layers are either provided as input, or modeled using a damping depth and annual cycle. The soil thermal balance is then composed of the change in heat storage in the top layer and a heat flux between the top layer and the damping depth.

For application of DHSVM in the boreal forest, a third soil layer was added to the two originally present in the model. *Haddeland and Lettenmaier* [1995] found during field work in summer 1994, and subsequent model sensitivity studies, that the upper moss/organic layer plays an important role in the water balance of the black spruce sites. A significant portion of the roots of some boreal vegetation, especially black spruce, is found in this organic layer. Evaporation from this layer is parameterized in the same manner as for the other soil layers, that is, the soil evaporation is the minimum of the potential soil evaporation and soil desorption. The moss layer is then modeled by choosing soil parameters that are characteristic of organic soils, such as a high porosity and a low bulk density. A second adaptation has been to include a soil temperature limitation in the calculation of the stomatal resistance, $r_s$. *Jones* [1992], following *Jarvis* [1976], suggests that a multiplicative model with appropriate non-linear components should be used to incorporate the effects of ambient conditions on the stomatal resistance. DHSVM includes influences from soil temperature $T_{soil}$, vapor pressure deficit,$\Delta e$, soil moisture content $\theta$, and photosynthetically active

radiation flux (*PAR*) on the stomatal resistance. The multiplicative model is given by

$$r_s = f_1(T_{soil}) \cdot f_2(\Delta e) \cdot f_3(PAR) \cdot f_4(\theta) \cdot r_s^{min}, \tag{3.1}$$

where $r_s^{min}$ is a species-dependent minimum stomatal resistance, and $f_i$ is a function whose form can be obtained from controlled environment studies. The soil temperature relationship is given by *Haddeland and Lettenmaier* [1995] as

$$f_1(T_{soil}) = \begin{cases} \left(a + bT_{soil} + cT_{soil}^2\right)^{-1} & T_{soil} > 0°C \\ \infty & T_{soil} \le 0°C \end{cases}, \tag{3.2}$$

where $a$, $b$, and $c$ coefficients depending on vegetation type. The remaining functions are left unchanged from the original version of DHSVM as described by *Wigmosta et al.* [1994]. The relationships for vapor pressure deficit and PAR are taken from *Dickinson et al.* [1991], with the vapor pressure deficit feedback given by

$$f_2(\Delta e) = \begin{cases} \left(1 - \frac{\Delta e}{\Delta e_{max}}\right)^{-1} & 0 \le \Delta e < \Delta e_{max} \\ \infty & \Delta e \ge \Delta e_{max} \end{cases}, \tag{3.3}$$

where $\Delta e_{max}$ is the vapor pressure deficit above which complete stomatal closure occurs. The influence of the light level on the stomatal resistance is modeled by

$$f_3(PAR) = \frac{1 + R_p/R_p^c}{r_s^{min}/r_s^{max} + R_p/R_p^c}, \tag{3.4}$$

where $R_p$ is the amount of visible radiation, $R_p^c$ the amount of visible radiation at which $r_s = 2r_s^{min}$, and $r_s^{max}$ the maximum stomatal resistance. A piece-wise linear dependence on soil moisture is

assumed following *Feddes et al.* [1978]

$$f_4(\theta) = \begin{cases} 1 & \theta^* \leq \theta \leq n \\ \frac{\theta^* - \theta_{wp}}{\theta - \theta_{wp}} & \theta_{wp} < \theta < \theta^* \\ \infty & \theta_r \leq \theta \leq \theta_{wp} \end{cases}, \tag{3.5}$$

where $\theta^*$ is the moisture content above which the soil moisture does not limit transpiration, $n$ the total porosity, $\theta_{wp}$ the wilting point, i.e. the soil moisture content below which soil water is unavailable to the plants, and $\theta_r$ is the residual moisture content. Evapotranspiration is calculated for each root zone layer separately and independently, with a different canopy resistance term for each layer. The evapotranspiration from each layer is multiplied by the fraction of roots in the layer to find the actual amount of moisture transpired.

### *3.3 Point Model Application*

The detailed moisture and energy flux observations from the tower flux sites offer a unique opportunity for model development and evaluation. Hydrological models are typically evaluated on the basis of their ability to simulate observed stream hydrographs. This focus on hydrograph simulation is justified in the light of engineering and water resource applications, and because hydrographs are often the only observed data series available for comparison with model simulations. A further reason for focusing on streamflow is that it integrates the response of all hydrologic processes acting in a catchment to meteorological forcings and land surface characteristics. For a hydrologic model to produce reasonable hydrographs, it is necessary to include the relevant hydrologic processes. However, it is often impossible to evaluate the relative importance of different processes using only streamflow to assess model performance. Most hydrological model are overparameterized, and can produce similar results for different sets of model parameters [*Beven*, 1993; *Duan et al.*, 1992].The BOREAS data allow a thorough inspection of the appropriateness of hydrological models, since observations are available for most components of the energy and

Table 3.1: Climatic conditions near the southern (Prince Albert, Saskatchewan) and northern (Thompson, Manitoba) limits of the boreal forest.

| | Prince Albert | Thompson |
|---|---|---|
| Mean annual precipitation (mm) | 398 | 544 |
| Mean annual temperature (°C) | 0.1 | -3.9 |

water balance.

Detailed and complete surface observations of energy and moisture exchange between the land surface and atmosphere were collected at the tower flux sites. Taking advantage of these observations, this paper discusses the ability of DHSVM to simulate these moisture and energy fluxes at the tower sites, looking at small areas centered around the tower flux sites. By eliminating the complexity of a fully distributed run, such as the effects of spatial variability on forcing variables and terrain characteristics, we can instead focus on the ability of DHSVM to simulate separate components of the energy and water balance. If DHSVM can demonstrate skill in the simulation of these individual components, greater confidence can be placed in the results of the fully distributed runs that are our eventual goal.

### *3.4 Model Implementation*

Two tower flux sites in the southern modeling subarea (SMSA), and one in the northern modeling subarea (NMSA) (Figure 2.2) were selected to contrast the response of the boreal forest system to the different climatic conditions near the northern and southern limits of the boreal forest (Table 3.1). Temperature is the main limiting factor for vegetation growth in the north, while in the south moisture stress plays an important role. In each study area we selected the Old Black Spruce (OBS) site, since these sites represent the dominant tree species in most of the BOREAS study area. The black spruce (*Picea mariana*) in the boreal forest zones generally occurs in areas with poor drainage. In addition the Old Jack Pine (OJP) site in the SMSA was selected, since jack pine (*Pinus banksiana*) tends to grow under different hydrologic conditions than black spruce,

with a preference for well drained sandy soils. In this manner we can evaluate the performance of DHSVM over a range of climatic and hydrologic conditions. The data collected at the different tower flux sites are described in more detail by *Jarvis et al.* [1997] for SSA-OBS, *Baldocchi et al.* [1997] for SSA-OJP, and *Goulden et al.* [1997] for NSA-OBS.

Soil temperature limitations on the stomatal resistance were based on *Haddeland and Lettenmaier* [1995], who fitted curves to data given by *Stathers and Spittlehouse* [1990] for Norway spruce (*Picea abies*) and Scots pine (*Pinus sylvestris*), which were taken to be similar to black spruce and jack pine, respectively. The soil temperature relationship for black spruce, $f_1^{bs}$, is given by

$$f_1^{bs} = \begin{cases} \left(0.176 + 0.0770 T_{soil} - 0.0018 T_{soil}^2\right)^{-1} & T_{soil} > 0°C \\ \infty & T_{soil} \leq 0°C \end{cases}, \tag{3.6}$$

and the relationship for jack pine, $f_1^{jp}$, is given by

$$f_1^{jp} = \begin{cases} \left(0.0705 T_{soil} - 0.0013 T_{soil}^2\right)^{-1} & T_{soil} > 0°C \\ \infty & T_{soil} \leq 0°C \end{cases}. \tag{3.7}$$

Instead of modeling each tower flux site as one isolated pixel, the model was applied to a square grid mesh in the vicinity of the tower, with the tower at the center. The main motivation for this strategy is to account for the lateral redistribution of subsurface water, which DHSVM represents explicitly. If the model were run for a single point, an artificial slope would have to be imposed to drain water away from the pixel. While this might be defensible for the well-drained jack pine site, black spruce generally tend to grow in depressions with poor drainage, which collect water from neighboring higher areas. Therefore, a certain amount of lateral inflow to the black spruce pixel would have to be specified. By running the model over a somewhat larger area, this effect is recognized explicitly, and the need of imposing a somewhat arbitrary slope and inflow is avoided. By choosing the model area large enough, the boundary effects from the edge of the

Table 3.2: Vegetation parameters for the three tower flux sites

| Vegetation Parameter | | OBS | | OJP | |
|---|---|---|---|---|---|
| | | Overstory | Understory | Overstory | Understory |
| Type | | Wet coniferous | | Dry coniferous | |
| Height | (m) | 12.0/10.0 | 0.2 | 13.0/10.0 | 0.2 |
| LAI | | 3.0/2.5 | 2.0 | 3.0/2.5 | 2.0 |
| $r_s^{min}$ | (s/m) | 400 | 200 | 400 | 200 |
| $r_s^{max}$ | (s/m) | 5000 | 5000 | 5000 | 5000 |
| $\Delta e_{max}$ | (Pa) | 4000 | 4000 | 4000 | 4000 |
| $\alpha$ | | 0.08 | 0.1 | 0.08 | 0.1 |
| $C_n$ | | 3.5 | NA | 3.5 | NA |
| $R_p^c$ | ($W/m^2$) | 30 | 30 | 30 | 30 |
| $k$ | | 0.5 | 0.5 | 0.5 | 0.5 |
| $\theta^*$ | | 0.15 | 0.25 | 0.11 | 0.11 |

$\alpha$: albedo
$C_n$: canopy attenuation coefficient for wind
$k$: canopy attenuation coefficient for radiation

model grid mesh do not propagate to the center of the grid mesh before the end of the model run. In this application we set the subsurface flux across the outer edge of the model square equal to zero, thus leaving evapotranspiration and saturation excess overland flow the only mechanisms by which water can leave the model area.

The topography of each model area was based on DEMs of the northern and southern modeling subareas (NMSA and SMSA) with a spatial resolution of 100 m×100 m (courtesy L. Band and X. Wang, University of Toronto). For each site a square of 51×51 pixels (5.1 km×5.1 km) was selected, with the tower flux site at location (26, 26). Uniform vegetation and soil types were assigned to all the pixels in each block (Table 3.2 and Table 3.3). Vegetation and soil parameters were specified using a combination of observations made by BOREAS research teams and literature values. A model time step of 3 hours was selected to capture the diurnal cycle of moisture and energy fluxes.

Model forcings at each time step were shortwave radiation, longwave radiation, cloudiness, air temperature, humidity, wind, soil temperatures in the three soil layers, and precipitation. Short-

Table 3.3: Soil parameters for the three tower flux sites.

| Soil Parameter | | OBS | | | OJP | | |
|---|---|---|---|---|---|---|---|
| | | Top | Middle | Bottom | Top | Middle | Bottom |
| Layer depth | (m) | 0.2 | 0.4 | 0.3 | 0.2 | 0.4 | 0.3 |
| Overstory root fraction | | 0.5 | 0.4 | 0.1 | 0.2 | 0.5 | 0.3 |
| Understory root fraction | | 0.9 | 0.1 | 0.0 | 0.7 | 0.3 | 0.0 |
| $n$ | | 0.8 | 0.5 | 0.4 | 0.4 | 0.4 | 0.4 |
| $\lambda$ | | 0.25 | 0.378 | 0.553 | 0.378 | 0.378 | 0.55 |
| $h_b$ | (m) | 0.0726 | 0.1466 | 0.0869 | 0.1466 | 0.1466 | 0.0869 |
| $\theta_{FC}$ | ($m^3/m^3$) | 0.6 | 0.207 | 0.125 | 0.207 | 0.207 | 0.125 |
| $\theta_{WP}$ | ($m^3/m^3$) | 0.2 | 0.095 | 0.055 | 0.095 | 0.095 | 0.055 |
| $\rho_b$ | ($kg/m^3$) | 250 | 1300 | 1600 | 1300 | 1300 | 1600 |
| $K_s^v$ | (m/s) | $6.0\times10^{-6}$ | $5.5\times10^{-6}$ | $1.94\times10^{-6}$ | $5.5\times10^{-6}$ | $5.5\times10^{-6}$ | $1.94\times10^{-6}$ |
| $K_s^h$ | (m/s) | $2.0\times10^{-6}$ | $2.0\times10^{-6}$ | $2.0\times10^{-6}$ | $2.0\times10^{-6}$ | $2.0\times10^{-6}$ | $2.0\times10^{-6}$ |
| $c_{\text{solid}}^{\text{eff}}$ | (W/m K) | 0.3 | 5.7 | 4.6 | 5.0 | 5.0 | 5.0 |
| $C_{\text{soil}}^{\text{dry}}$ | ($J/m^3$ K) | $0.58\times10^6$ | $1.4\times10^6$ | $1.4\times10^6$ | $1.4\times10^6$ | $1.4\times10^6$ | $1.4\times10^6$ |

$\lambda$: pore size distribution index
$h_b$: air entry pressure
$\theta_{FC}$: soil moisture at field capacity
$\rho_b$: bulk density
$K_s^v$: saturated hydraulic conductivity in vertical direction
$K_s^h$: saturated hydraulic conductivity in horizontal direction
$c_{\text{solid}}^{\text{eff}}$: effective solids thermal conductivity
$C_{\text{soil}}^{\text{dry}}$: volumetric heat capacity of the soil

wave radiation, longwave radiation, air temperature, humidity and wind were taken from data assembled by J. Kimball (University of Montana). These data are based on observations from the tower flux sites, with missing values replaced by observations from the nearest reporting station. For the model run these data were aggregated to a three hour time interval. Cloudiness was calculated based on the ratio of top of the atmosphere clear sky radiation, corrected for zenith angle, to the measured shortwave radiation, thus giving a measure of the transmissivity of the atmosphere. A rain radar operated near the southern edge of the SMSA from May to September 1994 [*Schnur et al.*, 1997]. Precipitation estimates from this radar, with a spatial resolution of 2×2 km, were used for the pixels around the OBS and OJP sites in the south. For the OBS site in the north observations from the rain gage nearest the tower flux site were used. The precipitation from this gage, TB22, was used for all pixels near the SSA-OBS site in the north. Precipitation was applied

Table 3.4: Initial soil moisture content ($m^3/m^3$).

| Soil layer | SSA-OBS | NSA-OBS | SSA-OJP |
|---|---|---|---|
| Top | 0.30 | 0.30 | 0.10 |
| Middle | 0.30 | 0.30 | 0.10 |
| Bottom | 0.30 | 0.30 | 0.15 |

uniformly over the three hour time step. Although the duration of convective storms is often less than the model time step, this should not significantly affect the results of our point model runs. The hydrologic response to precipitation events is relatively slow in the BOREAS region, due to the modest relief and the absence of Hortonian type overland flow.

Model runs were made for the period May 21 to September 21, 1994, covering all three summer IFCs. Initial soil moisture contents were set equal to 0.30 for all three soil layers in the OBS sites (Table 3.4). This is equal to half the field capacity in the top layer, and slightly exceeds the field capacity in the lower layers. At the OJP sites the initial soil moisture content was set to 0.1 for the upper two layers, and to 0.15 for the bottom layer. These moisture contents are similar to soil moisture measurements made at the tower flux sites by *Cuenca et al.* [1997]. Soil moisture contents for the upper layer were set below field capacity, because the amount of precipitation during the weeks preceding the start of the model period was small in both the SMSA and the NMSA.

## *3.5 Results*

This section focuses on DHSVM's ability to simulate the different components of the energy balance,

$$R_{\text{net}} = H + LE + G + \Delta Q_{st}, \tag{3.8}$$

Table 3.5: Total precipitation and mean temperature at the tower sites during summer 1994.

| Tower flux site | Mean precipitation (mm) | | | | Temperature (°C) | | | |
|---|---|---|---|---|---|---|---|---|
| | IFC1 | IFC2 | IFC2 | period | IFC1 | IFC2 | IFC2 | period |
| SSA-OBS | 60.7 | 90.6 | 20.2 | 476.3 | 12.9 | 17.9 | 12.3 | 14.3 |
| SSA-OJP | 48.9 | 98.2 | 21.4 | 374.3 | 13.7 | 17.9 | 13.6 | 14.9 |
| NSA-OBS | 52.8 | 39.0 | 21.4 | 194.2 | 13.9 | 16.9 | 13.4 | 14.6 |

where $R_{net}$ is the net energy received by the surface, $H$ is the sensible heat flux, $LE$ is the latent heat flux, $G$ is the ground heat flux, and $\Delta Q_{st}$ is the change in ground heat storage. The sign convention we use here and in the following discussion is that $R_{net}$ is taken to be positive towards the surface, while all components on the right-hand side of (3.8) are taken to be positive away from the surface. The current implementation of DHSVM contains only a rudimentary algorithm to deal with the ground heat flux and the ground heat storage. Therefore, one objective of comparing observed and simulated latent and sensible heat fluxes is to gain a better indication of the importance of the soil thermal component during the summer months.

### *3.5.1 Southern Modeling Subarea*

In the SMSA the total amount of precipitation during the period May 21 to September 21, 1994, was 476 mm at SSA-OBS and 374 mm at SSA-OJP (Table 3.5). The period between the end of IFC1 and the start of IFC2 was particularly wet, with total precipitation amounts of 282 mm at SSA-OBS, and 214 mm at SSA-OJP. Temperatures varied only slightly between the tower sites, with the average temperature at the SSA-OBS site slightly lower than at the SSA-OJP site. During IFC2, temperatures were 4°–5°C higher than during IFC1 and IFC3. IFC3, which took place during the first few weeks of September 1994, was characterized by shorter day lengths and lower sun angles, leading to a sharp reduction in net available energy. The amount of observed net radiation during this period was only 50–60% of that observed during IFC1 and IFC2. In addition, precipitation amounts were much lower, with only about 20 mm of rainfall during the three week period.

Table 3.6: Observed and simulated net radiation.

| Site | Period | Number of observations | Mean observed ($W/m^2$) | Mean simulated* ($W/m^2$) | Mean simulated entire period ($W/m^2$) | Absolute bias ($W/m^2$) | Relative bias (%) | RMS error ($W/m^2$) |
|---|---|---|---|---|---|---|---|---|
| SSA-OBS | IFC1 | 192 | 144.1 | 150.5 | 150.5 | 6.4 | 4.5 | 27.5 |
| | IFC2 | 184 | 154.2 | 151.0 | 151.0 | -3.3 | -2.1 | 31.6 |
| | IFC3 | 153 | 88.2 | 93.1 | 96.1 | 4.8 | 5.5 | 27.1 |
| | May 21–Sept 21 | 950 | 132.0 | 132.9 | 132.1 | 1.0 | 0.7 | 30.3 |
| SSA-OJP | IFC1 | 183 | 133.4 | 131.7 | 130.2 | -1.7 | -1.3 | 50.5 |
| | IFC2 | 174 | 150.8 | 136.9 | 130.7 | -13.9 | -9.2 | 55.4 |
| | IFC3 | 138 | 87.1 | 86.5 | 83.6 | -0.7 | -0.8 | 38.0 |
| | May 21–Sept 21 | 888 | 125.0 | 119.1 | 114.7 | -5.9 | -4.7 | 50.5 |
| NSA-OBS | IFC1 | 131 | 148.9 | 145.7 | 145.7 | -3.2 | -2.2 | 45.7 |
| | IFC2 | 141 | 121.8 | 115.9 | 120.1 | -5.9 | -4.9 | 46.0 |
| | IFC3 | 148 | 82.7 | 82.3 | 85.7 | -0.3 | -0.4 | 59.6 |
| | May 21–Sept 21 | 827 | 122.0 | 118.3 | 118.6 | -3.7 | -3.1 | 46.9 |

* Mean simulated is calculated based on only those model time steps for which concurrent observations were available. Mean simulated entire period is based on all model time steps during the period.

*SSA-OBS*

The SSA-OBS site had the highest amount of precipitation of the three tower sites discussed. Average observed and simulated net radiation agreed to within 1% for the entire modeling period, and to within 5.5% for any of the three IFCs (Table 3.6). The modeled net radiation appeared to be slightly out of phase with the observations, increasing slightly more rapidly than the observed net radiation flux in the morning, and decreasing slightly more rapidly in the afternoon (Figure 3.2).

This phase difference was more pronounced in the average daily cycle of the sensible heat flux. Both modeled and observed fluxes peaked during the time interval from noon until 3PM, but the model underpredicted the observed flux in the morning and overpredicted in the afternoon (Figure 3.3). Average simulated peak values were about 10% lower than observed peak values. Over the entire modeling period, DHSVM underestimated the sensible heat flux by 4.0 $W/m^2$ or 6.2% (Table 3.7). The largest deviations between observed and modeled fluxes occurred during

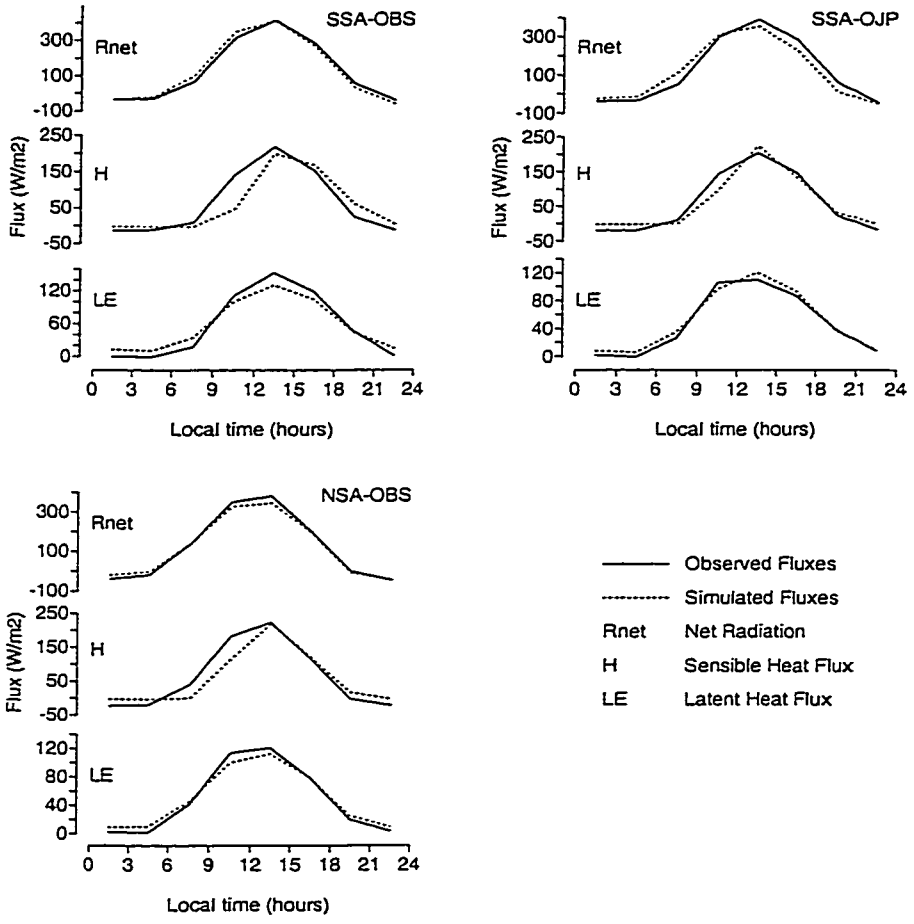


Figure 3.2: Average diurnal cycle of observed and simulated net radiation, sensible and latent fluxes for the three tower flux sites, May 21, 1994 – September 21, 1994.

IFC2, when the model underpredicted the average sensible heat by 8.9 W/m$^2$ or 11.7%. The latent heat flux did not demonstrate the phase shift exhibited by the net radiation and sensible heat flux, but the daily peak values were underpredicted by 22.3 W/m$^2$, or 14.5%. The night time latent heat flux during the period from 9PM until 6AM was overpredicted by about 12 W/m$^2$. Although the model bias was only 1.0% for the entire summer period, the bias was 11.2 W/m$^2$ or 21.6% during IFC1, and -7.3 W/m$^2$ or -10.0% during IFC2 (Table 3.8).

For each of these fluxes, and for each IFC the root mean square error (RMSE) was calculated

Table 3.7: Observed and simulated sensible heat.

| Site | Period | Number of observations | Mean observed ($W/m^2$) | Mean simulated* ($W/m^2$) | Mean simulated entire period ($W/m^2$) | Absolute bias ($W/m^2$) | Relative bias (%) | RMS error ($W/m^2$) |
|---|---|---|---|---|---|---|---|---|
| SSA-OBS | IFC1 | 189 | 76.2 | 71.8 | 70.7 | -4.4 | -5.8 | 47.7 |
| | IFC2 | 181 | 76.4 | 67.5 | 66.4 | -8.9 | -11.7 | 67.7 |
| | IFC3 | 150 | 36.7 | 41.0 | 45.5 | 4.3 | 11.6 | 53.4 |
| | May 21–Sept 21 | 931 | 65.1 | 61.1 | 60.3 | -4.0 | -6.2 | 58.4 |
| SSA-OJP | IFC1 | 172 | 69.4 | 73.7 | 68.1 | 4.2 | 6.1 | 45.3 |
| | IFC2 | 171 | 71.4 | 72.8 | 67.4 | 1.3 | 1.8 | 38.4 |
| | IFC3 | 129 | 52.4 | 47.9 | 42.6 | -4.6 | -8.7 | 43.9 |
| | May 21–Sept 21 | 865 | 62.6 | 63.8 | 59.6 | 1.2 | 1.9 | 41.1 |
| NSA-OBS | IFC1 | 128 | 84.0 | 84.1 | 78.7 | 0.2 | 0.2 | 47.3 |
| | IFC2 | 138 | 55.8 | 49.6 | 51.9 | -6.2 | -11.1 | 53.7 |
| | IFC3 | 120 | 30.7 | 35.1 | 37.8 | 4.4 | 14.2 | 48.9 |
| | May 21–Sept 21 | 699 | 62.7 | 59.1 | 56.3 | -3.6 | -5.7 | 52.1 |

* See note at bottom of Table 3.6.

Table 3.8: Observed and simulated latent heat.

| Site | Period | Number of observations | Mean observed ($W/m^2$) | Mean simulated* ($W/m^2$) | Mean simulated entire period ($W/m^2$) | Absolute bias ($W/m^2$) | Relative bias (%) | RMS error ($W/m^2$) |
|---|---|---|---|---|---|---|---|---|
| SSA-OBS | IFC1 | 189 | 52.0 | 63.2 | 62.6 | 11.2 | 21.6 | 31.2 |
| | IFC2 | 181 | 73.0 | 65.7 | 65.2 | -7.3 | -10.0 | 36.2 |
| | IFC3 | 150 | 40.3 | 41.6 | 40.1 | 1.3 | 3.3 | 20.4 |
| | May 21–Sept 21 | 931 | 56.9 | 57.5 | 56.2 | 0.6 | 1.0 | 29.6 |
| SSA-OJP | IFC1 | 172 | 47.9 | 58.5 | 56.0 | 10.5 | 22.0 | 44.5 |
| | IFC2 | 167 | 63.3 | 59.4 | 57.1 | -3.9 | -6.1 | 31.7 |
| | IFC3 | 129 | 32.4 | 39.4 | 37.9 | 6.9 | 21.3 | 27.1 |
| | May 21–Sept 21 | 865 | 49.0 | 52.6 | 50.3 | 3.6 | 7.4 | 33.6 |
| NSA-OBS | IFC1 | 131 | 52.0 | 47.9 | 53.0 | -4.2 | -8.0 | 30.6 |
| | IFC2 | 133 | 49.7 | 49.9 | 52.3 | 0.2 | 0.4 | 23.8 |
| | IFC3 | 119 | 35.5 | 42.2 | 39.7 | 6.7 | 18.8 | 24.6 |
| | May 21–Sept 21 | 620 | 48.4 | 49.5 | 48.9 | 1.1 | 2.2 | 26.0 |

* See note at bottom of Table 3.6.

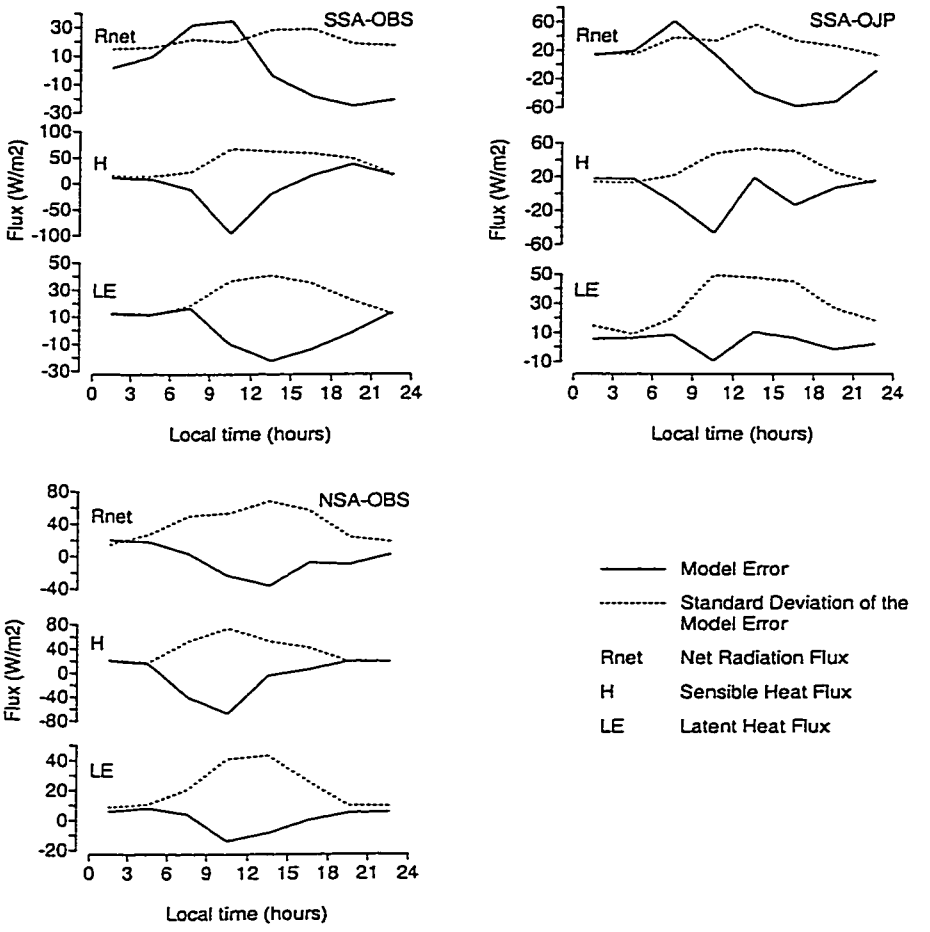


Figure 3.3: Mean diurnal cycle of the model error and the standard deviation of the model error, for net radiation, sensible and latent fluxes for the three tower flux sites, May 21 to September 21, 1994.

as

$$\mathrm{RMSE} = \frac{1}{n}\sqrt{\sum_{t=1}^{n}\left(x_{\mathrm{sim}}^{t} - x_{\mathrm{obs}}^{t}\right)^{2}}, \tag{3.9}$$

where $n$ is the total number of observations, $x_{\mathrm{obs}}^{t}$ the observed quantity for a certain time step $t$ , and $x_{\mathrm{sim}}^{t}$ the simulated quantity for the same time step. The phase shift between the modeled

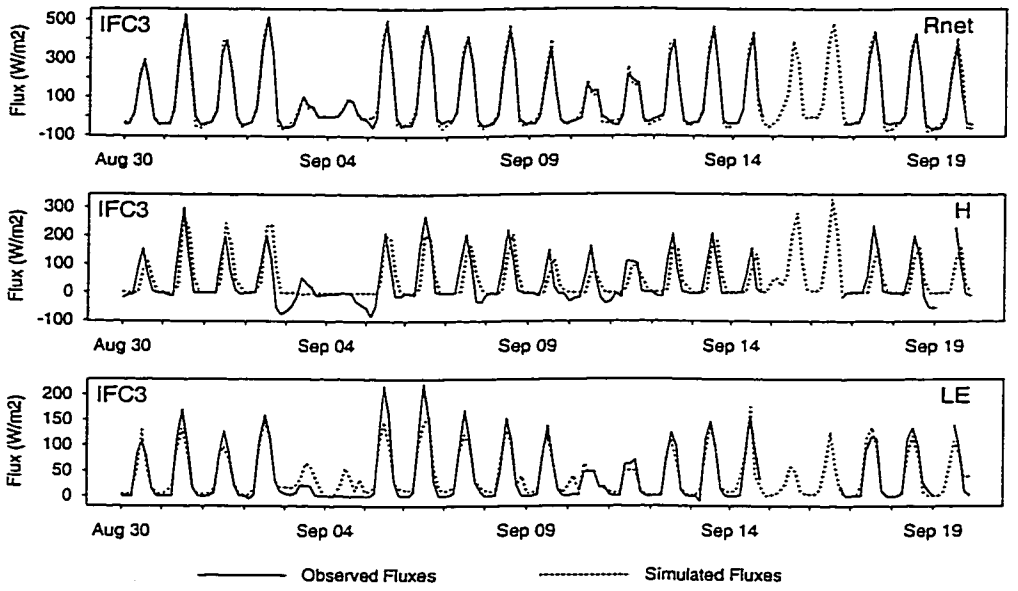


Figure 3.4: Observed and simulated net radiation, sensible and latent heat fluxes during for old black spruce in the southern study area.

and observed sensible heat fluxes resulted in relatively high RMS errors of 58.4 W/m$^2$ for the entire period, and 67.7 W/m$^2$ during IFC2. The corresponding errors for the latent heat flux were 29.6 W/m$^2$ and 36.2 W/m$^2$ respectively. The standard deviation of the model error reaches its highest values in late morning to early afternoon, when the fluxes are greatest (Figure 3.3). Modeled and observed fluxes for IFC3 are shown in Figure 3.4. Although the figure demonstrates that DHSVM follows the changes in the diurnal cycle of the observed fluxes quite well over a 3 week period, it also clearly shows the phase shift in the modeled and observed sensible heat flux.

*SSA-OJP*

Meteorological conditions at SSA-OJP were comparable to those at SSA-OBS, with the average temperature during IFC1 and IFC3 about 1°C higher. The total amount of precipitation during

the entire period was about 100 mm less than at SSA-OBS. The phase shift between the observed and modeled net radiation and sensible heat flux at SSA-OBS was also observed for SSA-OJP (Figure 3.2), although the phase shift for the sensible heat flux was much less pronounced. Model bias for the average net radiation was -5.9 W/m$^2$ or -4.7% for the entire period, and reached a maximum of -13.9 W/m$^2$ or -9.2% during IFC2. The modeled sensible heat flux matched the observed flux closely, with the maximum difference occurring during IFC3 when the model bias was -4.6 W/m$^2$ or -8.7%. Average daily peak values were overestimated by 20.5 W/m$^2$ or 10.0%. As in the case of SSA-OBS, the latent heat flux at SSA-OJP was overestimated during IFC1 and IFC3 and underestimated during IFC2, with an overall bias of 3.6 W/m$^2$ or 7.4%. No phase shift was apparent in the diurnal cycle, but nighttime evapotranspiration was overpredicted, as was the daily peak value. The diurnal cycle of the bias and standard deviation for the net radiation, sensible and latent heat flux are presented in Figure 3.3.

### *3.5.2 Northern Modeling Subarea*

The summer of 1994 was one of the driest on record for the NMSA [*Sellers et al.*, 1995], with total precipitation during the period May 21 to September 21, 1994, only 194.2 mm at NSA-OBS. Temperatures at the tower site were similar to those observed in the SMSA. Net incoming radiation was highest during IFC1, about 140 W/m$^2$, but declined during IFC2 and IFC3. The decrease in net radiation during IFC2 may partly be attributed to haziness caused by smoke from a number of large forest fires that burned in northern Canada during this period [*Sellers et al.*, 1995]. As in the SMSA, net radiation fell sharply during IFC3 as a result of lower sun angle (lower maxima), and shorter days (smaller totals).

#### *NSA-OBS*

The simulated net radiation again showed a slight phase shift compared to the observed radiation (Figure 3.2). The average simulated net radiation flux was 3.7 W/m$^2$ or 3.1% lower than the observed over the entire model period, with the largest deviation during IFC2, when the model bias

was -5.9 W/m$^2$ or 4.9% (Table 3.6). The sensible heat flux showed a more distinctive phase shift, albeit not as prominent as for SSA-OBS. The sensible heat flux was overpredicted during IFC1 and IFC3 and underpredicted during IFC2, with an overall bias for the entire period of -3.6 W/m$^2$ or -5.7% (Table 3.7). The RMS error ranged from 47.3 W/m$^2$ during IFC1 to 53.7 W/m$^2$ during IFC2 and was 52.1 W/m$^2$ for the model period. The simulated latent heat flux was close to the observed flux during IFC1 and IFC2, but was overestimated by 6.7 W/m$^2$ or 18.8% during IFC3. However, because evapotranspiration was low during IFC3 the model bias for the entire period was only 1.1 W/m$^2$ or 2.2%. As at the other sites, no phase shift was observed in the diurnal cycle of the latent heat flux, although nightly evaporation was overpredicted by about 7 W/m$^2$. The diurnal cycle of the bias and standard deviation of the model bias for the net radiation, sensible and latent heat flux are presented in Figure 3.3. During the period June 8–12, 1994, the second part of IFC1, the latent heat flux was underestimated by -22.7 W/m$^2$ or -38.1%. During this period the modeled soil moisture in the upper layer fell below the wilting point, thereby inhibiting further transpiration from this layer. In DHSVM the amount of transpiration from each layer is weighted by the root density in that layer. If the soil water content in a certain layer falls below the wilting point or freezes, no further transpiration is allowed from that layer. At the same time, DHSVM does not allow other soil layers to make up for this shortfall of soil moisture, even if they do not have any moisture limitations, because the weights for the root density are fixed.

### *3.6 Discussion*

A number of patterns can be discerned from the model simulations. First, DHSVM is well able to simulate the average sensible and latent heat fluxes during the entire model period. Average net radiation was predicted to within 5% for all three sites (Table 3.6), which is quite likely within the range of the measurement error. Average sensible heat fluxes were predicted to within 6.2% for SSA-OBS, 2.0% for SSA-OJP, and to within 5.8% for NSA-OBS (Table 3.7). Average latent heat fluxes were simulated to within 7.4% of the observed values for these three sites (Table 3.8). *Sellers et al.* [1995] noted that despite the abundance of water in the area, the evaporative flux was

low and fairly constant between 1 and 2 mm/day, even during warm and sunny days, suggesting a strong biophysical control on this flux.

To investigate the influence of environmental controls on the modeled latent heat flux, we executed two model runs for SSA-OBS in which we removed the soil temperature and the vapor pressure deficit factors from the calculation of the stomatal resistance. In the first run the factor $f_1(T_{soil})$ in (3.1) was set equal to 1 for all time steps, and in the second run the factor $f_2(\Delta e)$ was set to 1 for all time steps. As expected, the change in the biophysical controls on the stomatal resistance resulted in a large change in the relative contribution of the different components of the soil-vegetation system to the total evapotranspiration. In both cases the contribution of the vegetation, and in particular the overstory, increased significantly, with the largest increase resulting from the change in the soil temperature control. However, the total evapotranspiration was insensitive to the change in the biophysical controls. This is a direct result of the representation of the evapotranspiration process in DHSVM. As explained in Section 3.2, the soil evaporation is the minimum of the atmospheric demand and the amount the soil can deliver during a time step. For almost all time steps the amount the soil can deliver is larger than the atmospheric demand, and soil evaporation is therefore only modulated by the aerodynamic resistance and the amount of transpiration from the vegetation layers. Thus, if the evaporation from the vegetation is increased, the evaporation from the soil is decreased by a similar amount, and the net effect on the total evapotranspiration is negligible. Notwithstanding that the model was able to predict the total evapotranspiration reasonably well on average, this characterization does not appear to be physically realistic, and will likely be changed in the future.

The evaporative fraction, defined as $LE/(H+LE)$, was often less than one, corresponding to high Bowen ratios $(H/LE)$. Based on the average latent heat fluxes calculated, the evaporative flux at the tower sites ranged from 1.9 mm/day at SSA-OBS to 1.4 mm/day at NSA-OBS, in good agreement with the observations. DHSVM produced realistic simulations of the relative magnitudes of the latent heat fluxes, with the highest evaporative fluxes observed and modeled at SSA-OBS, followed by SSA-OJP, and NSA-OBS. Nonetheless, our expectations for DHSVM are

more demanding than simply reproducing seasonally averaged fluxes, for which a less detailed model might have provided adequate results. We also would like the model to capture the diurnal energy and water balance dynamics, and their changes during the season. In this respect, the model was less successful. For the two flux tower sites in the SMSA the latent heat flux during the first IFC was overpredicted, while the latent heat flux during the second IFC was underpredicted. As a result, the increase in modeled evaporation between IFC1 and IFC2 was relatively small, 2.5 $W/m^2$ for SSA-OBS and 0.9 $W/m^2$ for SSA-OJP, while the observed latent heat fluxes for the same time steps increased by 21.0 $W/m^2$ and 15.4 $W/m^2$ respectively. At the same time the observed sensible heat flux showed a small increase from IFC1 to IFC2 of 0.2 $W/m^2$ for SSA-OBS and 2.0 $W/m^2$ for SSA-OJP, while the modeled sensible heat flux showed a small decrease of 4.3 $W/m^2$ and 0.7 $W/m^2$ respectively.

Overprediction of the latent heat flux during IFC1 may have been due in part to inaccurate initial conditions, i.e., too much moisture in the soil profile. We suspect that the failure of soil temperature controls on transpiration to be reflected in total evapotranspiration, as explained above, probably played a role as well. In any event, the underprediction of the latent heat flux during IFC2 was more revealing. As a result of the large amount of precipitation between IFC1 and IFC2 moisture stress was practically non-existent. In addition air temperatures were 4°–5°C higher than during IFC1. Despite this, modeled latent heat flux were only slightly higher.

It appeared that DHSVM underpredicted the amount of evapotranspiration on days with high humidity and low incoming shortwave radiation. These tend to be days with precipitation, or days following a rainstorm. This may suggest that either the model does not allow for sufficient canopy interception storage that can evaporate at the potential rate, or that the feedback of the light level on the stomatal resistance given by (3.4) is too severe. Either problem can be fairly easily remedied; by allowing for more interception storage, or changing the parameters that govern the influence of the light level on the stomatal resistance, respectively. More model testing, e.g., using additional moisture and energy flux data collected during summer, 1996 (not yet available[1]), and/or by using

[1]This was true at the time of writing of the original article in 1996/97. The complete BOREAS data set was made

additional tower sites, is expected to provide insight into the nature of model changes that will be required.

A feature of the results that may prove to be more indicative of a misrepresentation of physical processes is the phase shift in the diurnal cycle in the simulation of the net radiation and the sensible heat flux. This phase shift is most pronounced for the black spruce sites. These sites were simulated using the same soil profiles, consisting of a 0.2 m organic soil layer near the surface with a high porosity. The phase sift in the sensible heat flux for the jack pine site, which has a well-drained, sandy soil, was much less prominent. DHSVM simulates the change in soil heat storage only in the top 0.1 m, and assumes that the temperature of this layer is equal to the radiant surface temperature [*Arola and Lettenmaier*, 1996]. The soil heat capacity of this layer is calculated as a weighted average of the heat capacities of the constituent elements, i.e. the soil matrix and the soil moisture. Since water has a large thermal capacity, the heat capacity of this top layer increases rapidly with increasing soil moisture. At the SSA-OBS site, where the phase shift is most prominent, the simulated and observed fluxes start to become out of phase in the middle of June when the soil moisture content in the top soil layer reaches field capacity. The thermal capacity of this layer then becomes so large that the soil only heats up slowly in the morning and cools down slowly in the evening. As a result the sensible heat flux is underpredicted in the morning and overpredicted in the evening. Because soil surface temperatures are too low in the morning, the outgoing longwave radiation is underpredicted, with the result that net radiation is overpredicted. The reverse is true in the late afternoon. The reason we focus on the change in soil heat storage is that the modeled soil heat storage term is much larger than the modeled ground heat flux during the morning hours when the phase shift is most prominent. However, comparison of the modeled ground heat flux with some measured ground heat fluxes showed that the modeled ground heat flux had a larger amplitude in the diurnal cycle than observed. Since the latent heat flux is calculated independent of the surface radiant temperature and the sensible heat flux, no phase shift is noticeable between the modeled and observed fluxes. Here the only solution appears

---

available on CD-ROM in spring 2000, see *Newcomer et al.* [2000].

Table 3.9: Breakdown of the simulated evaporative flux in individual components, May 21, 1994 – September 21, 1994.

| Site | Overstory Transpiration | Understory Transpiration | Evaporation from Interception Storage | | Soil Evaporation | Total |
|---|---|---|---|---|---|---|
| | | | Overstory | Understory | | |
| | (mm) | (mm) | (mm) | (mm) | (mm) | (mm) |
| SSA-OBS | 72.9 | 26.1 | 28.6 | 9.2 | 106.4 | 243.2 |
| SSA-OJP | 74.8 | 19.0 | 21.3 | 6.6 | 96.3 | 218.0 |
| NSA-OBS | 56.5 | 35.8 | 10.9 | 5.2 | 103.4 | 211.8 |

to be a more complete description of the soil thermal balance, including both the soil heat flux and the change in soil heat storage. It is anticipated that this adaptation will prove to be even more crucial when DHSVM is run over an entire hydrological year, including snow accumulation and soil freeze in the fall, and the snow melt and soil thaw in the spring.

Although DHSVM was able to simulate the total latent heat flux at the tower sites quite accurately, further investigation is needed to determine how well DHSVM partitions the evaporative flux in the individual components. Table 3.9 shows the accumulated totals of the individual components for the entire modeling period. As expected, overstory transpiration is in all cases more important than transpiration from the understory, and the evaporation from interception storage is strongly dependent on the amount of precipitation. Thus evaporation from interception storage accounted for 15.5% and 12.8% of total evaporation for SSA-OBS and SSA-OJP, respectively, while it accounted for only 7.6% of total evaporation at NSA-OBS.

However, direct evaporation from the soil appears to play a far greater role than expected in our model runs, accounting for 44% of total evapotranspiration in the south, and about 50% in the north. This is different from the conclusion reached by *Sellers et al.* [1995] that "most of the incoming solar radiation is intercepted by the vegetation canopies rather than by the moist underlying moss/soil surface, which generally makes only a small contribution to the total sensible and latent heat fluxes". *Haddeland and Lettenmaier* [1995], based on field observations near the NSA-OBS site, reported that the moss fraction of the daily total evaporative flux ranged from

less than 10% to almost 70%, during the period September 2–13, 1994. Typical contributions ranged from 20% to 25%. For the same period the modeled contribution of the soil evaporation to the daily evaporative flux varied from 30% to 70%, with typical values between 40% and 50%. The total amount of modeled evapotranspiration for this 12 day period was 14.8 mm, with 48.9% directly from the soil, 43.8% from the under- and overstory combined, and 7.2% from interception storage. We hope to explore this issue further when more final data sets for the tower flux sites become available which include latent heat flux measurements at different heights in the canopy. If the observations support a relatively high contribution of direct soil evaporation, this could help explain the near-constant observed latent heat fluxes during the 1994 season. When transpiration shuts down during bright sunny days as a result of biophysical feedback mechanisms such as a vapor pressure deficit control, direct soil evaporation may be able to supply most of the evaporative flux. This is the pattern that was observed in our model simulations. Since water availability is generally not limiting in the boreal forest areas, direct evaporation from the soil could potentially be an important component of the latent heat flux.

### *3.7 Conclusions*

BOREAS offers a unique opportunity for the modeling community to compare model simulations with observations of energy and moisture fluxes in the boreal forest. Few existing data offer comparable detail, not only in spatial and temporal resolution, but also in the amount of auxiliary data gathered, such as soil and biophysical characteristics. At this stage, much of the data from the tower flux sites is still in preliminary form[2], and thus caution is needed when interpreting the results, and any conclusions must be viewed as preliminary.

This first evaluation of DHSVM's performance in the boreal forest ecosystem indicates several strengths and weaknesses. Average seasonal sensible and latent heat fluxes were simulated accurately, and the mean diurnal cycle in the latent heat flux closely matched the observations at

[2]This was true at the time of writing of the original article in 1996/97. The complete BOREAS data set was made available on CD-ROM in spring 2000, see *Newcomer et al.* [2000].

the two black spruce, and one jack pine sites. However a phase shift was observed in the simulation of the sensible heat flux and net radiation. This timing problem was attributed to the soil heat algorithm, which is probably too simplistic. Because our ultimate goal is to run the model in fully distributed mode for an entire hydrologic year, an improved soil thermal model is essential. Another point that requires more study is the model representation of evapotranspiration. The model atmospheric demand was always smaller than the potential soil delivery rate, and the result of which was that the soil always evaporated at a modified (accounting for transpiration and canopy evaporation) potential rate. As a result, the total model evapotranspiration was insensitive to biophysical controls, even though these controls strongly influenced the partitioning of the evaporative flux into its constituent components. In addition, the soil evaporation appears to be overestimated, although this preliminary conclusion requires confirmation using more complete data sets at the tower flux sites and the results of summer 1996 field work.

Chapter 4

# A SIMPLIFIED APPROACH FOR PREDICTING SHORTWAVE RADIATION TRANSFER THROUGH BOREAL FOREST CANOPIES

This chapter has appeared as B. Nijssen and D. P. Lettenmaier, A simplified approach for predicting shortwave radiation transfer through boreal forest canopies, *J. Geophys. Res.*, *104*, 27,859–27,868, 1999.

## *4.1 Introduction*

Approximately one fourth of the global land surface is covered by forests [*Kirschbaum et al.*, 1996b], which are disproportionally important to the global and regional balances of water, energy, and carbon. Therefore it is especially important that the land-atmosphere transfer schemes incorporated in surface hydrological models accurately predict the effects of forest canopies on energy and moisture fluxes. Modeling efforts have featured prominently among land surface change studies because of (1) logistical impracticalities in conducting large-scale perturbation experiments (e.g., removing the boreal forest [*Bonan et al.*, 1992]), (2) the need for evaluations of potential effects of climate and land surface change [e.g., *Kirschbaum et al.*, 1996b], (3) the controlled environment offered by models (e.g., forest harvest effect studies [*Storck et al.*, 1998]), and (4) the small cost of model simulations compared to field studies. However, the effectiveness of models as a tool for land surface change studies depends largely on whether the sensitivities to changes in land surface characteristics observed in the prototype are mirrored by the sensitivities that the model exhibits to equivalent changes in input parameters. If semi-empirical methods are used to study vegetation change effects, it can be difficult to determine how changes in model parameters relate to changes in land surface characteristics. The use of physically based representations in simulation models facilitates this process, to the extent that model parameters can be

related directly to measurable land surface characteristics.

Notwithstanding the desirability of greater physical realism in land surface models, it must be recognized that the quality and quantity of data available to describe land surface processes is limited. A detailed physical model whose parameters can only be obtained at great expense will be of limited use, other than in highly focused research investigations. Input parameters that cannot be easily obtained often become nothing more than tuning or calibration parameters, whose ultimate values bear little connection to the physical characteristics they represent [*Beven*, 1989; *Grayson et al.*, 1992]. Thus the goal is to identify physically realistic models that can display the appropriate sensitivities, while at the same time only employing those parameters that can be obtained routinely. The quest for simple models obviously means that not all processes can be resolved to great detail, but for many applications use of a simple model may be more intellectually honest than use of a complicated model whose parameters are only poorly known [*Grayson et al.*, 1992].

Particularly for regional or smaller-scale studies there is great interest in so-called spatially distributed models which allow land surface characteristics to vary spatially. These models typically operate at resolutions similar to those of high-resolution digital elevation models (typically 30 m-1000 m), and land surface processes often have to be calculated for tens or hundreds of thousands of points [*Storck et al.*, 1998]. Even with the rapid increase in computer processor speeds, the sheer volume of calculations remains a concern, and computational simplicity is an additional model requirement. The purpose of this paper is to develop a simple radiative canopy transfer model that predicts the shortwave radiative flux to the soil or snowpack under a boreal forest canopy, based on radiation measurements above the canopy and commonly available canopy characteristics.

### *4.2 Canopy Radiative Transfer*

A variety of canopy radiation models has been developed to model the distribution of shortwave radiation in and below the canopy as a function of above-canopy shortwave radiation [e.g., *Dick-*

*inson*, 1983; *Ni et al.*, 1997; *Roujean*, 1996; *Sellers*, 1985]. These models range from complex representations of the optical properties of individual canopy elements to simple models that employ bulk canopy parameterizations.

Accounting for the effects of both the optical characteristics of canopy elements and the canopy structure on radiation transfer is problematic for two reasons. First, the complex three-dimensional structure of plant canopies makes radiation modeling difficult, even though the individual processes of shading, absorption, reflection, and transmission in plant canopies are fairly well understood. Second, even if an attempt is made to model these processes explicitly, as in the GORT model [*Ni et al.*, 1997], it is difficult to acquire the required canopy information.

Most simple canopy radiation models use some variation of Beer's law, in which the effects of canopy structure are not explicitly represented. According to Beer's law, irradiance decreases exponentially with increasing path length through the absorbing medium [*Monteith and Unsworth*, 1990]. *Larsen and Kershaw* [1996] have shown that Beer's-law-type models are inadequate to model the within-canopy distribution of light interception but that they can be adequate to predict the average light conditions below the canopy. In such models the canopy is represented by one or more plane-parallel, scattering and absorbing layers with uniform properties in the horizontal plane. Vegetation elements are assumed to be randomly distributed in space. In most applications, two parameters are used to account for inhomogeneities in the spatial distribution of canopy cover. Within a tree stand, inhomogeneities are accounted for by a clumping factor. The leaf area index for a vegetation stand is multiplied by the clumping factor to derive an effective leaf area index value. If leaves are randomly distributed the clumping factor equals unity but is smaller than unity for canopies in which the leaf distribution is nonrandom [*Chen et al.*, 1997a]. Open spaces between tree stands are accounted for by a canopy cover fraction. The vegetation is assumed to be randomly distributed within this fraction, and the remaining area is assumed to be bare. The length scale of the bare patches is assumed to be large in relation to the size of individual plants.

For application in plant canopies bulk coefficients are used and Beer's law is written as

$$R_s^u = R_s^o e^{-f}, \tag{4.1}$$

where $R_s^u$ is the downward shortwave radiation below the plant canopy, $R_s^o$ is the downward shortwave radiation above the canopy, and $f$ is a bulk canopy optical thickness dependent on leaf area index and other variables such as solar zenith angle and canopy structure [*Ross*, 1975]. The models differ in the way they prescribe $f$ [*Chen et al.*, 1997a; *Pomeroy and Dion*, 1996; *Yamazaki et al.*, 1992].

The canopy radiation model used in the distributed hydrology-soil-vegetation model (DHSVM) [*Wigmosta et al.*, 1994] is typical of this approach. DHSVM uses a two layer canopy, in which transmission through the top layer is modeled on the basis of Beer's law. A fractional ground cover $F$ can be specified for the overstory or top canopy layer, similar to the one suggested by *Sellers* [1985] and *Jones* [1992]. The transmittance of shortwave radiation is specified by a Beer's law relationship, with

$$f = -kL, \tag{4.2}$$

where $k$ is a constant, canopy-dependent attenuation coefficient, and $L$ is the effective leaf area index of the overstory.

In addition to the assumptions inherent to all radiative transfer approaches, a number of simplifying assumptions are implicit in this radiation model, particularly the following:

1. Shortwave radiation in the visible and infrared ranges of the spectrum is not treated separately. Consequently, the albedos and transmission coefficients are bulk coefficients that specify an effective reflection and transmission for the entire shortwave region.

2. Above-canopy direct and diffuse radiation are transmitted equally efficiently.

3. Multiple scattering by the canopy, which is important in the infrared range of the shortwave spectrum, is not explicitly represented.

4. Other than the leaf area index, the only canopy-dependent parameter affecting transmission is the attenuation coefficient $k$. The attenuation coefficient accounts for all canopy structural properties other than the leaf area index. Unlike many of the other canopy radiative transfer models, there is no dependence of $k$ on the path length through the canopy, which for direct radiation varies with the cosine of the solar zenith angle.

The major advantage of this formulation compared with more complex formulations is that the number of canopy parameters is limited, and leaf area index is routinely available for many species. The major disadvantage is that the attenuation coefficient, which accounts for all canopy structural effects, is not known a priori. Consequently, the attenuation coefficient becomes a calibration parameter for many real-world applications. Because few below-canopy radiation measurements are available, this calibration has to be performed indirectly, for example, by evaluating snowmelt rates under the canopy as compared to snowmelt rates in the open. Because the calibration is performed indirectly, the difference between the final, calibrated attenuation values can be large, even for similar canopies. In addition, a fixed attenuation coefficient is unable to respond to environmental changes, such as the amount of direct and diffuse radiation and the solar zenith angle.

Replacing the simple formulation currently used with any of the more complex canopy radiation models does not necessarily solve the problem. Replacement of the single, constant canopy attenuation coefficient by a more physically realistic formulation is only desirable if the new model parameters can either be obtained from routinely measured quantities or if the physically realistic range of the new parameters is better defined.

For most land-atmosphere transfer schemes and spatially distributed hydrological models, the main quantity of interest is the total amount of shortwave radiation incident on the soil or snow surface and the total amount of radiation absorbed by the canopy. The main canopy characteristic that is routinely available is the effective leaf area index.

## 4.3 Model Formulation

A simple canopy radiative transfer model is proposed, which is based on Beer's law, but which accounts explicitly for penetration, multiple scattering, and multiple reflections between the ground and the canopy. The algorithm treats direct and diffuse above-canopy radiation separately and models transmission of direct radiation as a function of solar zenith angle.

### *4.3.1 Penetration*

Following *Ross* [1975], we assume that the direct radiation penetrates the canopy according to

$$\tau_b = e^{-\frac{LG(\theta)}{\cos\theta}}, \tag{4.3}$$

where $\tau_b$ is the penetration function for direct radiation, $\theta$ is the solar zenith angle, and $G(\theta)$ is the average projected leaf area in the direction $\theta$. For many plant canopies, $G(\theta)$ can be approximated by a linear equation of the form

$$G(\theta) = a + b\cos\theta, \tag{4.4}$$

where $a$ and $b$ are functions of the leaf angle distribution, with $a > 0$ [*Goudriaan*, 1977; *Ross*, 1975; *Sellers*, 1985].

For a horizontal, plane surface the penetration function for diffuse radiation ($\tau_d$) can be obtained by integrating the component of $\tau_b$ normal to the surface over the upper hemisphere, [i.e., *Ross*, 1975, equation (20), p. 20]

$$\tau_d(L) = \frac{R_{dp}(L)}{R^o_{sd}} = \frac{1}{R^o_{sd}} \int_{2\pi} d(n)\tau_b(L,n)\cos\theta d\Omega, \tag{4.5}$$

where $R_{dp}(L)$ is the amount of diffuse radiation that has penetrated to a depth $L$ in the canopy, $R^o_{sd}$is the downward diffuse shortwave radiation above the canopy, $d(n)$ is the radiance of the sky in the direction $n$, and $d\Omega$ is the solid angle $\sin\theta d\theta d\phi$.

Combining (4.3), (4.4), and (4.5), under the assumption that the diffuse radiance of the sky is constant, leads to

$$\begin{aligned}\tau_d(L) &= \frac{1}{\pi}\int_{2\pi}\tau_b(L,n)\cos\theta d\Omega \\ &= 2\int_0^{\pi/2} e^{-\frac{G(\theta)L}{\cos\theta}}\cos\theta\sin\theta d\theta \\ &= 2e^{-bL}\int_0^{\pi/2} e^{-\frac{aL}{\cos\theta}}\cos\theta\sin\theta d\theta. \end{aligned} \tag{4.6}$$

Now, let $x = \cos\theta$, then $dx = d(\cos\theta) = -\sin\theta d\theta$, and the integration limits change to 0 and 1. Thus

$$\begin{aligned}\tau_d(L) &= 2e^{-bL}\int_0^{\pi/2} e^{-\frac{aL}{\cos\theta}}\cos\theta\sin\theta d\theta \\ &= 2e^{-bL}\int_1^0 -e^{-\frac{aL}{x}}x dx = 2e^{-bL}\int_0^1 x e^{-\frac{aL}{x}}dx \\ &= e^{-bL} \\ &\quad \left[\left\{(1-aL)e^{-aL} + (aL)^2 E_i(1,aL)\right\} - \right. \\ &\quad \left. \lim_{x\downarrow 0}\left\{\left(x^2 - aLx\right)e^{\frac{-aL}{x}} + (aL)^2 E_i\left(1,\frac{aL}{x}\right)\right\}\right], \end{aligned} \tag{4.7}$$

where $E_i(n,x)$ with $n$ a nonnegative integer is the exponential integral, defined as

$$E_i(n,x) = \int_1^\infty \frac{e^{-xt}}{t^n}dt. \tag{4.8}$$

For $a > 0$, the last term of (4.7) vanishes, resulting in

$$\tau_d(L) = e^{-bL}\left[(1-aL)e^{-aL} + (aL)^2 E_i(1,aL)\right]. \tag{4.9}$$

For a random or spherical leaf distribution, $a = \frac{1}{2}$, and $b = 0$, and thus

$$\tau_d(L) = \left(1 - \frac{L}{2}\right) e^{-\frac{L}{2}} + \frac{L^2}{4} E_i\left(1, \frac{L}{2}\right). \tag{4.10}$$

The total penetration function for shortwave radiation ($\tau_p$), for a random leaf angle distribution without accounting for scattering and multiple reflections, is found by combining (4.3), (4.4), and (4.10), resulting in

$$\begin{aligned} \tau_p &= \tau_b \frac{R^o_{sb}}{R^o_s} + \tau_d \frac{R^o_{sd}}{R^o_s} \\ &= e^{\frac{-L}{2\cos\theta}} \frac{R^o_{sb}}{R^o_s} + \left\{ \left(1 - \frac{L}{2}\right) e^{\frac{-L}{2}} + \left(\frac{L}{2}\right)^2 E_i\left(1, \frac{L}{2}\right) \right\} \frac{R^o_{sd}}{R^o_s}, \end{aligned} \tag{4.11}$$

where $R^o_{sb}$ is the downward direct shortwave radiation above the canopy. A random leaf angle distribution is often the first assumption if no additional information about the canopy structure is available, and appears to be a good first assumption for many plant canopies [*Chen et al.*, 1997a; *Sellers et al.*, 1996].

### *4.3.2 Scattering*

The assumption that multiple scattering is minimal is likely to be valid for transmission of photosynthetically active radiation (PAR) through the canopy, because most of the radiation in this part of the spectrum is absorbed by the leaves [*Ni et al.*, 1997]. Multiple scattering in the infrared region is substantial, and this effect cannot be neglected when considering the transmittance of total shortwave radiation through a vegetation canopy [*Ni et al.*, 1997]. Traditionally, more complex models, such as two-stream approximations, are used to account for multiple scattering. However, for deep canopies and assuming isotropic scattering and exponential decrease of transmission with depth, *Monteith and Unsworth* [1990] note that the ratio of attenuation coefficients for total shortwave radiation and PAR is approximately $\sqrt{a_{\text{total}}/a_{\text{PAR}}}$, where $a_{\text{total}}$ is the absorption over the

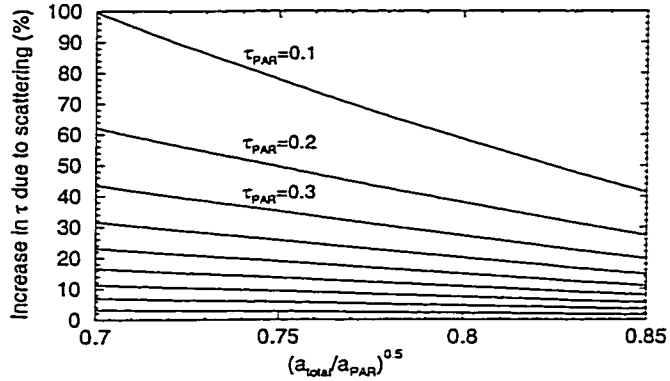


Figure 4.1: Increase in transmittance due to multiple scattering in the canopy according to equation (4.12) as a function of $\sqrt{(a_{\text{total}}/a_{\text{PAR}})}$. The curves from top to bottom are for $\tau_{\text{PAR}}$ values from 0.1 to 0.9.

entire shortwave region, and $a_{\text{PAR}}$ is the absorption in the PAR region of the spectrum. Consequently, under the above assumptions, the transmission of total radiation $\tau_{\text{total}}$ can be expressed as a function of the transmission for PAR radiation $\tau_{\text{PAR}}$ as

$$\tau_{\text{total}} = \tau_{\text{PAR}}^{\sqrt{a_{\text{total}}/a_{\text{PAR}}}}. \tag{4.12}$$

Because multiple scattering is small in the PAR region of the spectrum, (4.11) can be used as an estimator for $\tau_{\text{PAR}}$, and (4.12) can be used to account for the effects of multiple scattering. In the following, $\tau_{\text{PAR}}$ is taken to be equal to $\tau_p$, calculated according to (4.11).

As *Monteith and Unsworth* [1990] point out, the quantity $\sqrt{a_{\text{total}}/a_{\text{PAR}}}$ is relatively constant for a wide range of canopy types and generally falls in the range 0.70 to 0.85. Thus even though $a_{\text{total}}$ and $a_{\text{PAR}}$ exhibit some variation with leaf age and location of the leaf in the canopy [*Middleton and Walter-Shea*, 1995], the total quantity varies little, and a constant, vegetation-dependent value of $\sqrt{a_{\text{total}}/a_{\text{PAR}}}$ is used. Figure 4.1 shows the increase in transmittance due to scattering as a function of $\sqrt{a_{\text{total}}/a_{\text{PAR}}}$ for $\tau_{\text{PAR}}$ from 0.1 to 0.9. The increase in transmittance because of scattering increases with decreasing $\tau_{\text{PAR}}$ and $\sqrt{a_{\text{total}}/a_{\text{PAR}}}$. For small values of $\tau_{\text{PAR}}$, implying

a dense canopy, multiple scattering can account for almost half the radiation reaching the forest floor. For open canopies, with values of $\tau_{PAR}$ close to unity, the contribution of multiple scattering is small.

### *4.3.3 Multiple Reflections*

In the DHSVM radiation model, *Wigmosta et al.* [1994] account for single reflections between the forest canopy and the forest floor or understory. However, it is straightforward to account for multiple reflections.

Shortwave radiation above the canopy ($R_s^o$) is separated into a direct component ($R_{sb}^o$) and a diffuse component ($R_{sd}^o$). Part of this incoming radiation is directly reflected back to the atmosphere ($\alpha_o R_s^o$, with $\alpha_o$ the bulk canopy albedo). The direct and diffuse radiative fluxes are transmitted through the overstory according to the transmittances $\tau_b$ and $\tau_d$. The total transmitted radiation ($\tau_{\text{total}} R_s^o$) is treated entirely as diffuse radiation when it is reflected from the ground surface, with the assumption that the reflected radiation is isotropic. Part of the radiation reflected by the soil or understory ($\alpha_u \tau_{\text{total}} R_s^o$, with $\alpha_u$ the bulk ground or understory albedo) is transmitted through the canopy and returns to the atmosphere ($\alpha_u \tau_d \tau_{\text{total}} R_s^o$), while another part is reflected to the soil ($\alpha_o \alpha_u \tau_{\text{total}} R_s^o$). The same process then repeats, and the total radiation incident on the ground surface ($R_s^u$) can be determined by summing the individual terms, resulting in

$$\begin{aligned} R_s^u &= \tau_{\text{total}} R_s^o \left(1 + \alpha_o \alpha_u + {\alpha_o}^2 {\alpha_u}^2 + \cdots + {\alpha_o}^n {\alpha_u}^n + \cdots\right) \\ &= \tau_{\text{total}} R_s^o \sum_{i=0}^{\infty} (\alpha_o \alpha_u)^i = \frac{\tau_{\text{total}}}{1 - \alpha_o \alpha_u} R_s^o \end{aligned} \tag{4.13}$$

The last step can be made since both $\alpha_o$ and $\alpha_u$ are by definition less than unity.

Note that the albedos $\alpha_o$ and $\alpha_u$ do not represent single-leaf albedos but rather bulk albedos of the overstory and understory/ground surface for the entire shortwave region. Bulk canopy albedos will generally have much smaller values than single-leaf albedos due to shading within the canopy. One assumption implicit in the above model is that the spectral composition of the incident radiation does not change as it passes through the canopy. This assumption allows the same albedo

values for incoming and reflected radiation. The spectral composition of the scattered radiation depends strongly on the optical properties of the leaves and the amount of scattering. Because most of the PAR is absorbed along its path through the canopy, radiation in the green and near-infrared part of the spectrum is enhanced [*Ross*, 1975]. Nonetheless, this spectral shift is neglected in our simple model.

### *4.3.4 Application of Method*

Equations (4.11), (4.12), and (4.13) constitute the algorithm to predict shortwave radiation below the canopy, given diffuse and direct shortwave radiation above the canopy. Application of the method consists of the following five steps:

1. Calculate the transmission coefficient for direct radiation ($\tau_b$) according to (4.3) and (4.4).

2. Calculate the transmission coefficient for diffuse radiation ($\tau_d$) using (4.9) or (4.10), depending on the leaf angle distribution function.

3. Combine the two coefficients weighted by the amount of diffuse and direct radiation according to (4.11), resulting in $\tau_p$.

4. Apply (4.12) to adjust $\tau_p$ for scattering, resulting in $\tau_{\text{total}}$.

5. Finally, apply a correction for reflections between the ground or the understory and the overstory, and multiply by the total above canopy radiation according to (4.13).

The model requires as input an estimate of above-canopy diffuse and direct radiation. Separation of total shortwave radiation into diffuse and direct components is not routinely available. Two methods to separate total above-canopy shortwave radiation into diffuse and direct components are discussed in section 4.4 below.

## 4.4 Model Application

To evaluate model performance, two applications are discussed in detail. First, model results are compared with predictions of the GORT (Geometric-Optical and Radiative Transfer) model [*Ni et al.*, 1997], which uses a more detailed representation of the transfer of shortwave radiation through the canopy. Second, the model is used to simulate the below-canopy radiation at two sites, where below-canopy radiation was measured. Both sites were part of the Boreal Ecosystem-Atmosphere Study (BOREAS). The first site is a mature jack pine site in the BOREAS southern study area (SSA), northeast of Prince Albert, Saskatchewan. The second site is a mature black spruce site in the same study area. For a detailed description of the BOREAS project and site characteristics, the reader is referred to *Sellers et al.* [1995] and *Sellers et al.* [1997]. *Baldocchi et al.* [1997] provide more specific information about the mature jack pine site, and *Jarvis et al.* [1997] provide details about the mature black spruce site.

### 4.4.1 Comparison With GORT

The GORT model [*Ni et al.*, 1997] estimates the direct and diffuse radiation that passes through gaps in the canopy using a geometric-optic approach and estimates the solar radiation scattered by the canopy elements and the understory using a radiative transfer approach. As *Pomeroy and Dion* [1996] point out, this approach is very successful in demonstrating the effects of canopy structure on radiation transmission but is not readily applicable using normal forest inventory measures.

*Ni et al.* [1997] simulate the sum of diffuse and direct transmittance and the total shortwave transmittance as a function of solar zenith angle for mature jack pine, using the GORT model. Their simulations were made for clear days during which they assumed that the direct radiation above the canopy decreases with increasing solar zenith angle according to

$$R_{sb}^{o} = \frac{\cos\theta}{\cos\theta + 0.09} R_{s}^{o}. \tag{4.14}$$

Figure 4.2 compares the results from the GORT model and our simple model for the mature jack

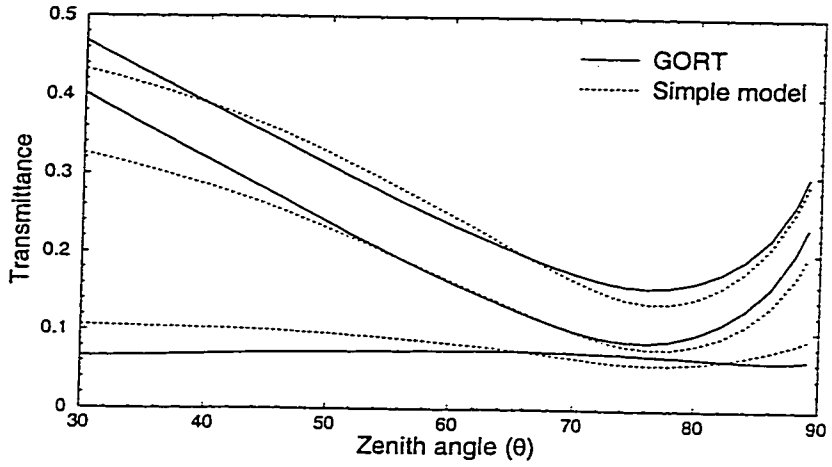


Figure 4.2: Transmittance as a function of solar zenith angle at the mature jack pine site as simulated by GORT and the simple model. The lines are based on equations (4.11), (4.12), and (4.14) and account for multiple reflections according to equation (4.13). Canopy characteristics are from *Ni et al.* [1997]. The top lines represent total transmittance corrected for multiple scattering $\tau_{\text{total}}/(1-\alpha_o\alpha_u)$, the middle lines represent the transmittance for direct and diffuse radiation ($\tau_{\text{PAR}}$), and the bottom lines represent the transmittance due to multiple scattering and reflections.

pine site. The same canopy parameters were used as in *Ni et al.* [1997] ($L = 1.89$, $\sqrt{a_{\text{total}}/a_{\text{PAR}}} = 0.810$). Bulk canopy and understory albedos were taken from *Betts and Ball* [1997], with $\alpha_o$ = 0.090 (mean summer albedo for the mature jack pine site) and $\alpha_u$ = 0.75 (mean winter albedo for a snow-covered grassland). The mean observed summer albedo is used for the overstory in summer and winter, since *Pomeroy and Dion* [1996] found no appreciable influence of intercepted snow in the boreal jack pine canopy on the canopy albedo. The GORT curves in Figure 4.2 show the incident radiation less than 4 m above the forest floor. The zenith angles in Figure 4.2 are constrained to angles greater than 30° (zenith angles at the mature jack pine site are never smaller than 30.4°).

Comparison of the total shortwave transmission curves in Figure 4.2 shows a similar shape for both curves, with a maximum transmittance for $\theta = 30°$ and a minimum near $\theta = 76°$. The transmittance increases for zenith angles larger than $\theta = 76°$, because almost all the radiation is

diffuse, and diffuse transmittance is larger than direct transmittance for large zenith angles (for a random canopy, with $L = 1.89$ in (4.3) and (4.10), $\tau_d > \tau_b$ for $\theta > 49.1°$). The location of the minimum is largely a function of the shape of (4.14). For a solar zenith angle of 30° the total shortwave transmittance is 0.468 for GORT and 0.433 for the simple model, while the minimum at $\theta = 76°$ is 0.157 for GORT and 0.137 for the simple model.

The components that make up the total shortwave transmittance show somewhat different patterns. The sum of direct and diffuse transmittance agrees very well for the two models for zenith angles greater than about 50°, with a minimum at $\theta = 76°$ of 0.087 for GORT and 0.079 for the simple models. For smaller zenith angles the simple model predicts smaller transmittances than GORT, differing by as much 0.076 for a zenith angle of 30°. This difference is made up for by an increase in the scattering component. In the simple model, scattering increases if the transmittance increases according to (4.12). Consequently, the scattering curve has the same shape as the direct and diffuse transmittance curve, albeit that the curve is much less sensitive to zenith angle. The scattering curve from GORT shows the opposite pattern, with maximum scattering when the direct transmittance is at a minimum.

The general pattern for the mature black spruce site is the same. Again, the simple model predicts a lower transmittance for direct and diffuse radiation at small zenith angles compared to GORT. In the range of zenith angles from 40° to 60° the simple model predicts somewhat larger transmittances for direct and diffuse radiation than GORT.

### *4.4.2 Comparison With Observations*

The individual components in the model can be compared with observations, if it is assumed that transmission of PAR through the canopy is only minimally affected by multiple scattering and multiple reflections. This assumption is arguably reasonable, because of large absorption by canopy elements in the PAR range [*Ni et al.*, 1997]. Under this assumption, measurements and simulations of transmitted PAR radiation are compared to evaluate (4.11), which describes penetration of direct and diffuse radiation into the canopy. Measurements and simulations of total

transmitted shortwave radiation can also be compared to evaluate the contributions of scattering and multiple reflections and overall performance of the model.

*PAR transmission.*

Calculation of PAR transmission through the forest canopy using (4.11) requires that the incoming PAR or shortwave radiation be separated into direct and diffuse components. As noted in section 4.4.1, (4.14), as used by *Ni et al.* [1997] to separate diffuse and direct radiation, is only appropriate for clear days. Only a small number of days during the BOREAS observation periods could be identified as categorically being clear. Therefore a different method was used on the basis of the clearness index ($k_t$), as defined by *Erbs et al.* [1982]. The clearness index is the ratio of total shortwave radiation above the canopy to total shortwave radiation at the top of the atmosphere [*Erbs et al.*, 1982]. High values of the clearness index indicate clear skies, while low values of the clearness index indicate cloudy skies. When the clearness index is smaller than 0.24, almost all the incoming radiation is diffuse, while for large values of $k_t$, the sky is mostly clear and most of the incoming radiation is direct. *Erbs et al.* [1982] developed a regression relationship between the clearness index and the fraction of incoming shortwave radiation that is diffuse.

Figure 4.3 compares 30 min averages of simulated and observed below-canopy PAR calculated using (4.11) at the mature jack pine site, for different levels of the clearness index. The PAR measurements were made at the top of the canopy and near the ground surface by a set of hemispherical optical sensors during the summer of 1994 [*Roujean*, 1999]. At each level, six or more sensors were used to obtain an estimate of the average PAR. Shortwave radiation values at the top of the canopy, used to calculate the clearness index, were measured using an Eppley pyranometer [*Shewchuk*, 1997]. The effective leaf area index was taken from *Chen et al.* [1997b], who performed extensive leaf area index measurements throughout the BOREAS study areas. The effective leaf area index for mature jack pine varied from 1.75 to 1.87 during the 1993 IFC and the 1994 IFCs [*Chen et al.*, 1997b], with an average value of 1.79. No calibration was performed to produce Figure 4.3.

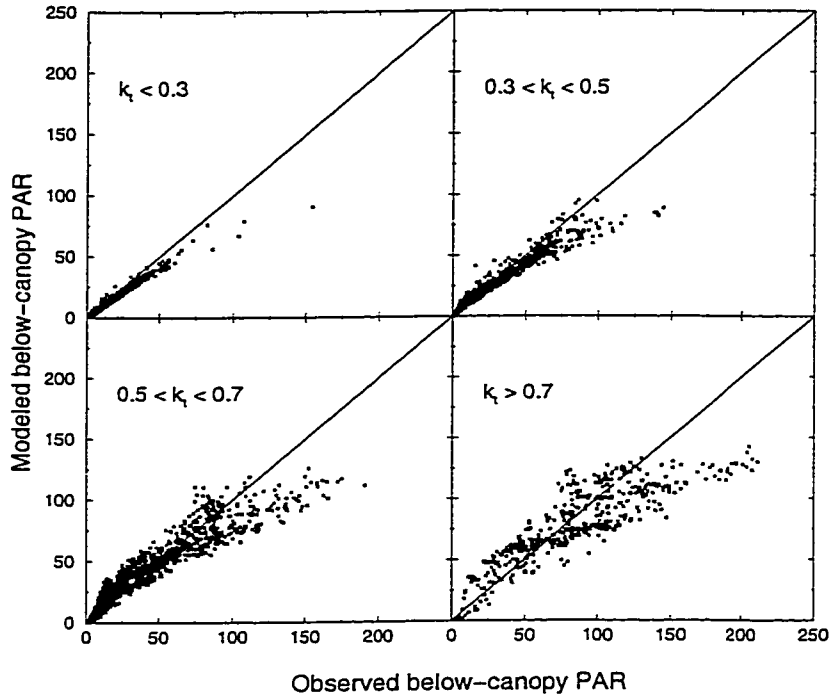


Figure 4.3: Simulated versus observed below-canopy PAR at the mature jack pine site for different levels of the clearness index ($k_t$) (30 min averages). Modeled values are based on equation (4.11). Measured above- and below-canopy PAR values are from *Roujean* [1999], and the total radiation values used to calculate the clearness index are from *Shewchuk* [1997].

The simple model tends to underpredict the observed below-canopy PAR values, particularly for the highest observed below-canopy PAR values on clear days. The bias is smaller on cloudy days, when most of the radiation is diffuse, or generally when radiation levels are low. This is consistent with the results from the previous section, which show that the simple model underpredicted the transmission of direct and diffuse radiation for small zenith angles, compared to the GORT model. Because the transmission of direct radiation at a particular point is highly dependent on local effects of tree geometry, the scatter increases with increasing radiation levels and increasing amounts of direct radiation.

Figure 4.4 shows 30 min averages of observed versus modeled below-canopy PAR at the ma-

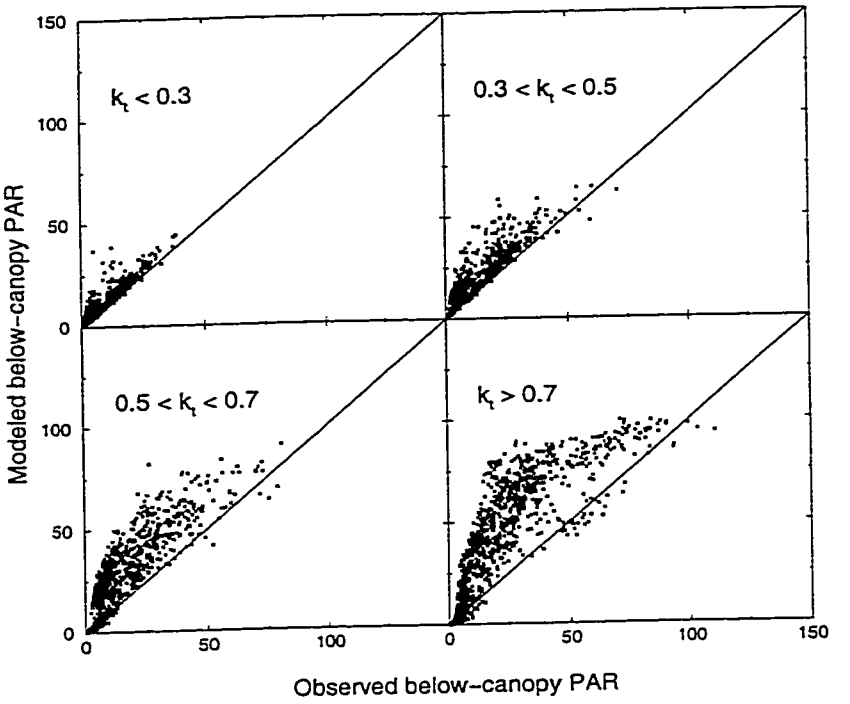


Figure 4.4: Simulated versus observed below-canopy PAR at the mature black spruce site for different levels of the clearness index ($k_t$) (30 min averages). Modeled values are based on equation (4.11). Measured above- and below-canopy PAR values are from *Roujean* [1999], and the total radiation values used to calculate the clearness index are from *Jarvis et al.* [1997].

ture black spruce site. The effective leaf area index for mature black spruce was 2.34 [*Chen et al.*, 1997b], resulting in a $\tau_d$ of 0.175. Above- and below-canopy PAR is taken from *Roujean* [1999], and above-canopy shortwave radiation is taken from *Jarvis et al.* [1997]. Attenuation through the mature black spruce is much stronger than attenuation through the jack pine, with below-canopy PAR generally less than 100 W/m$^2$. In contrast to the jack pine site, the model consistently overpredicts the observed below-canopy PAR, with greater positive bias for higher levels of below-canopy radiation.

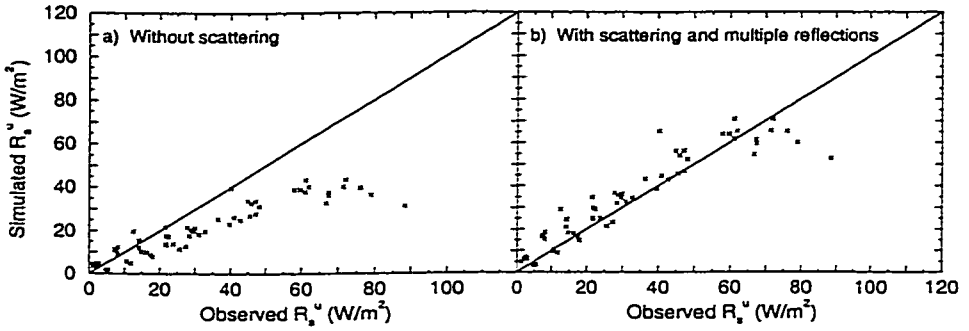


Figure 4.5: Scatterplots of simulated versus observed below-canopy shortwave radiation for mature jack pine (30 min averages): (a) transmittance based on equation (4.11) without scattering and reflections; (b) transmittance based on equations (4.11) and (4.12), including the effects of multiple scattering and reflections. Measured below-canopy radiation is from *Ni et al.* [1997], and measured above-canopy shortwave is from *Shewchuk* [1997].

*Total shortwave transmission.*

Shortwave radiation below the canopy was measured for a limited number of clear days during the winters of 1994 and 1996 using a set of 10 radiometers placed randomly on the ground surface [*Hardy et al.*, 1997; *Ni et al.*, 1997]. Figure 4.5 compares 30 min average, simulated and observed total below-canopy shortwave radiation at the mature jack pine site during February 1994. The same canopy characteristics were used as for Figure 4.2. As anticipated, the below-canopy radiation calculated using only (4.11) underestimates the observed flux, because it does not account for scattering and multiple reflections between the canopy and the snow surface (Figure 4.5a). Figure 4.5b shows the same data series as Figure 4.5a, with the contribution due to scattering computed using (4.12) and multiple reflections using (4.13). The simulated radiation values have a consistent upward bias but generally match the observed values, except for the highest observed radiation values. This negative bias for the highest below-canopy values was also observed in the simulated PAR (Figure 4.3a). These values occur as spikes near solar noon and probably include cases where a number of radiometers were in direct sunlight. Such conditions, while real, are not consistent with the spatial averaging implicitly assumed by the model. Figure 4.6 shows the

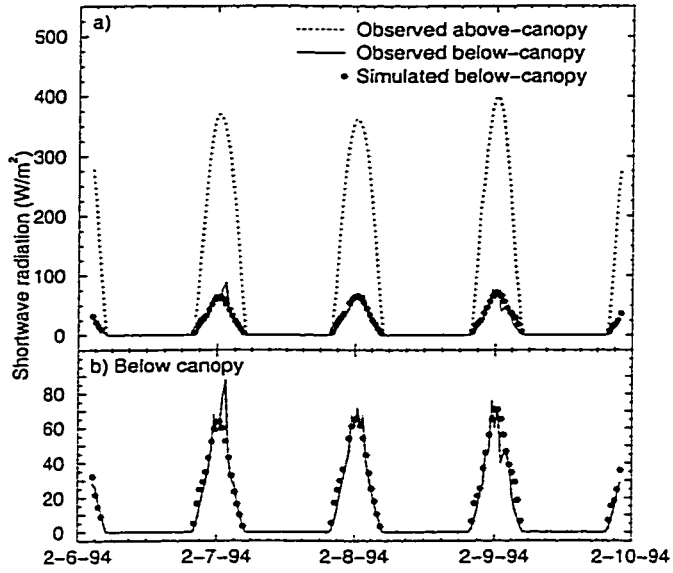


Figure 4.6: Time series of observed and simulated total below-canopy shortwave radiation at the mature jack pine site (30 min averages): (a) measured above- and below-canopy shortwave and simulated below-canopy shortwave; (b) measured below-canopy shortwave and simulated below-canopy shortwave. Data sources are the same as for Figure 4.5.

Figure 4.5b results as a time series.

Figure 4.7 shows results of application of the model for the mature black spruce site during the end of February 1996. During the period when below-canopy radiation was measured, no above-canopy radiation was observed at the same location. Above-canopy radiation values were taken from the nearest site at which observations were available, which is the mature jack pine site, about 29 km to the southeast. Above- and below-canopy radiation values were averaged over 1 hour intervals for this case, because the likelihood of a weather system affecting both sites within an hour is greater than for shorter time intervals.

The leaf absorption for black spruce is similar to that for jack pine, although reflectance is somewhat higher in the visible part of the spectrum and transmission somewhat lower [*Middleton and Walter-Shea*, 1995]. The same exponent was used in (4.12) as for jack pine. For the mature black spruce site the bias increases after applying the scattering correction, with modeled values

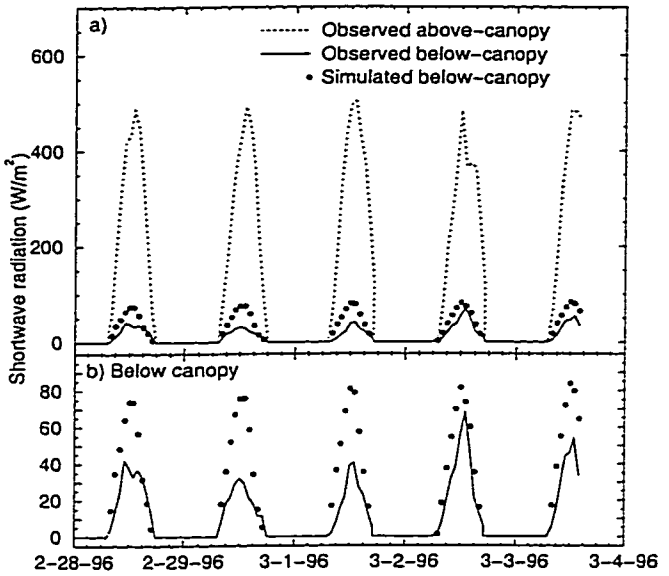


Figure 4.7: Time series of observed and simulated total below-canopy shortwave radiation at the mature black spruce site (60 min averages): (a) measured above and below-canopy shortwave and simulated below-canopy shortwave radiation; (b) measured below-canopy shortwave and simulated below-canopy shortwave radiation. Measured below-canopy radiation is from *Ni et al.* [1997], and measured above-canopy shortwave radiation is from *Shewchuk* [1997].

of total below-canopy radiation larger than observed values (Figure 4.7). Observed transmittance values at the black spruce site are very low early in the year, with most values in the range 0.03-0.13. In the model, the relative contribution of scattered radiation to total transmitted radiation is largest for low transmittance values (Figure 4.1). The increase in the transmittance due to scattering is also most sensitive to changes in $\sqrt{a_{\text{total}}/a_{\text{PAR}}}$ at low transmittance values. Model results at the black spruce site are therefore more sensitive to the formulation of multiple scattering than those at the jack pine site. Interestingly, the bias during the last two days is less than during the first three days, even though the above-canopy radiation values are very similar (Figure 4.7).

### *4.5 Discussion*

The simple model simulates the below-canopy PAR and shortwave well at the mature jack pine site but performs less well at the mature black spruce site. The rather large scatter in the plots of observed versus modeled below-canopy radiation can be attributed to a number of sources.

The model is simple and does not account for a number of effects that are included in more complex models. The model effectively represents the canopy by a single diffuse layer of canopy elements, represented by a single effective leaf area index. Thus many of the architectural effects of the canopy are not represented, which may largely be responsible for the poorer performance at the black spruce site than at the jack pine site. Even though the tree density is higher at the black spruce site, it is a more open stand than the jack pine stand, which has larger canopy crowns [*Roujean*, 1999]. The canopy of the mature jack pine thus conforms better to the model assumptions.

Second, the effective leaf index values vary rather widely in the BOREAS area. *Chen et al.* [1997b] report effective leaf area indices ranging from 1.09 to 4.10 for different mature jack pine stands in the BOREAS southern study area, and from 0.23 to 3.45 for different mature black spruce stands in the same area. Since the effective leaf area is the most important vegetation characteristic in the model, uncertainties in this value will influence the model results.

Third, measuring average below-canopy radiation levels is difficult, because of the highly heterogeneous structure of the forest canopy. The two data sets used to evaluate model predictions were carefully collected to address this concern [*Ni et al.*, 1997; *Roujean*, 1999], but problems remain. For example, at the black spruce site during the winter of 1996, above-canopy radiation levels were similar during each of the five days of observation, but below-canopy radiation levels differed widely. *Roujean* [1999] cautions that the mature black spruce site was rather dense, and most sensors were in the branches. Therefore PAR measurements may overestimate the radiation interception by the canopy at the plot level. At this point it is not entirely clear to what extent the upward bias produced by the model is due to model error and to what extent due to sampling problems below dense canopies. Examination of the probability density distribution of the normalized below-canopy radiation measurements showed that the distribution was characterized by

heavy tails, meaning that a large sample size is required to characterize the mean value.

Fourth, the separation of incoming above-canopy PAR and shortwave radiation into direct and diffuse radiation according to the clearness index gives reasonable results, but the relationship shows a large scatter [*Erbs et al.*, 1982]. Direct and diffuse radiation are attenuated differently, therefore errors in the separation will lead to errors in the prediction of transmitted radiation.

### *4.6 Conclusions*

Transmission of shortwave radiation through forest canopies is an important process that dominates the energy inputs to the understory or ground surface. As such, it affects the soil thermal balance, evaporation and transpiration from the understory, and the amount and rate of snowmelt. Although many canopy radiative transfer models exist in the literature, most are complex and require detailed information of canopy structural and optical characteristics which is not generally available, or are semi-empirical and contain calibrated parameters that do not exhibit the proper sensitivities to environmental changes. We have developed a simple canopy radiative transfer model based on Beer's law for use in a spatially distributed hydrology model. The new model requires knowledge only of the effective leaf area index and the bulk canopy and understory albedos. Nonetheless, more detailed knowledge about leaf angle distributions and leaf reflectances can easily be accommodated through the use of canopy specific values for $a$ and $b$ in (4.9) and for $a_{\text{total}}$ and $a_{\text{PAR}}$ in (4.12).

The model accounts for the transmission of diffuse and direct shortwave radiation and includes a term to account for multiple scattering in the canopy and multiple reflections between the canopy layers. The total transmitted radiation compared well with observed values over a range of solar zenith angles at a mature jack pine site. The results at a mature black spruce site were less positive. While the absolute model error in predicted below-canopy radiation was small compared to the above-canopy radiation, below-canopy radiation values were at times twice as large as the observed values. Because of the limited amount of available data, and the difficulty in making subcanopy radiation measurements that are representative for a stand, it is not clear to what extent

the discrepancy between measured and observed values is due to sampling error or to model error.

The model is not meant as a replacement for more complex methods. It does not, for instance, account for shifts in the spectral composition of radiation along its path through the canopy, nor does it model the vertical distribution of the radiative flux in the canopy. However, if the bulk shortwave radiation below the canopy is the primary quantity of interest, the proposed model can offer a simple solution using only commonly available canopy characteristics. If the vertical distribution of the radiation flux is the quantity of interest, more complex models such as those described by *Ni et al.* [1997] or *Roujean* [1996] may be more appropriate.

Chapter 5

# WATER BALANCE DYNAMICS OF A BOREAL FOREST WATERSHED: WHITE GULL CREEK BASIN, 1994–1996

## *5.1 Introduction*

As pointed out by *Metcalfe and Buttle* [1999], "information on water balance dynamics is an essential component of studies of the role of the boreal forest in surface-atmosphere interactions and climate change". Hydrological processes in the boreal forest not only influence the partitioning of incoming energy into sensible, latent and ground heat fluxes, but also play an important role in controlling biogeochemical cycles. For example, the production of methane in boreal wetlands is closely related to the water levels in these wetland areas [e.g. *Suyker et al.*, 1996]. However, there have been relatively few basin-scale studies of water balance dynamics in boreal forest watersheds.

Measurements taken as part of BOREAS allow the calculation of the water balance of the White Gull Creek basin, a 603 $km^2$ drainage basin that lies entirely within the BOREAS southern study area. Careful identification of the individual terms in the water balance makes it possible to address questions such as

- What is the importance of the winter snow pack to summer ET?
- What is the relative importance of snow melt and summer precipitation to stream discharge?
- What is the hydrologic response of the boreal forest to the interannual and interseasonal variations in meteorological conditions?
- How do the moisture fluxes in the boreal forest respond to extreme hydrologic events, such as spring snow melt and summer convective storms?

In turn, the answers to these questions will lead to a better insight into the hydrological processes that dominate the boreal forest and may give insights into vulnerabilities of the boreal environment to changes in climate. In addition, a calculation of the water balance will help to identify strengths and shortcomings in the data collected as part of BOREAS, and may provide important lessons for future large-scale field experiments. This chapter attempts to address these issues through a study of the water balance dynamics of the White Gull Creek basin in central Saskatchewan, Canada, for the period 1994-1996.

## *5.2 White Gull Creek Basin*

### *5.2.1 Basin Description*

The White Gull Creek Basin is located east of Candle Lake, Saskatchewan, Canada, about 60 km northeast of Prince Albert (Figure 5.1). The area upstream of the main discharge measurement location along Highway 106 (SW1) was about 603 $km^2$, although the wetlands present in the basin made it difficult to determine the basin boundaries. The basin falls within the BOREAS southern study area, near the southern limits of the boreal forest. White Gull Creek drains extensive wetland areas in a gently undulating to moderately rolling terrain with elevations ranging from 400 to 700 m. The surface geology is characterized by Pleistocene and Holocene glacial deposits on top of Cretaceous bedrock. Vegetation consists mainly of black spruce in poorly drained areas, and jack pine on well-drained and sandy soils. Mixed stands of aspen and white spruce are common on well-drained glacial deposits.

### *5.2.2 BOREAS Hydrological Field Measurements*

Discharge measurements in White Gull Creek were made by Environment Canada during the period 1994–1996 at site SW1 (Figure 5.1). Precipitation was measured year-round at sites operated by the Saskatchewan Research Council [*Shewchuk*, 1997, 2000]. Both Belfort weighing gauges equipped with an Alter shield as well as tipping bucket rain gauges were used at most of the sites. During the 1994–1996 growing seasons additional tipping bucket and Belfort rain gauges

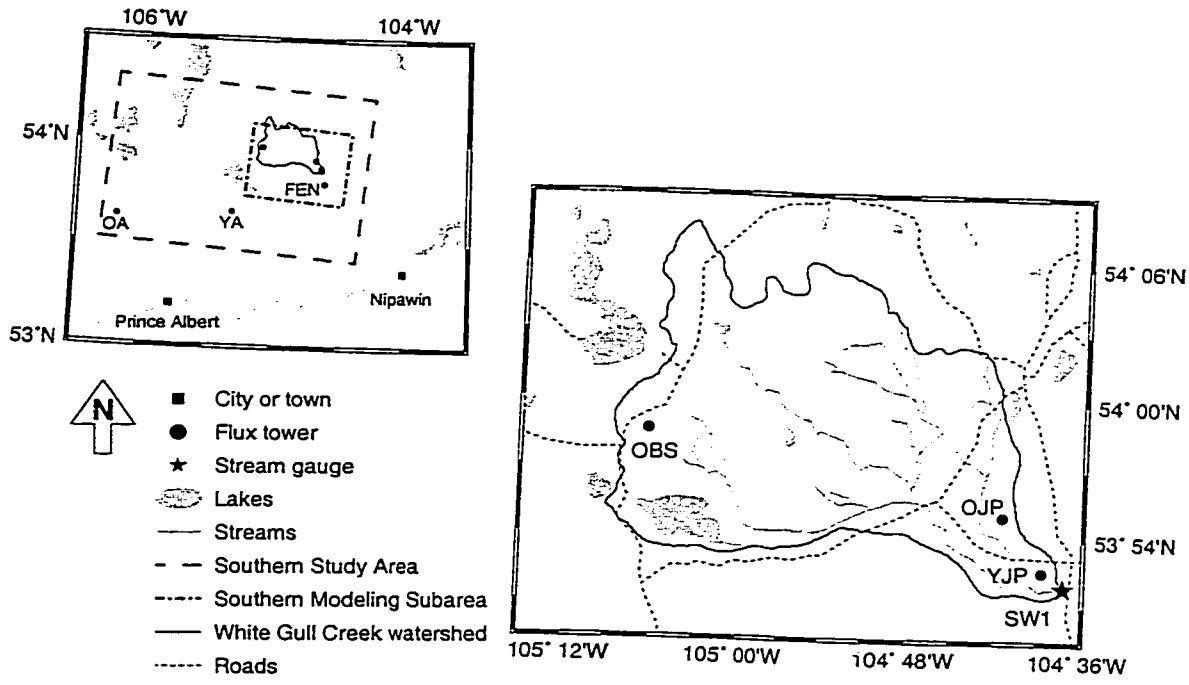


Figure 5.1: White Gull Creek Basin and location of the flux towers and stream gauge. OA - mature aspen, YA - young aspen, FEN - fen, OBS - mature black spruce, OJP - mature jack pine, YJP - young jack pine, SW1 - stream gauge.

were installed by the University of Waterloo [*Kouwen et al.*, 2000]. In the summer of 1994 a high-resolution rain radar ($\approx$ 2 km spatial resolution) was operated over the southern study area [*Schnur et al.*, 1997].

Meteorological conditions were measured year-round at sites operated by the Saskatchewan Research Council (SRC), as well as a number of permanent Canadian Atmospheric Environment Service (AES) sites. Flux towers installed in relatively homogeneous stands of vegetation measured latent, sensible and $CO_2$ fluxes, as well as meteorological conditions (Figure 5.1). The period during which each tower was operated varied, with some towers only operational during the 1994 intensive field campaigns and others operating for most of the growing seasons of 1994, 1995 and/or 1996. Three of the flux towers in the southern study area (mature black spruce, ma-

ture jack pine and young jack pine) were located within the boundaries of the White Gull Creek basin. The fen tower was located to the southeast, while the young aspen tower was located to the south. The mature aspen tower was located almost 70 km west of the basin in the Prince Albert National Park. Soil moisture at various depths was available at most sites for at least part of the period [*Cuenca et al.*, 1997].

Snow depth was monitored continuously at the SRC towers using an ultrasonic snow depth gauge. Snow surveys were made twice monthly by AES [*Goodison*, 2000]. In the winter of 1994 and 1996, snow water equivalent and snow properties such as density were determined near the time of peak snow accumulation [*Davis et al.*, 1997; *Davis*, 2000; *Hardy et al.*, 1997].

The meteorological data used in this study were taken from *Pauwels et al.* [1999] unless otherwise noted. *Pauwels et al.* combined observations from a large number of sources into continuous time series. A 2 km resolution gridded data product was used for the White Gull Creek basin, as well as a point data set for each of the towers. The data set provided hourly precipitation, air temperature, dew point temperature, incoming shortwave radiation, incoming longwave radiation, and surface pressure. Wind speeds were processed separately. The hourly data were aggregated to the daily timestep for the purpose of this study. The mean daily wind speed was lapsed to a common reference height of 40 m assuming a logarithmic wind speed profile and a vegetation-dependent roughness height and displacement height. The wind speeds at the reference heights were then interpolated to the 2 km grid cells covering the White Gull Creek basin using inverse distance weighting and a maximum of four nearest neighbors.

### *5.3 Precipitation and Runoff*

Long-term records (1975–1996) at Nipawin (53°20'N, 104°00'E, about 72 km southeast of the main discharge gauge at SW1) show that annual precipitation varied from 313 mm in 1992 to 533 mm in 1978, with a mean annual precipitation of 438 mm. Precipitation during the period 1994–1996 was 456 mm, 425 mm, and 490 mm (no observations in March 1996), respectively. Average annual precipitation over the White Gull Creek basin was 537 mm, 391 mm, and 465 mm

for the same three years. The higher precipitation in 1994 over the White Gull Basin occurred largely during the period January–April, when precipitation over the basin totaled 84.1 mm, while only 25.6 mm was measured at Nipawin. This may largely be due to underreporting of snow precipitation at the Nipawin site.

Precipitation values in the *Pauwels et al.* [1999] data set were based on precipitation gauges operated in and near the southern study area. During the summer additional gauges were operated within the modeling subarea. Rain radar observations made during the summer of 1994 were blended into the data set by treating each rain radar pixel as a surface station located at the center of the pixel. *Schnur et al.* [1997] have shown that the accumulated gauge precipitation (based on a network of 12 gauges in the southern study area) was about 86% of the accumulated rain radar precipitation estimate for the period May 5–September 23, 1994. The area-averaged monthly rain accumulations estimated using gauges and radar agreed to within 8.7% for the month of July 1994.

Precipitation over the White Gull Creek basin is summer-dominant (Figure 5.2). At Nipawin about two thirds of the annual precipitation falls during May–September, with half of that amount falling in June and July. A similar partitioning of precipitation is seen over the White Gull Creek basin for the period 1994–1996. The heaviest precipitation occurred during July 1994, when 173 mm was recorded (at Nipawin, 145 mm of precipitation was recorded, the third wettest month during the period 1975–1996).

Areally averaged discharge at the SW1 gauge totaled 110 mm in 1994, 48 mm in 1995, and 127 mm in 1996. During the period 1994–1996 mean daily discharge (Figure 5.2) ranged from about 0.1 $m^3/s$ (0.014 mm/day) in early spring to 25.2 $m^3/s$ (3.6 mm/day) on July 21, 1994 after heavy precipitation. The early spring figure is an estimate, because White Gull Creek is frozen for most of the winter. Spring snow melt is an important source for runoff, although the largest runoff during the 1994–1997 was associated with heavy summer precipitation. The mean runoff ratio (runoff divided by precipitation) was 20.4%.

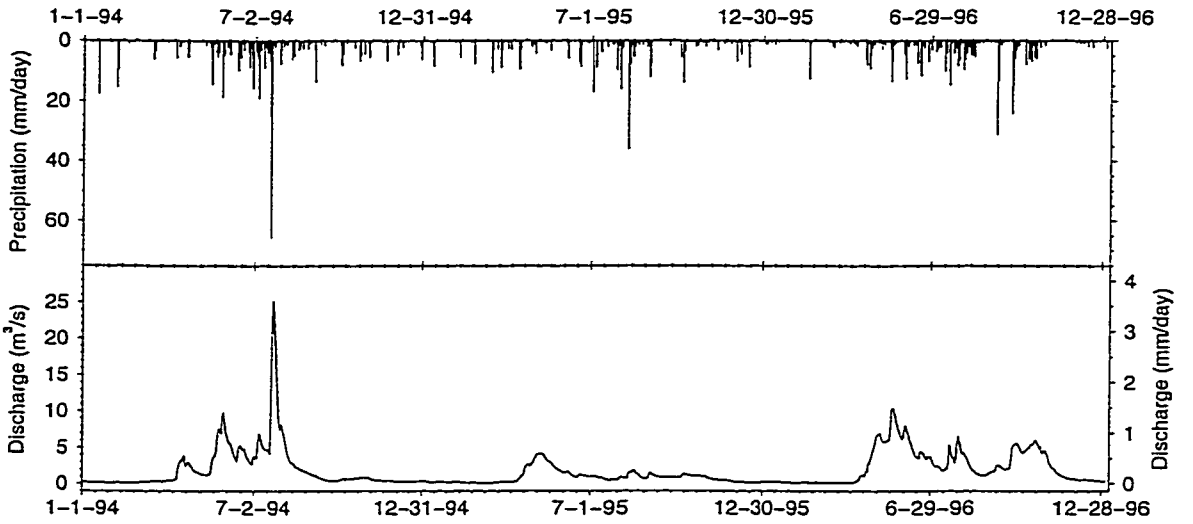


Figure 5.2: Mean daily precipitation over the White Gull Creek basin and discharge at SW1, 1994–1996.

### *5.4 Snow Accumulation and Melt*

The mean annual air temperature at the Nipawin station for the period 1975–1996 was 0.6°C, varying from a low of -44.4°C on January 18, 1996, to a high of 38.2°C on June 5, 1988. Mean daily air temperatures remained below 0°C from late October through the beginning of April (Figure 5.3). Average temperatures over the White Gull Creek basin during 1994–1996 were similar, with a maximum of 32.0°C on May 30, 1995 and a minimum of -40.0°C on February 1, 1996.

Snow accumulation during the 1994–1996 period started in the first week of November. Snow melt in 1995 started on April 11 at the forested sites and continued over a three week period, with a complete disappearance of snow by May 7. The open sites were completely snow-free about two weeks earlier [*Link and Marks*, 1999]. Based on snow course observations [*Goodison*, 2000] and sonic snow depth sensors at the mature aspen and jack pine towers [*Shewchuk*, 1997, 2000], the melt process in 1994 started in the first week of April and was completed by the second half

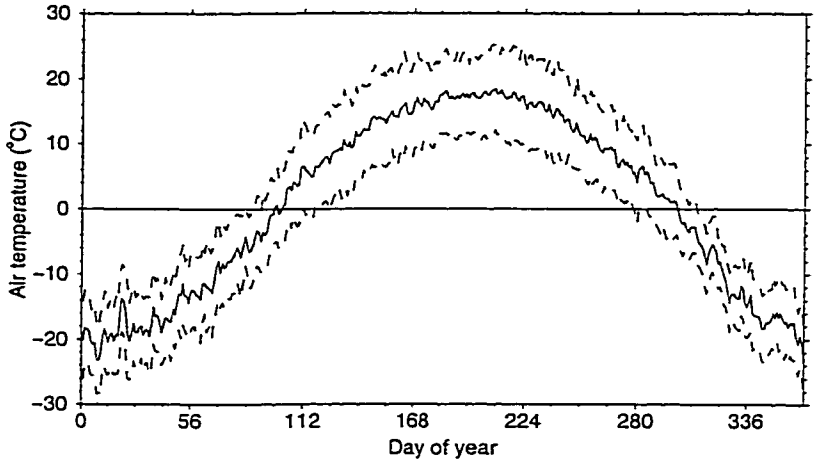


Figure 5.3: Mean daily minimum, mean and maximum air temperature at Nipawin, Saskatchewan (53°20'N, 104°00'E), 1975–1996.

of that month. Snow melt in 1996 started in the beginning of April, but fresh snow in the second half of the month delayed complete melt till about the second week of May. Ablation dates for the forested sites were similar, despite differences in canopy architecture [*Link and Marks*, 1999].

Figure 5.4 compares snow course measurements at five sites in the southern study area with accumulated precipitation for the 1994/95 and 1995/96 winters. The precipitation was accumulated for those days when the mean air temperature was smaller than 0°C. Because mid winter melt is rare in this region due to the low winter temperatures (Figure 5.3), the accumulated precipitation is expected to equal the accumulated snow minus any sublimation that would have occurred. *Link and Marks* [1999] in their simulations of the snow pack for the 1994-1995 winter, found that the latent heat flux was small. Although large latent heat fluxes can occur at air temperatures near 0°C [e.g. *Harding and Pomeroy*, 1996], Figure 5.4 indicates that during the winter of 1994–1995, gauge undercatch errors and sublimation roughly balanced, and the measured precipitation provides a reasonably accurate picture of the snow accumulated during the winter season. During the 1995–1996 winter, the snow courses indicated more snow on the ground than was measured as precipitation. At the start of the snow season, some of this discrepancy was likely due to the

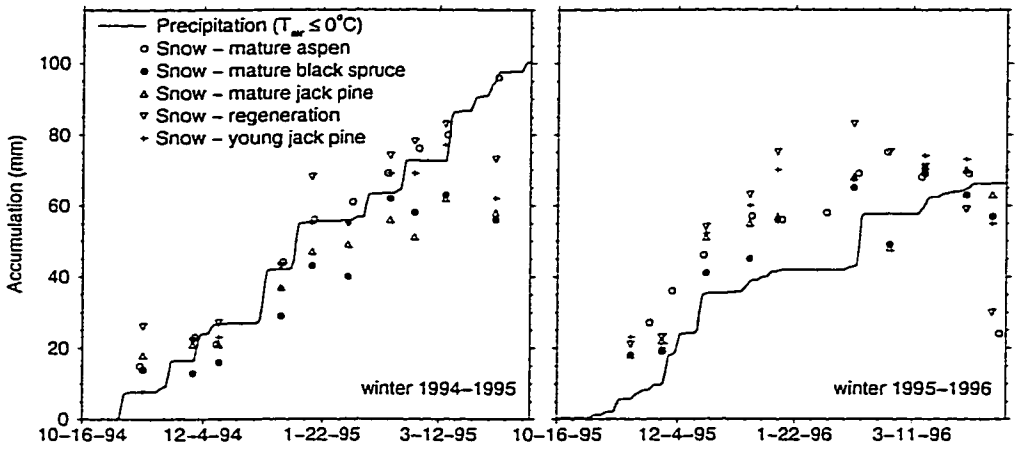


Figure 5.4: Accumulated precipitation during days when the mean daily air temperature was smaller than 0°C and snow course measurements at five locations in the southern study area for the winters 1994–1995 and 1995–1996.

simple snowfall temperature threshold of 0°C (a higher threshold would have shifted the solid line in Figure 5.4 upward, because temperatures in October are regularly above 0°C). However, even in mid winter, measured snow water equivalent increased faster than measured precipitation would suggest. During the winter far fewer precipitation gauges were operational than in the summer, increasing the likelihood that snowfall over part of the area would not be recorded. In addition, some gauge undercatch is likely to have occurred. Winter accumulated precipitation was about 20–30 mm smaller than maximum accumulated snow. Maximum accumulated snow for each of the three winters based on the snow course observations [*Goodison*, 2000] was 46 mm in 1994, 73 mm in 1995 and 71 mm in 1996, with maximum accumulation around the middle of March.

## *5.5 Evaporation*

### *5.5.1 Background*

One of the important early findings from BOREAS was that despite the abundance of water, evapotranspiration is limited, even on warm days with low humidity, suggesting a strong biophysical

control [*Sellers et al.*, 1995]. Evapotranspiration rates were less than 2 mm/day over the 1994 growing season, while sensible heat fluxes were often high, resulting in Bowen ratios larger than one on many days. These high sensible heat fluxes lead to the development of deep convective boundary layers over the BOREAS area.

*Betts et al.* [1999] studied the controls on evapotranspiration at the mature black spruce in the BOREAS northern study area using 3 years of 30 min averaged data. They analyzed the flux data using a Monin-Obukhov framework and a simple bulk surface model using a single vegetative resistance ($r_{veg}$) for the forest ecosystem, that is, no separation was made between the transpiration from the canopy and evapotranspiration from the understory/moss/soil layer. Based on observed fluxes, they calculated the corresponding $r_{veg}$ and examined its relationship with environmental conditions. They found that the latent heat flux remained small during the spring and increased only slightly with increased photosynthetic photon flux density, because early in the year the ground was still frozen. Consequently, at high radiation levels the sensible heat flux was high, leading to deep boundary layers and low humidity over the forest in spring. Even in summer, the increase of evaporation with increased radiation and temperature was weak, indicating that the latent heat flux was largely controlled by $r_{veg}$. Evaporation was about 50% higher when the canopy and moss were wet as compared to a dry canopy. As expected, the additional evaporation from a wet surface was less subject to photosynthetic control. At all humidities $r_{veg}$ increased with increased temperatures. At the same temperature the resistance was lowest in summer and was as much as 250 s/m higher when the soil was frozen. Under cloudy skies $r_{veg}$ was 50 s/m lower, because diffuse radiation penetrates the canopy more efficiently than beam radiation (see Chapter 4). Although vegetative resistance is normally not treated as a function of windspeed, the calculated $r_{veg}$ showed a considerable dependence on wind speed, with a decrease in $r_{veg}$ with increased wind speed. This was partially explained as a measurement problem of the fluxes at low wind speeds and by the absence of a leaf boundary layer resistance in the simple flux model. Regression analysis of $r_{veg}$ with environmental conditions explained 63.5% of the variance.

For a water balance study it is important to have a continuous record of evapotranspiration at

some temporal resolution. Although detailed measurements of the latent heat flux were made at all the towers, no continuous record of evapotranspiration existed for the period 1994–1996 at any of the sites. Consequently, evapotranspiration needed to be estimated based on other sources. Daily evapotranspiration was estimated based on environmental conditions at the towers and mapped to the White Gull Creek basin based on land cover type and leaf area index using an approach described in the following sections.

### *5.5.2 Flux Tower Estimates*

Latent heat flux measurements were made at the tower sites using eddy correlation and/or bowen ratio methods. To estimate the evapotranspiration on those days when measurements were not available, the following approach was adopted. As in *Grelle et al.* [1999] a bulk canopy resistance $r_c$ was calculated based on the Penman-Monteith combination equation, for those days when latent heat flux measurements were available. These calculated $r_c$ values were then related to measured environmental conditions using multiple linear regression, similar to the procedure followed in *Betts et al.* [1999]. Evapotranspiration was then estimated by combining the estimated $r_c$ values with the Penman-Monteith equation

$$LE = \frac{\Delta R_n + \rho_a c_p \left(e_s(T_a) - e\right)/r_a}{\Delta + \gamma\left(1 + r_c/r_a\right)}, \tag{5.1}$$

where $LE$ is the latent heat flux in W/m$^2$, $\Delta$ is the slope of the saturated vapor pressure curve at the air temperature ($T_a$) in Pa/°C, $R_n$ is the net radiation in W/m$^2$, $\rho_a$ is the air density in kg/m$^3$, $c_p$ is the specific heat of air at constant pressure in J/kg/°C, $e_s(T_a)$ is the saturated vapor pressure at the air temperature in Pa, $T_a$ is the air temperature in °C, $e$ is the actual vapor pressure in Pa, $r_a$ is the aerodynamic resistance in s/m, $\gamma$ is the psychrometric constant in Pa/°C, and $r_c$ is the bulk canopy resistance in s/m. More correctly, the $R_n$ term represents the energy available for turbulent heat exchange, and should be corrected for the ground heat flux $G$, change in energy storage $\Delta S$, advected energy and energy absorbed by biochemical processes in the plant. Of these terms $G$ can be a large component of the instantaneous energy balance, but tends to be small when

averaged over a day except during periods of soil freeze up and thaw. Similarly, $\Delta S$ tends to be small averaged over a day, except during periods of snow melt. Because these are the periods when the evapotranspiration tends to be low, these terms were neglected here. On a seasonal basis, *Jarvis et al.* [1997] reported that at the mature black spruce site during the 1994 growing season (May 23–September 21), 93% of the total net radiation flux density was accounted for by the latent heat (44%) and the sensible heat (49%) fluxes. The remaining 7% was split among the soil heat flux (3%), chemical energy (1%) and an unexplained residual of 3%.

When $LE$ is measured, $r_c$ can be calculated as

$$r_c = \frac{\Delta R_n r_a + \rho_a c_p \Delta e - r_a (\Delta + \gamma) LE}{\gamma LE}, \tag{5.2}$$

where $\Delta e = (e_s(T_a) - e)$. The aerodynamic resistance $r_a$ can be calculated as [*Shuttleworth*, 1993]

$$r_a = \frac{\ln[(z_u - d)/z_{om}] \ln[(z_e - d)/z_{ov}]}{k^2 U}, \tag{5.3}$$

where $z_u$ and $z_e$ are the respective measurement heights for the wind speed and the humidity in m, $z_{om}$ and $z_{ov}$ are the respective roughness lengths for momentum and mass exchange in m, $d$ is the displacement height in m, $U$ is the wind speed at the reference height in m/s, and $k$ is von Karman's constant (0.41). Following *Shuttleworth* [1993], $d$, $z_{om}$, and $z_{ov}$ were estimated based on the height of the vegetation $h_c$ ($d = 0.67h_c$, $z_{om} = 0.123h_c$, and $z_{ov} = 0.0123h_c$).

All terms on the right-hand side of (5.2) other than $R_n$ were available or could be calculated using the meteorological data set from *Pauwels et al.* [1999]. Although the net radiation was measured routinely at many of the sites, this variable was not included in the *Pauwels et al.* data set, because the specific purpose of that data set was as a forcing data set for land surface schemes, which normally calculate a surface temperature and thus outgoing longwave radiation directly. Interpolation of net radiation between the sites was difficult, because the radiative surface temperature and thus outgoing longwave radiation are highly dependent on local conditions. Therefore, the net radiation was estimated using measured incoming shortwave and longwave radiation, esti-

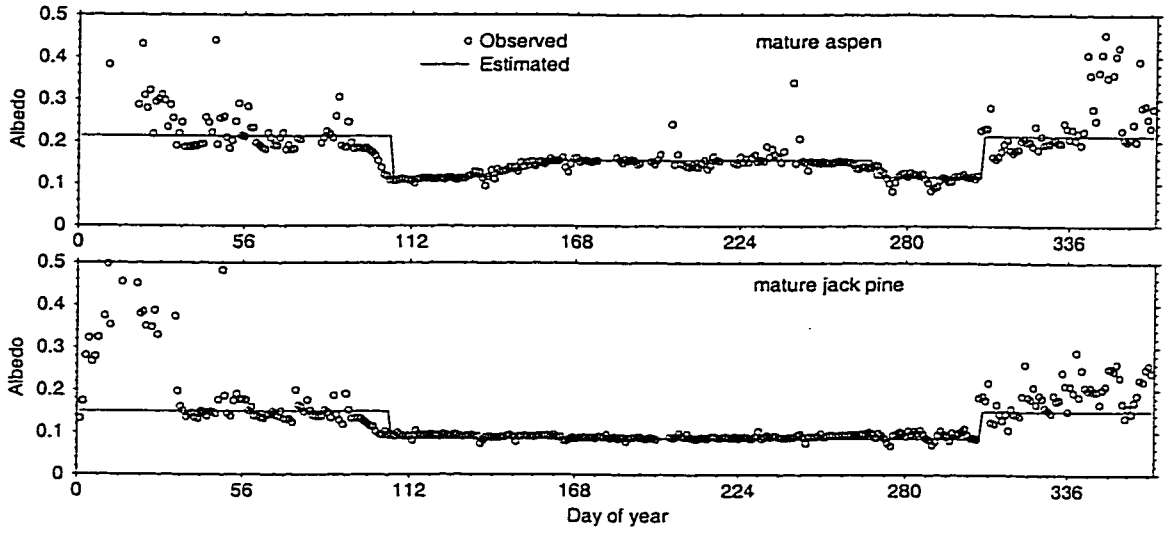


Figure 5.5: Observed and estimated shortwave albedo at the mature aspen and mature jack pine sites for 1994.

mated shortwave albedo and estimated emitted longwave radiation. Shortwave albedos were taken from *Betts and Ball* [1997], with transitions from snow covered to snow free conditions based on the snow data discussed in Sections 5.2.2 and 5.4. For the aspen sites, which are deciduous, albedo was linearly increased from the albedo for leaf-free aspen to leaf-covered aspen in the weeks following snow melt. The transition period was selected based on measured incoming and outgoing shortwave radiation at the aspen sites (Figure 5.5).

The surface radiative temperature ($T_s$) was measured by SRC at 15 minutes intervals at the mature aspen and the mature jack pine site using staring radiometers [*Shewchuk*, 2000]. These values were converted to outgoing longwave radiation and averaged over each 24-hour period. Outgoing longwave radiation was also estimated hourly using the air temperature ($T_a$) as an estimate of $T_s$, assuming that the surface emitted as a black body and averaging the resulting hourly outgoing longwave values over each 24-hour period. Figure 5.6 compares the estimated and observed outgoing and net longwave radiation at the mature aspen and mature jack pine sites for the period

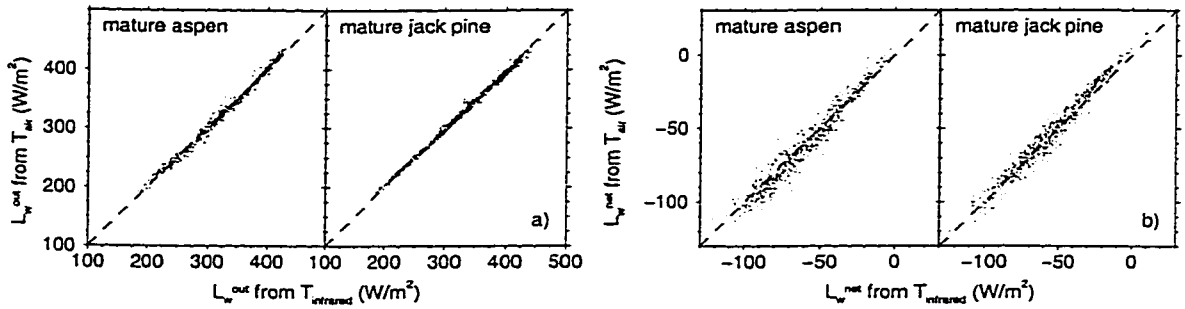


Figure 5.6: Measured and estimated daily a) outgoing and b) net longwave radiation at the mature aspen and jack pine sites. The outgoing longwave radiation along the horizontal axis is based on observed infrared temperatures.

1994–1996. The bias in net longwave radiation was 0.83 W/m$^2$ (1.4%, n=909) and -2.78 W/m$^2$ (5.2%, n=954) at the aspen and jack pine sites, respectively.

Figure 5.7 compares observed and estimated net radiation at the mature aspen and the mature jack pine sites. The bias was -5.1 W/m$^2$ (-8.6%, n=964) and 1.0 W/m$^2$ (1.7%, n=1028) for the aspen and jack pine sites, respectively. The bias at the aspen site was most pronounced during the winter months, when evaporation was at a minimum.

Any missing values in the original 30-minute latent heat measurements were filled in by averaging the two adjacent values. If either or both adjacent values were missing, the value was flagged as missing. Average daily heat fluxes were calculated for those days when fewer than three 30-minute values were missing.

The following sections discuss the latent heat flux estimates for the six vegetation types around the flux towers in the southern study area. Table 5.1 shows for each vegetation type the properties used for the estimation of the canopy resistance and the latent heat flux.

*Mature black spruce*

The mature black spruce site was located in the northwest corner of the White Gull Creek basin (Figure 5.1) and was representative of the dominant vegetation type in the North American boreal

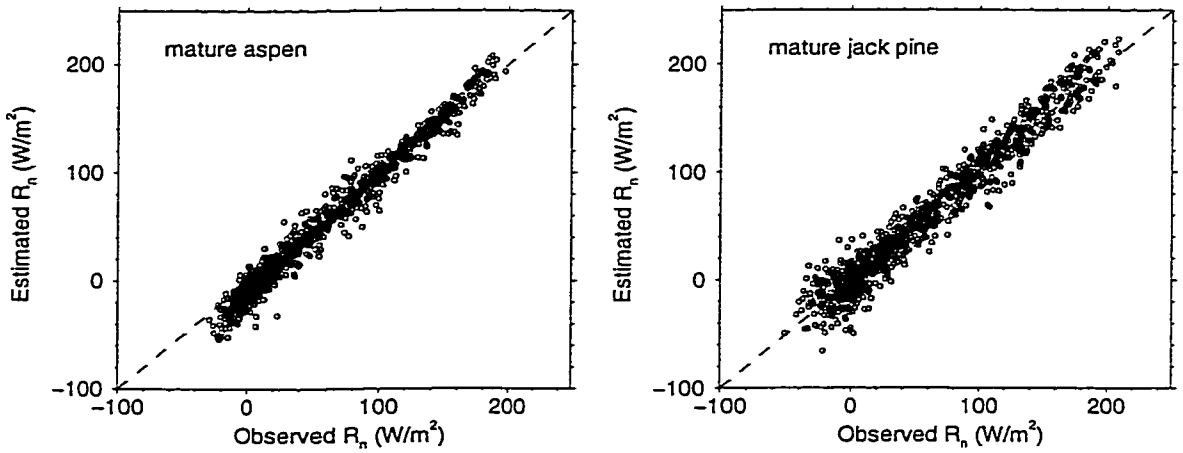


Figure 5.7: Measured and estimated daily net radiation at the mature aspen and jack pine sites.

forest. The flux tower operated during the 1994 growing season (May 24 – September 20) and during much of 1996 (March 25 – November 28) [*Jarvis and Moncrieff*, 2000]. Mean daily latent heat fluxes were available for 363 days (116 in 1994 and 247 in 1996). The data were filtered for those periods when snow was not present (day of year $>$ 132 and day of year $<$ 300). As pointed out by *Betts et al.* [1999], estimates of $r_c$ are less reliable at low fluxes, and we therefore required that $LE > 15$ W/m$^2$. Finally, a few large outliers were filtered by requiring that $r_c < 1000$ s/m.

Table 5.1: Vegetation characteristics used in the estimation of $r_c$ and $LE$.

| Site | Vegetation Height (m) | Albedo Summer | Albedo Winter |
|---|---|---|---|
| Mature black spruce | 10 | 0.081 | 0.108 |
| Mature aspen | 21.5 | [a]0.156 | 0.214 |
| Mature jack pine | 13.5 | 0.086 | 0.150 |
| Fen | 1 | 0.135 | 0.480 |
| Young aspen | 3 | [a]0.156 | 0.214 |
| Young jack pine | 4.5 | 0.086 | 0.150 |

[a]An albedo of 0.116 was used for the period with no snow and no leafs

The final data set contained 259 values, of which 114 were in 1994 and 145 in 1996.

Many of the same relationships between $r_c$ and environmental conditions were found as reported by *Betts et al.* [1999] for 30-minute data at the mature black spruce site in the BOREAS northern study area. The resistance $r_c$ decreased with humidity, incoming shortwave radiation and wind speed, and increased with air temperature. As in *Betts et al.* [1999], a wetness and cloudiness index were created to further stratify the data. The wetness index was calculated in the same way as in *Betts et al.* [1999], and was similar to an antecedent precipitation index. The index was incremented with the amount of precipitation on the previous day and decremented by 1 on dry days. The maximum allowed value of the index was 5. The cloudiness index was calculated as the ratio between measured total incoming shortwave radiation and the calculated amount of shortwave radiation at the top of the atmosphere for the same time period. Lower values of the cloudiness index indicated reduced transmission of shortwave radiation through the atmosphere and increased cloudiness. The resistance generally decreased with increased wetness of the canopy, presumably because evaporation from the canopy and moss storage is not controlled by the stomata. As in *Betts et al.* [1999], a significant dependence of $r_c$ on the wind speed was found.

Multiple linear regression of $r_c$ against air temperature, wind speed, atmospheric pressure, relative humidity, incoming shortwave radiation, incoming longwave radiation, precipitation, net radiation, wetness index and clearness index showed that only five terms were significant. The resulting model explained 81.8% of the variance in $r_c$, giving

$$\begin{array}{rcccccc} r_c & = & 893 & -7.82RH & -26.8U & -8.80WS & -0.435R_s \quad +7.86T_a \\ & & \pm 41 & \pm 0.41 & \pm 3.1 & \pm 2.35 & \pm 0.087 \quad \pm 1.03 \end{array} \tag{5.4}$$

where $RH$ is the relative humidity in %, $WS$ the wetness index as defined above, $R_s$ the total incoming shortwave radiation in W/m$^2$, and $U$ and $T_a$ as before. The values in the second line are the standard errors of the regression coefficients. Unlike in *Betts et al.* [1999], nonlinear terms such as $T_a^2$ and products of the radiative flux and the wetness index were not found to be significant in the regression. *Betts et al.* used 30-min data, consequently their data set was much larger.

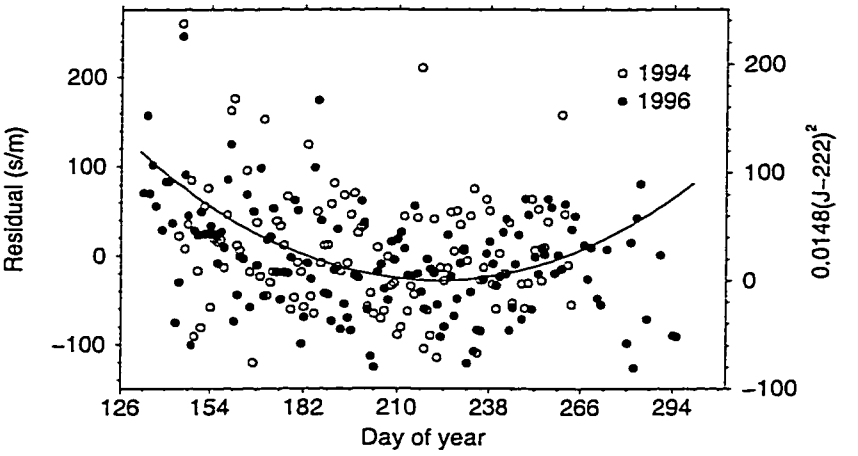


Figure 5.8: Model residuals by year according to (5.4) with superimposed the $J$-terms in (5.6) as a function of day of year.

The predicted latent heat flux was much more strongly affected by a systematic bias at low $r_c$ values than at high $r_c$ values, because

$$\frac{\partial LE}{\partial r_c} = -\frac{1}{(1+\Delta/\gamma)\, r_a + r_c} LE. \tag{5.5}$$

To avoid extremely high predicted latent heat fluxes for estimated $r_c$ values much lower than those observed, the calculated $r_c$ value was set to a minimum value ($r_c^{min}$) if it was smaller than this minimum. The minimum resistance was set to 80% of the lowest observed $r_c$ value. For the mature black spruce site $r_c^{min}$ was set to 25 s/m.

Although none of the other meteorological variables improved the regression, the model residuals clearly showed a dependence on the day of the year (Figure 5.8). They decreased during the first part of the growing season, reached a minimum around the beginning of August and then slowly increased again. Inclusion of a linear and quadratic day of year ($J$) term in the regression, improved the explained variance to 84.4% and reduced the residual standard error from 64.3 to

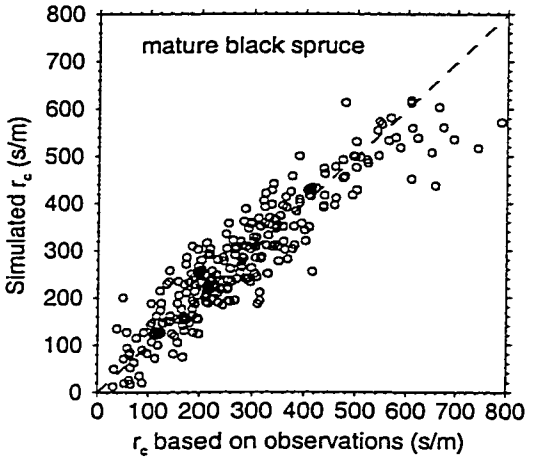


Figure 5.9: Observed and simulated $r_c$ at the mature black spruce site.

59.9 s/m. The resulting model was

$$\begin{array}{rcccccccc} r_c & = & 1489 & -6.89RH & -27.9U & -10.3WS & -0.436R_s & +11.8T_a & -6.57J & +0.0148J^2 \\ & & \pm 125 & \pm 0.43 & \pm 2.9 & \pm 2.3 & \pm 0.084 & \pm 1.3 & \pm 1.48 & \pm 0.0036 \end{array} \quad (5.6)$$

The bias in the mean was +1.5 s/m (n = 259), with a root mean squared error (RMSE) of 58.8 s/m (note that the bias was introduced by imposing $r_c^{min}$, the multiple linear regression model itself was unbiased). Equation (5.6) underpredicted $r_c$ for the highest $r_c$ values (Figure 5.9) many of which occur near the beginning of the growing season in May, or near the end in September. *Betts et al.* [1999] also found that their regression model for $r_c$ underestimated the highest $r_c$ values.

The sum of the $J$ and $J^2$ terms in (5.6) reaches a minimum for $J = 222$ or approximately August 10. The soil temperature at 0.2 m at the mature black spruce site is above 0°C for about 5 months of the year and reaches a maximum of about 11°C in the first week of August, both in 1994 and 1996. Soil temperature at 0.5 m reaches its maximum about 1 week later. Although

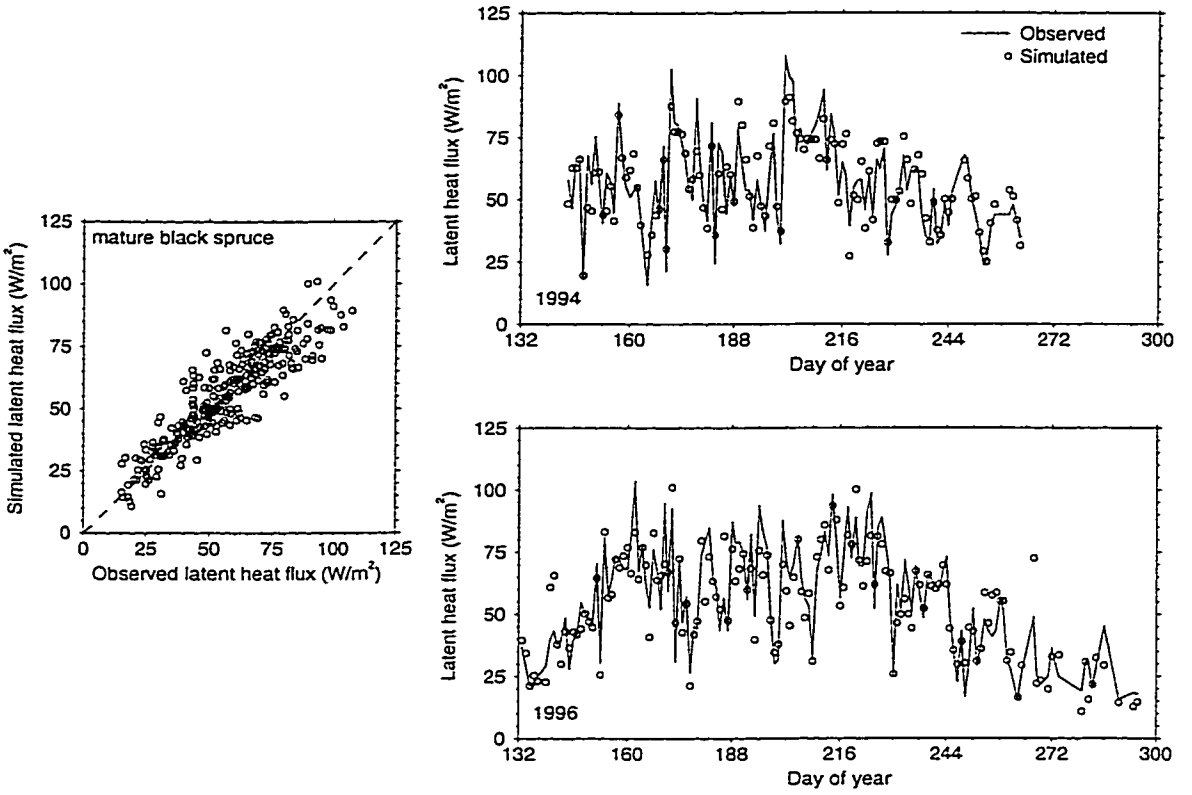


Figure 5.10: Observed and simulated latent heat at the mature black spruce site for the snow free periods in 1994 and 1996.

correlation does not indicate causality, the increased temperatures in the root zone may facilitate water uptake by the shallow rooting black spruce trees. *Grelle et al.* [1999] in a study of surface conductance and evaporation at the NOPEX Norunda site in central Sweden [e.g. *Grelle et al.*, 1997], also found that monthly variations in the surface conductance showed low resistances in the summer and high resistance in the winter. In their case, high resistances in the spring of 1996 were attributed to the very cold winter of 1995–1996 (at the NOPEX site) and potential root and foliage damage. Given that the residuals in Figure 5.8 are highest in the spring, a similar explanation may be valid for the BOREAS mature black pine site.

Figure 5.10 shows the observed and simulated latent heat flux, where the latter was simulated

using the estimated net radiation and $r_c$ according to (5.6). The calculated latent heat flux explained 80.3% of the variance in the observed latent heat flux. The bias in the mean was -1.6% or -0.9 W/m$^2$ (about 0.03 mm/day in equivalent water depth) with an RMSE of 9.1 W/m$^2$ (16.3%).

*Mature aspen*

The mature aspen site was located west of the White Gull Creek basin (Figure 5.1) in the Prince Albert National Park. The vegetation at the aspen site was representative of the dominant deciduous forest type in the North American boreal forest. Flux data were collected during 1994 (February 2 – September 19 [*den Hartog et al.*, 2000]) and 1996 (April 20 – December 31 [*Black and Nesic*, 2000]). Mean daily latent heat fluxes were available for 363 days (173 in 1994 and 190 in 1996). The data were filtered for those periods when the aspen canopy was developed (June 11 – September 16, but note that leaf growth continued until mid-July [*Blanken et al.*, 1997]). In addition, we required that $LE > 15$ W/m$^2$ and that $r_c < 400$ s/m. The final data set contained 162 values, of which 75 in 1994 and 87 in 1996. No attempt was made to separate the hazelnut understory, which accounted for 25% of the forest evaporation [*Blanken et al.*, 1997], from the aspen overstory. Instead, a bulk canopy conductance was calculated.

The $r_c$ values at the mature aspen site were generally much lower than at the coniferous sites. *Blanken et al.* [1997] noted that the aspen canopy had a large maximum canopy conductance, larger than most forests and more similar to well-watered crops. The multiple linear regression model relating $r_c$ to environmental conditions explained 80.7% of the variance in $r_c$, giving

$$\begin{array}{rcccccccc} r_c & = & 1384 & -2.82RH & -23.5U & -0.931Rs & +8.84T_a & +298CX & -9.91J & +0.0225J^2 \\ & & \pm 193 & \pm 0.34 & \pm 2.7 & \pm 0.225 & \pm 0.95 & \pm 92 & \pm 2.16 & \pm 0.0054 \end{array} \qquad (5.7)$$

For high values of the clearness index $CX$, the sky was mostly clear, and most of the incoming shortwave radiation was direct beam radiation, while for low values most of the incoming shortwave radiation was diffuse. The increase in $r_c$ with increased $CX$ occurred because diffuse

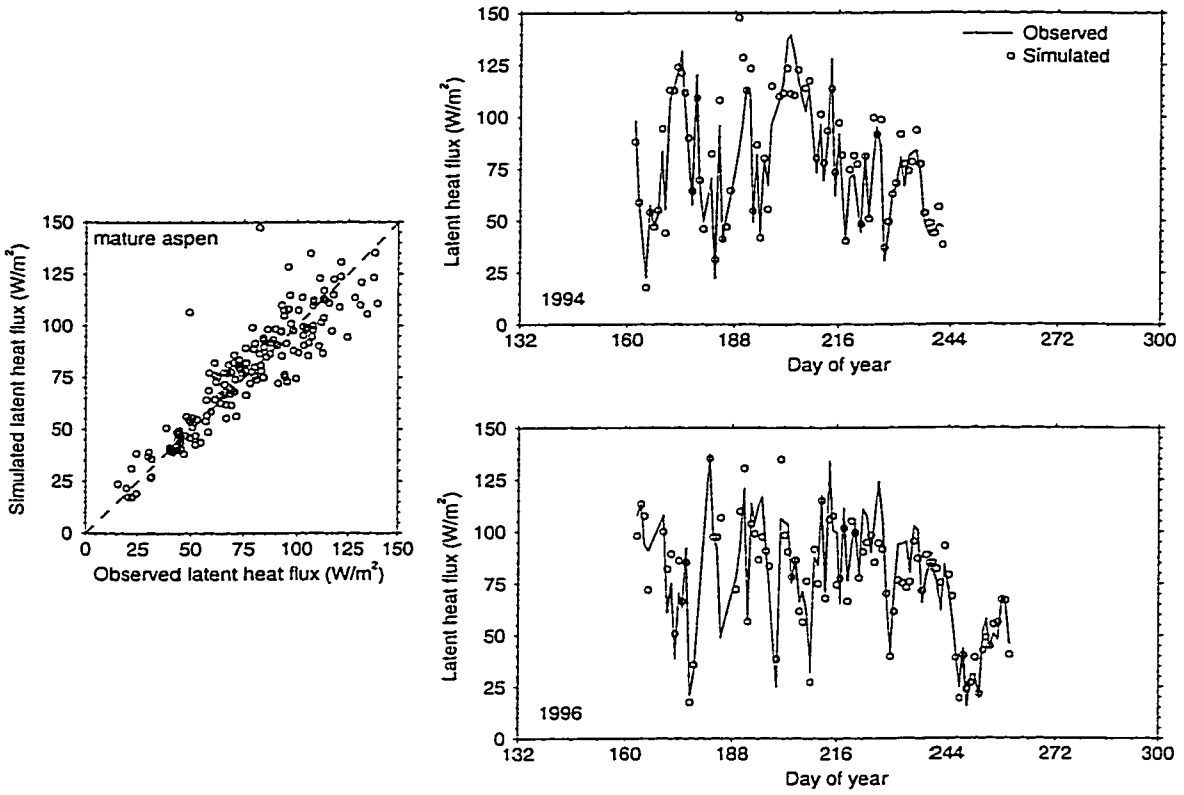


Figure 5.11: Observed and simulated latent heat at the mature aspen site for the periods in 1994 and 1996 when the canopy is fully developed.

radiation penetrates the canopy more efficiently than direct radiation [*Goulden et al.*, 1997; *Nijssen and Lettenmaier*, 1999]. Thus at the same radiation level, the canopy will photosynthesize and hence transpire more when the radiation is diffuse. The minimum canopy resistance $r_c^{min}$ was set to 20 s/m. Addition of the $J$ terms increased the explained variance from 75.7% to 80.7% and reduced the residual standard error from 31.4 to 28.1 s/m. The contribution of these terms to $r_c$ reaches a minimum around day 204 (July 23). The strong relationship between the canopy resistance and humidity or vapor pressure deficit at the aspen site was also noted by *Blanken et al.* [1997] and *Hogg and Hurdle* [1997].

Figure 5.11 shows the observed and simulated latent heat flux, where the latter was simulated

using the estimated net radiation and $r_c$ according to (5.7). The bias in the mean is +3.2 W/m$^2$ (4.1%) during 1994 ($n = 75$), -1.8 W/m$^2$ (-2.3%) in 1996 ($n = 87$), and 0.5 W/m$^2$ (0.7%) for the entire period ($n = 162$), with an RMSE of 12.3 W/m$^2$ (15.8%), 11.8 W/m$^2$ (15.0%) and 12.0 W/m$^2$ (15.4%), for the respective periods. The modeled latent heat flux explained 82.7% of the variance in the observations.

*Blanken et al.* [1997] found that the mean daytime dry-canopy conductance ($g_c$) at the aspen site was linearly related to the total LAI at the site ($g_c = aLAI + b$). Because the intercept $b$ was small compared to the product $aLAI$, the canopy resistance was approximately inversely proportional to the total LAI. The assumption was made that LAI increased linearly in spring between leaf emergence in the third week of May and the middle of June and decreased linearly in the fall between the start of senescence in the middle of September and the end of October. The canopy resistance for these periods was estimated using

$$r_c = r_{c*} \frac{LAI_*}{LAI_t}, \tag{5.8}$$

where $r_{c*}$ is the canopy resistance calculated according to (5.7), $LAI_*$ is the total forest LAI in the middle of June and at the start of senescence (set at 80% of maximum LAI), and $LAI_t$ is the estimated LAI at time $t$.

*Mature jack pine*

The mature jack pine site was located in the eastern part of the White Gull Creek basin, about 7.5 km northwest of the SW1 gauge. The vegetation at the site consisted of a 13.5 m high jack pine stand (LAI 1.9–2.2) with a sparse understory vegetation consisting of bearberry, cranberry and lichen [*Baldocchi et al.*, 1997]. Flux measurements were collected from May 23–September 16, 1994 [*Baldocchi and Vogel*, 2000]. Mean daily flux measurements were available for 79 days. As for the mature black spruce, the observations were filtered for conditions when $LE > 15$ W/m$^2$ and $0 \leq r_c < 1000$ s/m, leaving 75 days in the final data set.

The canopy resistance model explained 78.3% of the variance in the observations and was

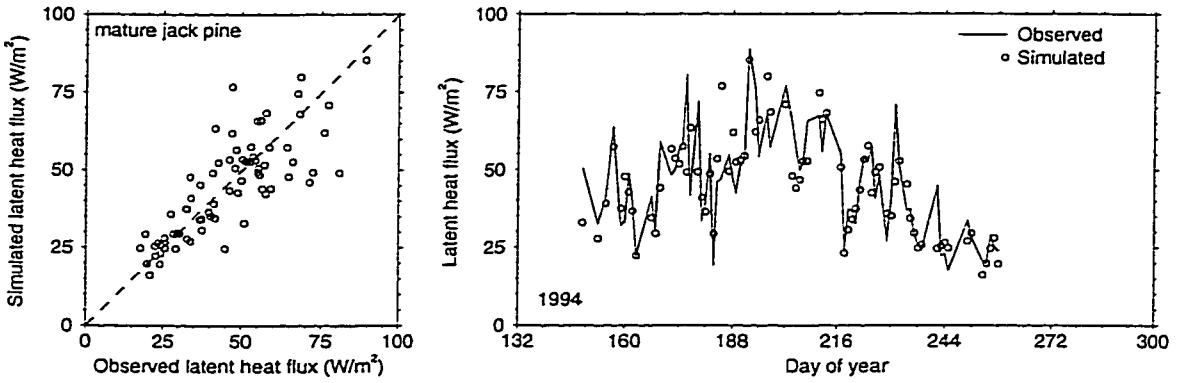


Figure 5.12: Observed and simulated latent heat at the mature jack pine site for the 1994 growing season.

given by

$$\begin{array}{rcccccccc} r_c & = & 2212 & -15.4RH & -31.6WS_* & -7.18R_s & +3.41R_n & +1998CX & -3.02J \\ & & \pm 273 & \pm 2.0 & \pm 8.4 & \pm 1.59 & \pm 1.17 & \pm 466 & \pm 1.00 \end{array}, \quad (5.9)$$

where $WS_*$ a wetness index similar to the one above, except that $WS_*$ was calculated based on the precipitation on the same day (whereas $WS$ in (5.6) is calculated based on the precipitation on the previous day). The minimum canopy resistance $r_c^{min}$ was set to 30 s/m. Unlike at the mature black spruce site, $r_c$ showed no temperature or wind speed dependence.

Figure 5.12 shows the observed and simulated latent heat flux, where the latter was simulated using the estimated net radiation and $r_c$ according to (5.9). The bias in the mean was -0.8 W/m$^2$ (-1.8%) during 1994 ($n = 75$), with an RMSE of 10.2 W/m$^2$ (22.4%). Despite the low bias, the modeled latent heat flux explained only 64.1% of the variance in the latent heat observations.

*Fen*

The fen site was located near the southeastern corner of the basin, 7 km due south of the SW1 stream gauge (Figure 5.1). The site was a minerotrophic, patterned fen, surrounded by black

spruce and jack pine forests. The fen was about 4000 m long in the north-south direction, and about 450 m in the east-west direction [*Suyker et al.*, 1997, 1996]. The vegetation at the fen was at most 0.5–1.5 m high, and the mean surface height was approximately 0.06 m above the mean hollow depth. The flux tower was located near the eastern edge of the fen and *Suyker et al.* [1997] state that acceptable wind directions for eddy correlation measurements were from 190°to 360°. However, because data were aggregated to daily fluxes and the wind speed varied throughout the day, we included all flux measurements in our daily averages. Flux measurements were collected from May 18 – October 7, 1994 and May 18 – October 9, 1995, with an interruption from June 1 – June 20, 1995 due to a nearby forest fire [*Verma et al.*, 2000]. Mean daily flux measurements were available for 258 days. The observations were filtered for conditions when $LE > 15$ W/m$^2$ and $r_c < 400$ s/m. However, the fen site was the only site where $r_c$ calculated from the observations using (5.2) was negative for a large number of days (39). Further inspection showed that 30 of these negative $r_c$ values occurred on rainy days. *Verma et al.* [2000] noted that dew or rain caused aberrant signals in some of the sensors at the fen site, and heavy dew or rain would cause complete deterioration of these signals. We therefore excluded all rainy days from the data set at the fen site and required that $r_c \geq 0$, leaving a total of 129 days of which 63 in 1994 and 66 in 1995.

The canopy resistance model explained 65.3% of the variance in the observations and was given by

$$\begin{array}{rcccccc} r_c & = & 892 & +0.103\Delta e & -1.55R_s & +812CX & -7.85J & +0.0155J^2 \\ & & \pm 191 & \pm 0.016 & \pm 0.51 & \pm 205 & \pm 2.31 & \pm 0.0066 \end{array}, \qquad (5.10)$$

with $r_c^{min}$ set to 6.5 s/m. As at the mature jack pine, dependence on windspeed was largely absent. Canopy resistance values at the fen site were much lower than those at the coniferous sites, and were similar to those at the mature aspen site. Consequently, evapotranspiration at the fen site was generally higher than at the coniferous forest sites and similar to that at the mature aspen site. The explained variance was slightly higher when using $\Delta e$ in the regression equation than when using both $RH$ and $T_a$.

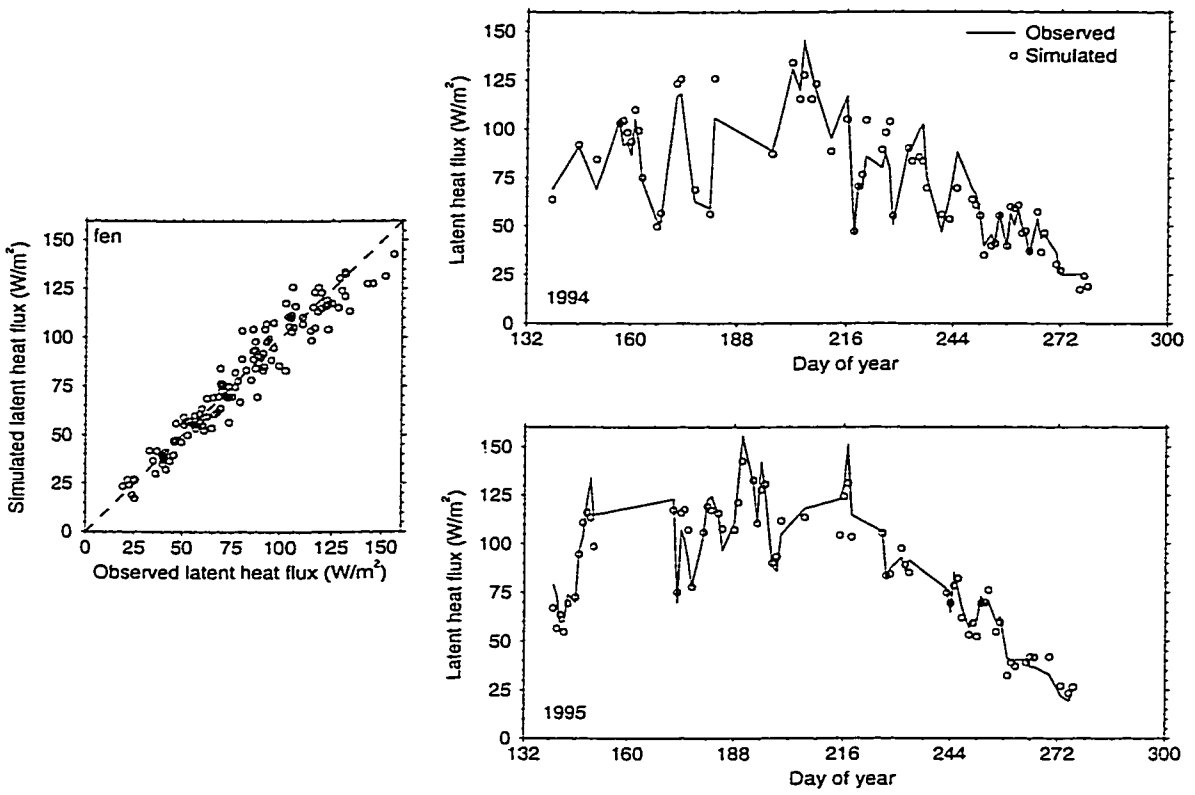


Figure 5.13: Observed and simulated latent heat at the fen site during the 1994 and 1995 growing seasons.

Figure 5.13 shows the observed and simulated latent heat flux, where the latter was simulated using the estimated net radiation and $r_c$ according to (5.10). The bias in the mean was +0.3 W/m$^2$ (0.4%) during 1994 ($n = 63$), -1.8 W/m$^2$ (-2.1%) in 1995 ($n = 66$), and -0.8 W/m$^2$ (-1.0%) for the entire period ($n = 129$), with an RMSE of 8.6 W/m$^2$ (11.8%), 8.0 W/m$^2$ (9.2%) and 8.3 W/m$^2$ (10.4%), for the respective periods. The modeled latent heat flux explained 93.4% of the variance in the observations.

Inclusion of all points for the fen site ($n = 257$), that is, including the days originally filtered out, resulted in a bias in the latent heat flux of -0.67 W/m$^2$ (-0.9%), an RMSE of 11.1 W/m$^2$ (15.3%), and an explained variance of 88.7% (Figure 5.14).

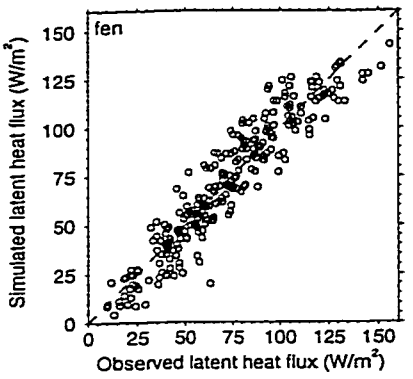


Figure 5.14: Observed and simulated latent heat at the fen site during the 1994 and 1995 growing seasons including all points.

*Young aspen and young jack pine*

Two flux towers were located in a young aspen and a young jack pine stand during part of the 1994 growing season. The records at these towers were short, which made it difficult to develop separate $r_c$ models. Instead, data from these two sites were used to evaluate whether the $r_c$ models developed for the mature aspen and the mature jack pine sites could be used to simulate the canopy resistance and consequently the latent heat flux at the other sites, which had similar vegetation types, but differed in developmental stage. The $r_c$ values based on (5.7) and (5.9) were scaled according to the LAI value following (5.8), with $LAI_*$ and $LAI_t$ replaced by the LAI values at the original and transfer sites, respectively. LAI values for the sites were based on an interpreted Landsat Thematic Mapper image from August 9, 1991 as explained in more detail in Section 5.5.3.

The young aspen site was located southwest of the White Gull Creek basin (Figure 5.1). The flux tower was placed in a clearing of $1 \times 2$ km, covered by dense young aspen with a mean height of 2.5–3 m. The site was surrounded by mature aspen and jack pine with heights up to 20 m [*Bessemoulin*, 2000]. Flux measurements were made from July 18 – September 20, 1994. Mean daily latent heat fluxes were available for 53 days. Senescence started in the beginning of September, as evidenced by the sharp increase in $r_c$ values. The same data filter was applied as

for the mature aspen site, leaving 44 mean daily latent heat fluxes. The LAI value for the young aspen site was estimated as 2.51, while that at the mature aspen site was 2.60 [*Chen et al.*, 1997b].

Figure 5.15a shows a scatterplot of the observed and simulated latent heat flux at the young aspen site. The simulated values had a bias of 5.69 W/m$^2$ (7.1%), an RMSE of 12.1 W/m$^2$ (15.1%), and explained 88.6% of the variance in the observations. This is comparable to the results at the mature aspen site, although the bias is larger. According to *Bessemoulin* [2000], the main source of measurement error at the young aspen site came from the Campbell hygrometer, which did not work correctly when the windows were wet (25 out of 44 days showed some precipitation). In addition, the wind term in (5.8) is likely to be different at the young aspen site, which has a much smaller canopy height (3 m versus 21.5 m at the mature aspen site).

The young jack pine was located about 5.5 km southeast of the mature jack pine site (Figure 5.1). The flux tower was placed in a 11–16 year old jack pine stand, with a height of 4–5 m. Flux data were collected from May 26 – September 20, 1994 [*Anderson et al.*, 2000]. Flux data were missing for a few hours a day for many days (particularly at night), and because of our strict screening criteria, only 35 mean daily latent heat fluxes were available. All 35 values passed the same data filter that was used for the mature jack pine site. The LAI value for the young jack pine site was estimated as 2.85, while that at the mature jack pine site was 2.40 (see Section 5.5.3).

The resulting observed and simulated latent heat flux estimates are shown in Figure 5.15b. The simulated values had a bias of -19.9 W/m$^2$ (-30.0%), an RMSE of 24.6 W/m$^2$ (37.1%), and explained only 60.5% of the variance in the observations. Although the explained variance is only slightly worse than at the mature jack pine, the bias and RMSE are much larger. It is not clear why this estimate is so much worse than at the aspen site. The young jack pine shows a much greater latent heat flux than the mature jack pine, despite having comparable LAI values. For the 26 coincident days for which observed mean daily latent heat fluxes were available for both sites, the mean flux was 40.9 W/m$^2$ at the mature jack pine site and 71.0 W/m$^2$ at the young jack pine site (simulated means 39.7 W/m$^2$ and 49.1 W/m$^2$, respectively). The sites were located within 5.5 km of each other at about the same elevation, and meteorological factors are therefore unlikely

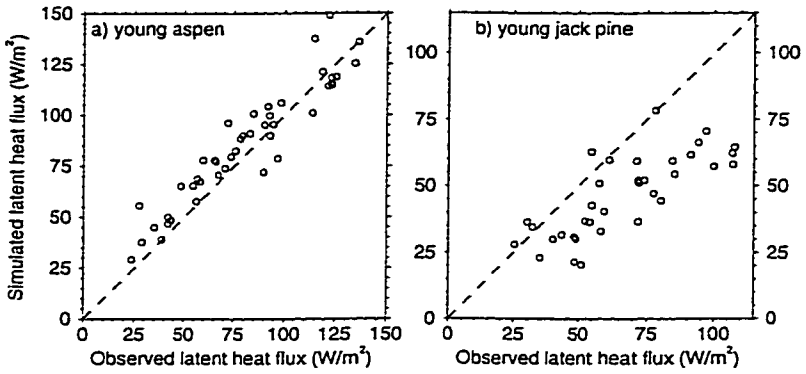


Figure 5.15: Observed and simulated latent heat at the a) young aspen and b) young jack pine sites.

to explain the difference. To obtain an unbiased estimate for the latent heat flux at the young jack pine site, the $r_c$ values needed to be about half those at the mature jack pine site. *Moore et al.* [2000], in a study of the growing season water balance at the mature jack pine stand in the BOREAS northern study area, reported that evaporation rates at their site were similar to those at the mature jack pine stand in the southern study area, despite smaller LAI, basal area and a more northernly location. They concluded that evapotranspiration did not scale with LAI at the jack pine sites.

*Winter-time evaporation*

The above models could only be used when the ground was snow-free. During the winter time, the vegetative resistance calculated using (5.2) increased rapidly, because the vegetation no longer transpired. However, *Grelle et al.* [1999] noticed at the NOPEX boreal forest site in Sweden that significant evaporation occurred even for air temperatures below 0°C. At their site evaporation during the winter season sometimes reached as high as 0.5 mm/day (about 14.5 W/m$^2$). Measurements taken at the mature black spruce and mature aspen site during snow covered periods in 1994 and 1996 showed small latent heat fluxes during the period November–March, which

rapidly increased during April and May. The mean measured latent heat flux at the mature aspen site during the period November–March was 3.43 W/m$^2$ ($n = 54$) and ranged from 0.2 W/m$^2$ to 11.9 W/m$^2$. Similarly, the measured flux at the mature black spruce site averaged 4.11 W/m$^2$ ($n = 37$), with a low of 0.9 W/m$^2$ and a high of 13.2 W/m$^2$. In this study, winter-time evaporation (November–March) was assumed constant at 4 W/m$^2$ (about 0.14 mm/day) for all sites.

*Harding and Pomeroy* [1996] reported a mean latent heat flux of 80 W/m$^2$ over a 36-hour period in March 1994 at a mature jack pine site in the BOREAS southern study area. This is equivalent to a water loss of 4 mm over the 36 hour period. These high fluxes occurred while the air temperature was near 0°C, wind speeds of about 4 m/s, and with a substantial load of snow intercepted by the jack pine canopy. During the snow melt period in April and early May evaporation increased as both the day length and temperature increased. Evaporation rates during this period were generally somewhat higher at the mature black spruce site than at the leafless mature aspen site. Evaporation at the black spruce averaged about 23.1 W/m$^2$ ($n = 42$), with a high of 67.8 W/m$^2$ and a low of 6.0 W/m$^2$. At the aspen site the mean evaporation was 13.6 W/m$^2$ ($n = 58$), with a high of 33.3 W/m$^2$ and a low of 2.9 W/m$^2$. Because none of the meteorological variables were strongly correlated with the evaporation, a constant evaporation rate of 23 W/m$^2$ was assumed for the black spruce site and 14 W/m$^2$ for the mature aspen site during the period from April 1 till the end of snow melt. The winter evaporation rate at the mature black spruce was used for all coniferous vegetation types, while the mature aspen evaporation was used for all other land cover types.

### *5.5.3 Areal Evaporation Estimate*

An areal estimate of daily evapotranspiration over the White Gull Creek basin was calculated by applying the LAI-weighted versions of equations (5.6), (5.7), and (5.10) to each 2 × 2 km grid cell covering the basin. The resulting evapotranspiration estimates were area-weighted according to the fraction of each grid cell covered by each vegetation type. Finally, the grid cell estimates were summed over the basin. No LAI-weighting was applied to the $r_c$ model for the mature jack

pine site, following the discussion in Section 5.5.2, because factors other than LAI appeared to determine the relative amount of evaporation between the jack pine sites.

Vegetation cover fractions were based on a classified Landsat Thematic Mapper (TM) image from September 2, 1994 [*Hall et al.*, 1997; *Hall*, 2000]. The high-resolution TM-based vegetation classification (spatial resolution about 30 m) offered an important advantage over the coarser Advanced Very High Resolution Radiometer (AVHRR) based classification (spatial resolution about 1 km) [*Steyaert et al.*, 1997]. Fen, bogs, small water bodies and small patches of dry jack pine could not be resolved within the wet conifer mosaic in the AVHRR classification. As a result the TM-based classification showed that about 1.00% of the southern study area (which encompasses the White Gull basin) was covered by dry conifer (mainly mature jack pine) and 7.63% by fen, while the AVHRR-classification showed the sum of the two classes to be about 1.54% [*Steyaert et al.*, 1997]. Similar results were found by *Potter et al.* [1999]. The White Gull Basin contained an even greater percentage of fen areas (12.9%, see Table 5.2). Because these vegetation types had very different evapotranspiration characteristics, it was important to distinguish the fen and wetland areas from the coniferous vegetation. Vegetation classes were mapped from the 13 vegetation classes defined by *Hall et al.* [1997] to black spruce, jack pine, aspen, fen and water as specified in Table 5.2.

The LAI for each vegetation type within each 2 × 2 km grid cell was based on an interpreted TM-image from August 9, 1991, which provided LAI values for each pixel [*Chen and Cihlar*, 1996; *Chen*, 1996; *Chen and Geng*, 2000]. This high-resolution LAI image (about 30 m) was combined with the vegetation image from *Hall et al.* [1997]. Although the two images had the same resolution, they were in different map projections. Consequently there was no direct one-to-one mapping between the vegetation type and the LAI. To minimize registration errors associated with reprojecting one of the images, the following procedure was used to calculate a cell average LAI for each vegetation type.

The LAI image was transformed to the same projection as the vegetation image. Next, the dominant vegetation type and the mean LAI were calculated for each 100 × 100 m (1 ha) area

Table 5.2: Remapping of the land cover classes defined in *Hall et al.* [1997], and the fraction of the White Gull Creek basin covered by each type.

| Land cover type defined in *Hall et al.* [1997] | | Land cover type used in this study | |
|---|---|---|---|
| Vegetation type | area (%) | Vegetation type | area[a] (%) |
| conifer (wet) | 37.20 | black spruce | 63.53 |
| new regeneration conifer | 2.26 | | |
| medium age regeneration conifer | 18.51 | | |
| mixed[b] | 7.92 | | |
| deciduous | 5.48 | aspen | 13.38 |
| new regeneration deciduous | 3.53 | | |
| medium age regeneration deciduous | 0.07 | | |
| mixed[*] | 7.92 | | |
| conifer (dry) | 6.20 | jack pine | 6.36 |
| fen | 12.91 | fen | 13.24 |
| water | 3.40 | water | 3.49 |
| disturbed | 2.40 | These land cover types occupied only | — |
| fire blackened | 0.09 | small portions of the basin and were | |
| grass | 0.02 | disregarded. The area they occupied | |
| | | was proportionally divided among the | |
| | | other land cover types weighted by area. | |

[a]Rescaled to total 100%

[b]Divided equally between black spruce and aspen

within each grid cell. If the dominant vegetation within a 1 ha area accounted for more than 80% of the area, the area was taken to be representative of that vegetation type and labeled as "pure". For each vegetation type within each grid cell, the LAI values of all "pure" 1 ha areas were averaged to obtain a grid cell average LAI. If a grid cell contained a vegetation type, but did not contain any "pure" pixels with that vegetation, the LAI for that vegetation type was taken from the surrounding grid cells. The LAI values for the tower sites were determined from the image in a similar manner. Within a square of 1100 × 1100 m, with the flux tower in the center cell, the above method was used to locate all "pure" pixels with the same vegetation type as the tower site. The LAI value at the tower site was then taken as the average of these cells. The resulting LAI values corresponded closely with those reported by *Chen et al.* [1997b]. Unfortunately, the mature

Table 5.3: LAI values at the tower flux sites as determined from the August 9, 1991 Landsat TM image [*Chen and Geng*, 2000]. The last column shows the number of "pure" cells of the vegetation type at the tower within the 1100 × 1100 m area surrounding the tower (see text for details). For vegetation types see Table 5.2.

| Tower flux site | LAI value | Number of "pure" cells ($n$) for each vegetation type |
|---|---|---|
| mature aspen* | 2.60 | — |
| young aspen | 2.51 | $n = 42$ (type 11) |
| mature black spruce | 4.36 | $n = 53$ (type 1) |
| mature jack pine | 2.40 | $n = 36$ (type 2) |
| young jack pine | 2.85 | $n = 4$ (type 9), $n = 3$ (type 10) |
| fen | 2.25 | $n = 4$ (type 5) |

* LAI value from *Chen et al.* [1997b]

aspen tower flux site fell outside the LAI image of *Chen and Geng* [2000]. The value for this site was therefore taken from *Chen et al.* [1997b].

About 3.40% of the area of the White Gull Creek basin was covered by open water (Table 5.2). No flux towers were operated over open water surfaces. Open water evaporation was estimated using (5.1), assuming $r_c = 0$ s/m, a displacement height of 0 m and a roughness length of 0.01 m [*Shuttleworth*, 1993].

Vegetation heights and albedos were set to the values at the tower flux sites (Table 5.1), with the heights for new and medium age regeneration conifer set at 3 and 7 m, respectively, and for new and medium age deciduous set at 3 and 10 m, respectively.

Figure 5.16 shows the mean estimated evapotranspiration during 1994 for each of the vegetation types, averaged over the White Gull Creek basin. The annual totals for each of the vegetation types are given in Table 5.4. Despite the year-to-year variations in precipitation, evapotranspiration varied slightly over the three years. Annual evapotranspiration over the White Gull basin was estimated at 338, 345, and 351 mm/year for 1994, 1995, and 1996, respectively (Figure 5.17). The highest evaporation estimates were for the open water surface, and were likely biased high, because water temperatures as estimated from the air temperature, which in turn were interpolated

Table 5.4: Mean annual estimated evapotranspiration over the White Gull Creek Basin by vegetation type.

| Vegetation type | Evapotranspiration (mm/year) | | |
|---|---|---|---|
| | 1994 | 1995 | 1996 |
| mature black spruce | 315 | 320 | 324 |
| medium-age regeneration coniferous | 279 | 287 | 292 |
| new regeneration coniferous | 212 | 226 | 229 |
| mature aspen | 422 | 437 | 458 |
| medium-age regeneration deciduous | 345 | 360 | 381 |
| new regeneration deciduous | 337 | 356 | 376 |
| mixed | 387 | 398 | 411 |
| mature jack pine | 250 | 240 | 243 |
| fen | 489 | 502 | 496 |
| water | 599 | 585 | 617 |
| White Gull Creek Basin | 338 | 345 | 351 |

from the towers, were likely biased upward. A lower water temperature would mean a lower saturated vapor pressure above the water surface, and consequently a smaller vapor pressure gradient between the water surface and the measurement level. However, only 3.49% of the White Gull Creek basin is covered by open water and the effect on the basinwide evapotranspiration estimate is consequently small under normal conditions.

The next highest evapotranspiration estimates were for the fen areas, whose evaporation totals were intermediate between those for open water and mature aspen. Most of this excess evapotranspiration in the fen areas as compared to the aspen forest occurred in late spring, when the aspen trees were still developing their canopies. The mature black spruce forest which occupied about 37.2% of the area showed a higher annual evapotranspiration than the mature jack pine forest, which grew in drier upland areas. The lowest evapotranspiration was estimated for the new regeneration coniferous forest, with an average LAI of 2.2 (as compared to 4.4 for the mature black spruce).

The annual evaporation estimates for the mature aspen site compared favorably with those from *Barr et al.* [2000], who reported evapotranspiration estimates at the mature aspen site for

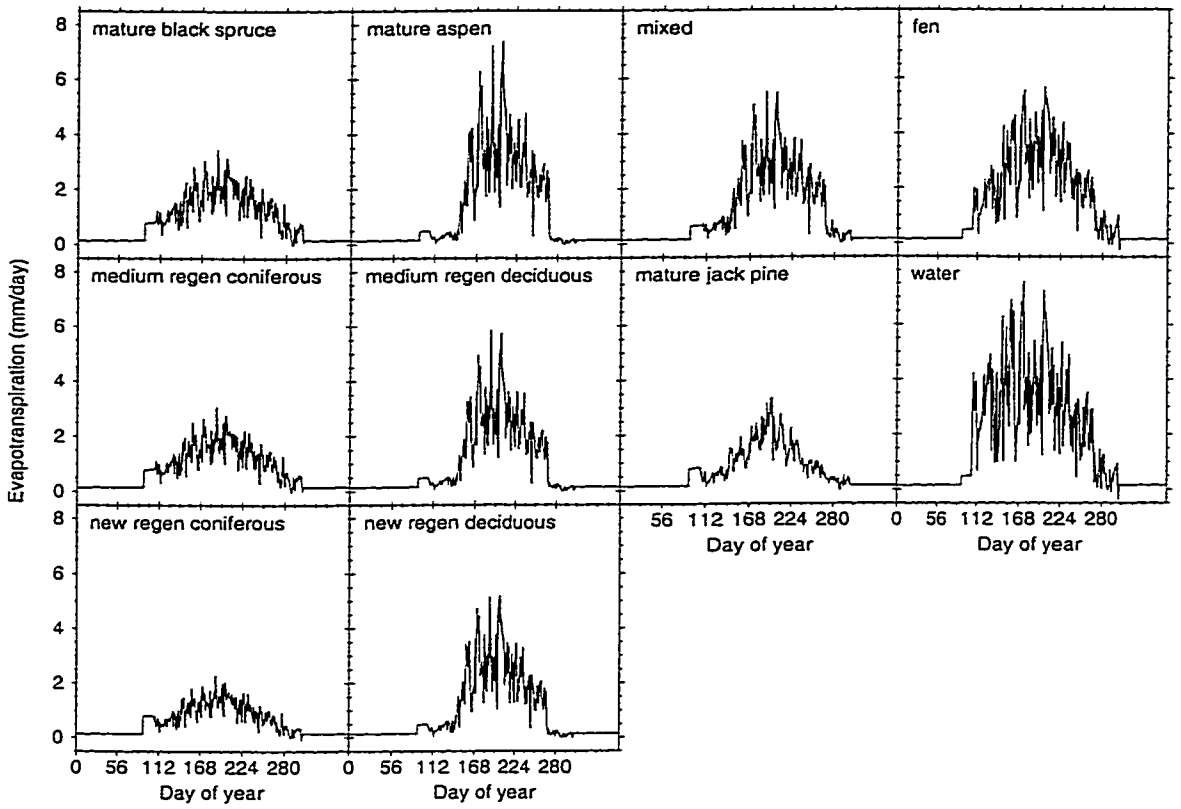


Figure 5.16: Mean daily evapotranspiration for each vegetation type during 1994, averaged over the White Gull Creek basin.

1997 and 1998. *Barr et al.* used a deep groundwater piezometer below the mature aspen site, which effectively integrated the mass loading over an area of about 10 ha. The piezometer-based evaporation estimates coincided to within 8% with those from eddy-correlation measurements. The piezometer-based evapotranspiration estimates ranged from 808 to 898 mm for the two year period 1997–1998, or 404 to 449 mm/year. Piezometer-based maximum daily evapotranspiration estimates were about 6.5 mm/day, although maximum eddy-correlation based estimates were no greater than about 5.5 mm/day. Evapotranspiration was very small from November through April, and reached a maximum during June–August. The average LAI for mature aspen over the White Gull Creek basin was 3.2, as compared to 2.6 at the mature aspen flux tower site.

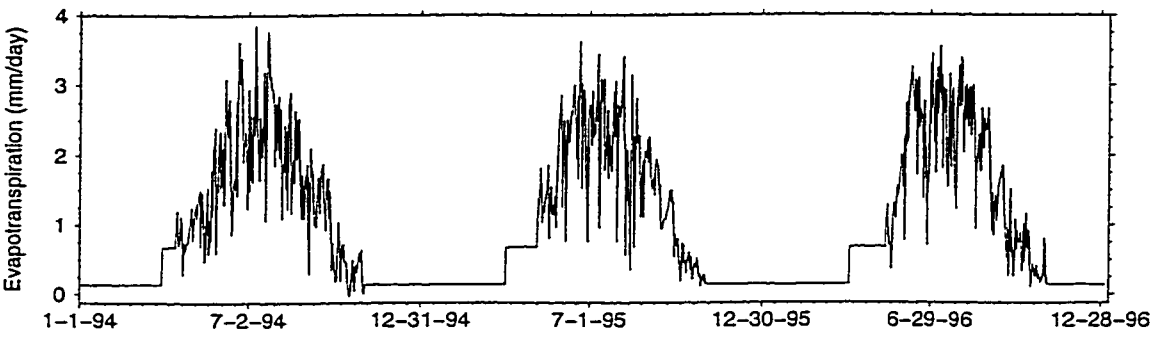


Figure 5.17: Mean daily evapotranspiration over the White Gull Creek basin, 1994–1996.

## *5.6 Storage*

The boreal landscape, with its wetlands and deep organic soils, provides a large amount of storage. The effects of this storage were evident in the hydrographs over the White Gull Creek basin. Streamflow response to precipitation was slow (Figure 5.2) and only occurred after extended periods of rainfall, after large precipitation events, and after snow melt. Following snow melt generated runoff in the spring of 1995, no significant streamflow events occurred during the remainder of the season, with total runoff for that year only 12% of precipitation. Most of the precipitation was stored within the basin and subsequently evaporated. Given the poorly developed channel network, it is likely that large portions of the basin are disconnected from the main drainage system for most of the year and only contribute to basin runoff after snow melt and during extreme events.

Figure 5.18 shows the water storage at the fen site and the soil moisture at the tower flux sites for the 1994 growing season. The fen collects water from the surrounding areas and the water level rises rapidly after medium to large rainfall events. The water level height was measured above the bottom of an average hollow [*Suyker et al.*, 1997]. The height of the hummocks in the fen ranged from 0.05 to 0.30 m above the average hollow surface, with a mean surface elevation of 0.06 m above the average hollow depth [*Suyker et al.*, 1997].

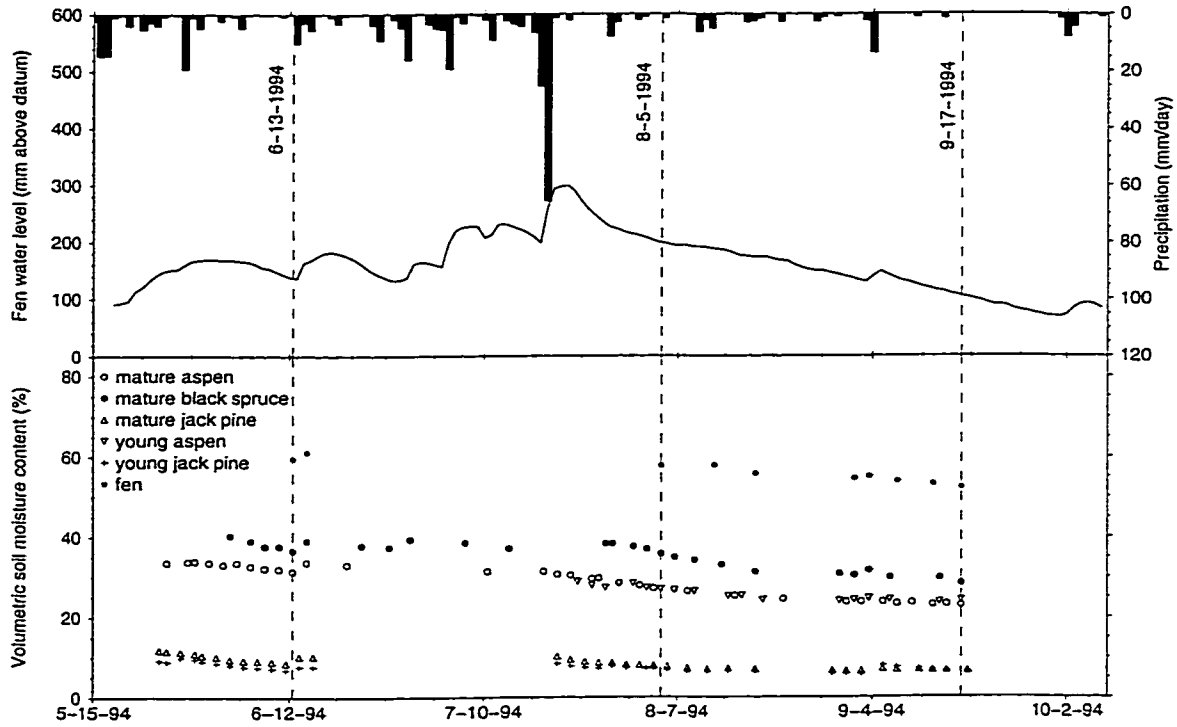


Figure 5.18: Water storage in the BOREAS southern study area. The top plot shows the water level at the FEN site and precipitation over the White Gull Creek basin [*Stuyker et al.*, 1997]. The bottom plot shows profile average volumetric moisture content at the flux tower sites [*Cuenca et al.*, 1997].

Soil moisture was measured by neutron probe and time domain reflectometry [*Cuenca et al.*, 1997]. The data in Figure 5.18 were integrated over the entire profile for which measurements were available, which was 1.2 m for the mature aspen, mature black spruce, young aspen and fen sites, 1.0 m for the young jack pine site and 1.7 m for the mature jack pine site. Unfortunately, few soil moisture observations were available from mid-June to late-July when the largest precipitation events occurred. Soil moisture contents were lowest at the jack pine sites, which were located on the sandy, well-drained upland sites [*Baldocchi et al.*, 1997; *Moore et al.*, 2000]. The highest soil moisture contents were measured at the fen site, where the substrate consisted of a thick peat layer (2–3 m in the center to 1 m on the edge).

Table 5.5: Annual water balance over the White Gull Creek Basin, 1994-1996.

| | Flux in (mm/year) | | |
|---|---|---|---|
| | 1994 | 1995 | 1996 |
| Precipitation | 537 | 391 | 465 |
| Discharge | 110 | 48 | 127 |
| Evapotranspiration | 338 | 345 | 351 |
| Δ Storage | 89 | -2 | -13 |

## *5.7 Synthesis and Discussion*

Table 5.5 shows the annual water balance of the White Gull Creek basin for the study period. The storage change was calculated as the residual of the measured precipitation and discharge and the estimated evapotranspiration. The sum of discharge and evaporation balanced the precipitation to within experimental error in 1995 and 1996. However, in 1994, precipitation exceeded the sum of discharge and estimated evapotranspiration by 89 mm. An important question is whether this "excess" precipitation was stored and carried over to the following years, or whether discharge and/or evapotranspiration in 1994 were underestimated.

Discharge forms only a minor component of the water balance in the White Gull Creek basin (Figure 5.19). During the period from June 28, 1994 till August 8, 1994, when discharge was the same as on June 28, 208 mm of precipitation fell on the White Gull Creek basin, 91 mm of which on July 18 and 19. During the same period the total discharge was only 49 mm, with a maximum discharge of 3.6 mm on July 21. Even early in the season after snow melt, total runoff remains small. In 1995, the main runoff peak occurred during the first half of May, but never exceeded 0.6 mm/day. Total runoff from the middle of April till the end of May was 23.4 mm in 1994, 18.3 mm in 1995 and 37.2 mm in 1996, with precipitation during those same periods of 96.4 mm, 40.5 mm, and 81.8 mm. Given maximum snow accumulation of 46 mm, 73 mm, and 71 mm (Section 5.4), most if not all snow is stored within the basin and replenishes storage depleted at the end of the previous growing season. In years with low summer precipitation such as 1995, a

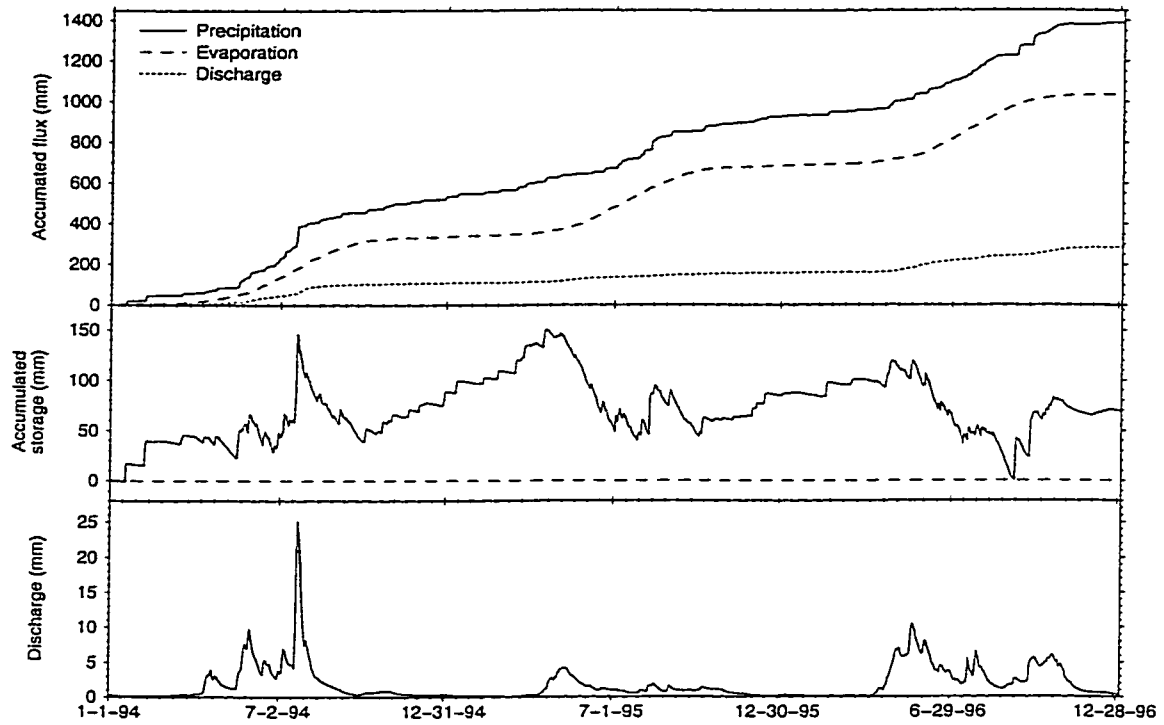


Figure 5.19: Accumulated fluxes, storage and discharge over the White Gull Creek basin, 1994–1996.

large part of the annual runoff is accounted for by snowmelt associated runoff. In 1994 the largest runoff event was associated with summer precipitation, while in 1996 the largest runoff occurred in the second half of May, as a result of both snow melt and about 27 mm of precipitation in the preceding week. Thus, most of the snowmelt water appears to be evaporated later in the summer, and does not directly contribute to stream flow.

If the "excess" precipitation in 1994 was stored within the basin, it did not contribute to increased discharge or evapotranspiration in the following two years. The net storage change over the three years was 74 mm. Figure 5.19 shows the accumulated fluxes and the estimated storage over the basin for the study period. Whereas in 1995 and 1996 storage in the basin reached a maximum at the end of the winter season, in 1994 storage reached a maximum in the middle of

summer, after a period of heavy precipitation in the first weeks of July (173 mm of precipitation fell during July 1994). This precipitation led to an increase in the fen water level from 165 mm above datum on July 1, 1994 to 299 mm above datum on July 23. However, a dry August and September (total precipitation 54 mm) dropped the fen water level to 68 mm above datum by October 1.

*Peck et al.* [1997], in a study of the soil moisture status of the BOREAS study area using gamma ray remote sensing, noted that field observations on September 9, 1993 showed considerable standing water to the north and northwest of the mature black spruce flux tower, whereas no standing water was observed in those areas in September, 1994, when the area had completely dried out. Soil moisture measurements in the BOREAS study southern area [*Cuenca et al.*, 1997] also indicated a steady dry-down during the 1994 growing season (Figure 5.18). Soil moisture contents during the 1994 growing season declined by about 100 mm from June 13 till September 17 at the black spruce, aspen and fen sites. Soil moisture changes at the jack pine sites were much smaller, because the well-drained sandy soils at those sites have a low water holding capacity. Surprisingly, the soil moisture content at the fen site declined by as much as 86 mm (integrated over the depth of the measurements), while the fen water level declined only by 23 mm.

This discrepancy between the fen water and the fen soil moisture calls into question the ability of soil moisture measurements to provide an adequate representation of the storage in the surrounding area. *Peck et al.* [1997] noted that the variability of the soil moisture and the water content of the moss layer was extremely high in the area surrounding the mature black spruce tower. The area to the southeast of the tower was much drier than the area to the north, northwest and southeast. The tower itself was also located in an area comparatively dry to much of the surrounding forest.

Basin discharge was reduced to pre-July levels by the second week of August, and was less than 1 $m^3/s$ (0.14 mm/day) after the first week in September (Figures 5.18 and 5.19). The water balance at the mature jack pine site between June 13 and September 17, 1994 consisted of 261 mm of precipitation, an estimated evapotranspiration of 155 mm, and a soil moisture storage change

of -35 mm, suggesting that 141 mm contributed to runoff and storage. Much of this water is likely to have been stored in the unsaturated zone above the water table. However, the mature jack pine forest only occupies about 6.2% of the area (Table 5.2). The aspen stands which occupy much of the remaining upland areas have a higher evapotranspiration, making less water available for storage and runoff than the jack pine trees.

Although some of the "excess" precipitation during 1994 may have contributed to recharge of a deeper-lying aquifer and the unsaturated zone in the upland areas, not enough information was available to determine the importance of these terms. It is unlikely that most of this "excess" precipitation contributed to interannual storage, because neither measured soil moisture, nor fen water level or discharge indicated an increased level of storage at the end of the 1994 growing season (Table 5.6). Consequently, errors in the precipitation and discharge measurements, or errors in the estimate of evapotranspiration remain as the most likely explanations of the "excess" precipitation in 1994. We analyze each of these possibilities in the remainder of this section.

Precipitation measurements almost invariably underestimate actual precipitation. Wind effects, wetting losses, and other systematic losses such as evaporation from the gauge during long, low intensity precipitation events can lead to significant errors [*Linsley et al.*, 1986]. However, an underestimation of precipitation would not help in explaining the "excess" precipitation during 1994 and it is difficult to think of a scenario that would lead to a consistent overestimation of precipitation. As discussed in Section 5.3, radar estimated precipitation in summer 1994 was greater than gauge precipitation. However, the radar-based rain estimate is likely to be somewhat higher than the gauge-based estimate, because it provides better spatial coverage. It is more likely that the accumulated precipitation for 1995 and 1996 is biased low than that the estimate for 1994 is biased high.

Errors in the discharge measurements may have occurred as well, but discharge formed only a minor component of the water balance in the White Gull Creek basin. To account for around 80 mm of moisture would have meant that discharge was underestimated by more than 40%. Again, this seems unlikely. However, some water may have bypassed the gauge during the high

Table 5.6: Water balance components during the 1994 growing season.

| Vegetation | Soil moisture | | | | | |
|---|---|---|---|---|---|---|
| | June 13, 1994 | | August 5, 1994 | | September 17, 1994 | |
| | (%) | (mm)[a] | (%) | (mm)[a] | (%) | (mm)[a] |
| mature aspen | 31.3 | 376 | 27.1 | 325 | 22.9 | 275 |
| mature black spruce | 36.5 | 438 | 35.8 | 430 | 28.3 | 340 |
| mature jack pine | 9.5 | 114 | 7.9 | 95 | 6.6 | 79 |
| young aspen | — | — | 26.8 | 322 | 24.1 | 289 |
| young jack pine | 7.3 | 88 | 6.9 | 83 | 6.4 | 77 |
| fen | 59.5 | 714 | 57.7 | 692 | 52.3 | 628 |
| | Water level (mm above datum) | | | | | |
| fen | | 137 | | 197 | | 104 |
| | Accumulated flux since June 13, 1994 | | | | | |
| Precipitation | | 0 | | 238 | | 287 |
| Discharge | | 0 | | 55 | | 66 |
| Evapotranspiration[b] | | 0 | | 130 | | 204 |

[a]Assuming an active soil depth of 1.2 m.
[b]As estimated in Section 5.5.3.

water levels in late July 1994, and may have exited the basin as groundwater, or may have contributed to recharge of a deeper lying aquifer. Unfortunately, no information is available to determine the extent to which this may have occurred. An additional source of error is that the rating curve used to relate water level height to discharge volume is normally least well defined for the highest flows, both because of the low frequency of occurrence and because of practical measurement difficulties at high flows.

An underestimation of the evapotranspiration is a more likely source of the discrepancy in the water balance. *Metcalfe and Buttle* [1999] estimated the water balance of a 2.4 km$^2$ fen area in the BOREAS northern study area and warned that the "a priori selection of homogeneous landscape features such as contiguous units of closed canopy forest and larger fens can overlook important areas such as open black spruce and treed muskeg". As a consequence, extrapolation of the evapotranspiration estimates from the towers can produce considerable errors in regional water balance

calculations. For example open-canopy black spruce forests tend to have larger evapotranspiration rates than closed-canopy black spruce forests because of their surface roughness, canopy ventilation, and surface wetness [*Metcalfe and Buttle*, 1999]. *Metcalfe and Buttle* [1999] made specific observations to calculate the storage terms in the water balance of their fen area explicitly. Consequently, they did not have to treat the storage as the residual of the remaining terms in the water balance. Unfortunately, this was not possible for the entire White Gull Creek area, which was about 250 times larger.

The problem that leads to an underestimation of the wetland area in classified AVHRR images as compared to high-resolution classified Landsat TM images, is also a factor at the smaller scales. Ephemeral storages and small perennial wetlands do not show on the TM images. In addition, the extent of these wetland areas varies with the moisture status of the area. During July 1994, after the large amount of precipitation in the third week of July, the basin was extremely wet, and most surface depressions were filled with water. Evapotranspiration during this period was therefore likely higher than was estimated using the equations and landscape categories in Section 5.5. If we assume that the entire White Gull Creek basin had evaporated as the fen in the three week period from July 20–August 10, 1994, basin average evapotranspiration during that period would have been 30 mm greater than estimated based on the vegetation types in Table 5.2. In addition, evaporation estimates for periods following rainfall when the canopy was wet, were likely underestimated. Most of the eddy-correlation systems worked poorly during periods of precipitation [e.g. *Verma et al.*, 2000], and precipitation days were therefore either unrepresented in the data sets used to develop the regression equations in Section 5.5, or explicitly removed. Systematic underestimation of evaporation during periods when the canopy was wet would mean that the water balance in 1995 and 1996 does not close as well as suggested in Table 5.5, but as mentioned, precipitation is also likely somewhat underestimated in those years.

The evaporation ratio (amount of evaporation divided by the amount of precipitation) was 63% in 1994, 88% in 1995 and 75% in 1996. However, if we assume that most of the "excess" precipitation in 1994 evaporated, the evaporation ratio for that year could be as high as 80%. The

discharge ratio was 20% in 1994, 12% in 1995 and 27% in 1996.

### *5.8 Conclusions*

Field measurements collected as part of the BOREAS experiment by a large number of science teams were combined to estimate the water balance components of the White Gull Creek basin in the BOREAS southern study area for the period 1994–1996.

Estimated evapotranspiration varied only little from year to year, and accounted for most of the precipitation over the area. Basin wide evaporation rates during the middle of the growing season were 2–3 mm/day, with evapotranspiration rates lower in the coniferous forests than in the deciduous stands and fen areas. The coniferous forests, black spruce and jack pine, exhibited a strong vegetative control over the evaporative flux, resulting in low evaporation rates over these forest types. Generally, the vegetative resistance to transpiration decreased with increasing humidity and cloudiness. Because atmospheric demand tends to be lower under these conditions, the vegetation controlled transpiration rate is relatively constant over the growing season and daily evapotranspiration totals strongly reflect the total daily net radiation.

Because the interannual variation in evapotranspiration was small, and because evapotranspiration accounted for the major part of the precipitation, annual discharge varied by a factor of two in response to changes in precipitation. The discharge ratio ranged from a low of 12% in 1995 to a high of 27% in 1996. Peak flows were small, with the largest flow no more than 3.6 mm/day in July 1994. The poorly developed channel network was already a clear indicator of the relatively low fraction of precipitation that becomes runoff.

Although snow covered the basin for about half the year, snow packs remained thin during the study period. The deepest snow pack occurred in 1996 when maximum accumulation was about 73 mm of water equivalent. Snow melt was an important contributor to streamflow in years with low summer precipitation such as 1995, but snow melt associated discharge rates were low. Most of the snow pack was stored within the basin and contributed to evapotranspiration later in the summer.

A major limitation in the calculation of the water balance was the difficulty of assessing basin storage. Although the measured precipitation and discharge and the estimated evapotranspiration rates suggested that about 89 mm of water was stored interannually from 1994 to 1995, none of the measurements of storage in the basin corroborated this conclusion. Some of this water may have contributed to recharge of a deeper-lying aquifer and the unsaturated zone in the upland areas, but not enough information was available to determine the importance of these terms. Most likely evapotranspiration during July and August 1994 was underestimated, because the basin was extremely wet after large amounts of precipitation in the first three weeks of July. If, as we suggest, most of the "excess" precipitation during 1994 evaporated, the representativeness of the evaporative fluxes measured at the towers is called into question. *Peck et al.* [1997] already noted that the site of the mature black spruce tower was drier than much of the surrounding black spruce forest.

This study demonstrates that even with carefully measured precipitation and discharge rates and carefully estimated evapotranspiration, enough uncertainty remains to make it difficult to estimate basin-wide storage. Although the fen water level and soil measurements provide some indication of storage, a limited number of carefully placed piezometers monitoring ground water levels in a number of places around the basin would have helped to complete the picture. In addition, measurements of lake water level and the extent of surface saturation following the July 1994 precipitation events would have been quite useful.

# Chapter 6

# CONCLUSIONS AND RECOMMENDATIONS

## *6.1 Conclusions*

The three studies here presented evaluate land surface hydrologic processes in the boreal forest using observations collected as part of the Boreal Ecosystem Atmosphere Study (BOREAS). The first study described the application of a spatially-distributed hydrologic model to selected BOREAS flux measurement sites. This model, the Distributed Soil-Hydrology-Vegetation Model (DHSVM), was originally developed for mid-latitude forested environments. Application of the model in a boreal forest environment showed that

- Average seasonal sensible and latent heat fluxes were simulated accurately, and the mean diurnal cycle in the latent heat flux closely matched the observations at two mature black spruce sites , and one mature jack pine site.

- A phase shift was observed in the simulation of the sensible heat flux and net radiation. This timing problem was attributed to the soil heat algorithm, which was too simplistic.

- The soil always evaporated at a modified potential rate, because model atmospheric demand was always smaller than the potential soil delivery rate. Consequently, total model evapotranspiration was insensitive to biophysical controls, even though these controls strongly influenced the partitioning of the evaporative flux into its constituent components.

To improve the model, a better representation of the transmission of shortwave radiation through the boreal forest canopy was developed. Simultaneous above and below canopy radiation measurements are only rarely made, largely because the subcanopy radiation environment is

usually highly variable, both in space and time. The availability of such measurements as part of the BOREAS project allowed the development of such a model. Although many canopy radiative transfer models exist in the literature, most are complex and require detailed information of canopy structural and optical characteristics which is not generally available, or are semi-empirical and contain calibrated parameters that do not exhibit the proper sensitivities to environmental changes. The new model accounts separately for the transmission of diffuse and direct shortwave radiation and includes a term to account for multiple scattering in the canopy and multiple reflections between the canopy layers. Comparison of model simulations with a more complex radiative transfer model (GORT) and with observations showed that

- The simple model predicted a lower transmittance for direct and diffuse radiation at small zenith angles compared to GORT, although the shape of the curve showing transmittance as a function of solar zenith angle was the same. In the range of zenith angles from 40° to 60° the simple model predicted somewhat larger transmittances for direct and diffuse radiation than GORT.

- The total transmitted radiation compared well with observed values over a range of solar zenith angles at a mature jack pine site.

- The absolute model error in predicted below-canopy radiation at a mature black spruce site was small compared to the above-canopy radiation, but below-canopy radiation values were at times twice as large as the observed values. Because of the limited amount of available data, and the difficulty in making subcanopy radiation measurements that are representative for a stand, it is not clear to what extent the discrepancy between measured and observed values was due to sampling error or to model error.

The new model is not meant as a replacement for more complex methods. It does not, for instance, account for shifts in the spectral composition of radiation along its path through the canopy, nor does it model the vertical distribution of the radiative flux in the canopy. However,

if the bulk shortwave radiation below the canopy is the primary quantity of interest, the proposed model can offer a simple solution using only commonly available canopy characteristics. If the vertical distribution of the radiation flux is the quantity of interest, more complex models such as those described by *Ni et al.* [1997] or *Roujean* [1996] may be more appropriate.

Early application of DHSVM in a spatially-distributed mode over the White Gull Creek basin in the BOREAS southern study area for the 1994 growing season showed that the model response to a wet period in July 1994 consisted of a greatly overestimated runoff peak [*Nijssen et al.*, 1996]. It was decided that rather than attempting further model refinements, a better understanding of catchment scale processes would result from a careful analysis of the water balance of the basin based for the 1994–1996 observation period.

The final study evaluates apparent water balance anomalies in the White Gull Creek Basin during the 1994–1996 period, with particular emphasis on the fate of precipitation that occurred during an unusually wet period in July 1994. To estimate evapotranspiration, multiple linear regression equations of canopy resistance as a function of environmental conditions were developed for each vegetation type using measurements made at the tower flux sites. The canopy resistances were scaled by the leaf area index (LAI) and combined with the Penman Monteith equation to derive a spatially distributed estimate of evapotranspiration. This evapotranspiration estimate was combined with observations of precipitation, discharge, snow accumulation and melt, soil moisture storage and fen water levels to estimate the water balance terms for the White Gull Creek basin. This study led to the following conclusions:

- Estimated evapotranspiration varied little from year to year and accounted for most of the precipitation over the area. Consequently, annual runoff ratios were small, but annual discharge varied by a factor of two in response to changes in precipitation.

- Basin wide evaporation rates during the middle of the growing season were 2 to 3 mm/day, with evapotranspiration rates lower in the coniferous forests than in the deciduous stands and fen areas. The coniferous forests exhibited a strong vegetative control over the evaporative flux.

- Snow covered the basin for about half the year, but snow packs remained thin during the study period. Snow melt was an important contributor to streamflow in years with low summer precipitation such as 1995, but snow melt associated discharge rates were low. Most of the snow pack was stored within the basin and contributed to evapotranspiration later in the summer.

- Although the measured precipitation and discharge and the estimated evapotranspiration rates suggested that about 89 mm of water was stored interannually from 1994 to 1995, none of the measurements of storage in the basin corroborated this conclusion. Some of this water may have contributed to recharge of a deeper-lying aquifer and the unsaturated zone in the upland areas, but not enough information was available to determine the importance of these terms. Most likely evapotranspiration during July and August 1994 was underestimated, because the basin was extremely wet after large amounts of precipitation in the first three weeks of July.

- If, as suggested, most of the "excess" precipitation during 1994 evaporated, the representativeness of the evaporative fluxes measured at the towers is called into question.

- A major limitation in the calculation of the water balance was the difficulty of assessing basin storage.

### *6.2 Recommendations*

The results from this study present a number of challenges and possibilities for further research. Whether and to what extent the flux tower measurements are representative of the exchange processes in the surrounding areas is an important issue, because flux towers have been the focus of many recent land surface-atmosphere experiments (e.g. FIFE [*Sellers et al.*, 1992], NOPEX [*Halldin and Gryning*, 1999], BOREAS [*Sellers et al.*, 1995], LBA [*LBA Science Planning Group*, 1996]). Even if the towers accurately measure the exchange processes in the flux measurement

source area, the question remains how to transfer these findings to the larger area. The simple method adopted in Chapter 5, that is, assuming that the canopy resistance scales with leaf area, may not be adequate for many cases. Most hydrological and land surface-atmosphere transfer models, which explicitly or implicitly perform this scaling, have enough degrees of freedom to allow calibration of model parameters to match observed fluxes. However, unless a better theoretical framework of this scaling process is developed, the question will remain how well these models perform in areas where no calibration data are available, or how well these models mirror the sensitivities to land surface and climatological changes experienced in the real world.

This study also demonstrates that even with carefully measured precipitation and discharge rates and carefully estimated evapotranspiration, enough uncertainty remains to make it difficult to estimate basin-wide storage. As a result, it is difficult to say with certainty how much of the "missing" water evaporated, how much by-passed the gauge and exited the basin as groundwater, and how much contributed to recharge of any aquifer system. Although the fen water level and soil moisture measurements provided some indication of storage, a limited number of carefully placed piezometers monitoring ground water levels would have helped to complete the picture. In addition, measurements of lake water level and the extent of surface saturation following the July 1994 precipitation events would have helped. Closure of the water balance can provide an important check on the measurements and can help in the development of scaling methods from the flux towers to larger areas. As such, it is no less important than closure of the energy balance which has received much more attention in most land surface-atmosphere exchange experiments.

Finally, the research findings provide some important directions for the development of a spatially distributed model of the hydrology of the boreal forest region. Unlike in mountainous regions, where much of the hydrology is dictated by difference in slope and aspect, available storage and land surface type govern the hydrology of the boreal forest. Coniferous forests exhibit a strong vegetative control on evapotranspiration during the growing season, while the deciduous vegetation transpires more freely when the canopy is fully developed. Because the degree of vegetation control is less in areas with standing water or open water surfaces, it is important to model the

temporal and spatial evolution of storage in the boreal forest. This is not only important to simulate the hydrology of the boreal forest, but many gas exchange processes are a direct function of the degree of saturation of the soil. The poorly developed drainage network and the low runoff ratios indicate that a detailed flow routing model may be both difficult to develop and unnecessary to capture the discharge process. The boreal forest landscape, at least in the White Gull Creek Basin, essentially acts as a low pass filter, with significant streamflow peaks only after snow melt and large summer precipitation events.

# BIBLIOGRAPHY

Anderson, D., R. Strieg, and K. Wickland, Exchange of trace gases, water and energy in disturbed and undisturbed boreal forests, in *Newcomer et al.* [2000].

André, J. C., J. P. Goutorbe, and A. Perrier, HAPEX-MOBILHY: A hydrologic atmospheric experiment for the study of water budget and evaporation flux at the climatic scale, *Bull. Amer. Meteor. Soc.*, *67*, 138–144, 1986.

Arola, A., and D. P. Lettenmaier, Effects of subgrid spatial heterogeneity on GCM-scale land surface energy and moisture fluxes, *J. Climate*, *9*, 1339–1349, 1996.

Baldocchi, D., and C. Vogel, Experimental and modeling studies of water vapor, sensible heat, and $CO_2$ exchange over and under a boreal forest, in *Newcomer et al.* [2000].

Baldocchi, D., C. Vogel, and B. Hall, Seasonal variation of energy and water vapor exchange rates above and below a boreal jack pine forest canopy, *J. Geophys. Res.*, *102*, 28,939–28,951, 1997.

Barr, A. G., G. van der Kamp, R. Schmidt, and T. A. Black, Monitoring the moisture balance of a boreal aspen forest using a deep groundwater piezometer, *Agric. For. Meteorol.*, *102*, 13–24, 2000.

Bessemoulin, P., Study of the boreal forest effects on surface/atmosphere fluxes (TF-06), in *Newcomer et al.* [2000].

Betts, A. K., and J. H. Ball, Albedo over the boreal forest, *J. Geophys. Res.*, *102*, 28,901–28,909, 1997.

Betts, A. K., M. L. Goulden, and S. C. Wofsy, Controls on evaporation in a boreal spruce forest, *J. Climate*, *12*, 1601–1618, 1999.

Beven, K., Changing ideas in hydrology — the case of physically-based models, *J. Hydrol.*, *105*, 157–172, 1989.

Beven, K., Prophecy, reality and uncertainty in distributed hydrological modelling, *Adv. Water Resour.*, *16*, 41–51, 1993.

Black, T. A., and Z. Nesic, Boreal forest atmosphere interactions: exchanges of energy, water vapor and trace gases, in *Newcomer et al.* [2000].

Blanken, P. D., T. A. Black, P. C. Yang, H. H. Neumann, Z. Nesic, R. Staebler, G. den Hartog, M. D. Novak, and X. Lee, Energy balance and canopy conductance of a boreal aspen forest: Partitioning overstory and understory components., *J. Geophys. Res.*, *102*, 28,915–28,927, 1997.

Bolle, H. J., EFEDA: European Field Experiment in a Desertification-Threatened Area, *Ann. Geophys.*, *11*, 173–189, 1993.

Bonan, G. B., and H. H. Shugart, Environmental factors and ecological processes in boreal forests, *Annu. Rev. Ecol. Syst.*, *20*, 1–28, 1989.

Bonan, G. B., and L. Sirois, Air temperature, tree growth, and the northern and southern range limits to *Picea mariana*, *J. Veg. Sci.*, *3*, 495–506, 1992.

Bonan, G. B., and K. Van Cleve, Soil temperature, nitrogen mineralization, and carbon source-sink relationships in boreal forests, *Can. J. Forest Res.*, *22*, 629–639, 1992.

Bonan, G. B., D. Pollard, and S. L. Thompson, Effects of boreal forest vegetation on global climate, *Nature*, *359*, 716–718, 1992.

BOREAS Science Team, BOREAS Experiment Plan, version 3.0, *Tech. rep.*, Goddard Space Flight Center, NASA, 1994.

BOREAS Science Team, BOREAS Experiment Plan, version 2.0, *Tech. rep.*, Goddard Space Flight Center, NASA, 1996.

Brooks, R. H., and A. T. Corey, Hydraulic properties of porous media, *Tech. rep.*, Colorado State University, 1964.

Chen, J., and X. Geng, Retrieval of boreal forest leaf area index from multiple scale remotely sensed vegetation indices, in *Newcomer et al.* [2000].

Chen, J. M., Evaluation of vegetation indices and modified simple ratio for boreal applications, *Can. J. Rem. Sens.*, *22*, 229–242, 1996.

Chen, J. M., and J. Cihlar, Retrieving leaf area index of boreal conifer forests using Landsat TM images, *Remote Sens. Environ.*, *55*, 153–162, 1996.

Chen, J. M., P. D. Blanken, T. A. Black, M. Guilbeault, and S. Chen, Radiation regime and canopy architecture in a boreal aspen forest, *Agric. For. Meteorol.*, *86*, 107–125, 1997a.

Chen, J. M., P. M. Rich, S. T. Gower, J. M. Norman, and S. Plummer, Leaf area index of boreal forests: Theory, techniques, and measurements, *J. Geophys. Res.*, *102*, 29,429–29,443, 1997b.

Cuenca, R. H., D. E. Stangel, and S. F. Kelly, Soil water balance in a boreal forest, *J. Geophys. Res.*, *102*, 29,355–29,366, 1997.

D'Arrigo, R., G. C. Jacoby, and I. Y. Fung, Boreal forests and atmosphere-biosphere exchange of carbon dioxide, *Nature*, *329*, 321–323, 1987.

Davis, R. E., Distributed energy transfer modeling in snow and soil for boreal ecosystems, in *Newcomer et al.* [2000].

Davis, R. E., J. P. Hardy, W. Ni, C. E. Woodcock, J. C. McKenzie, R. Jordan, and X. Li, Variation of snow cover ablation in the boreal forest: A sensitivity study on the effects of conifer canopy, *J. Geophys. Res.*, *102*, 29,389–29,395, 1997.

DeFries, R. S., and J. R. G. Townshend, NDVI-derived land cover classifications at global scales, *Int. J. Remote Sens.*, *15*, 3567–3586, 1994.

den Hartog, G., R. E. Mickie, H. H. Neumann, and N. B. A. Trivett, Boreal forest atmosphere interactions: exchanges of energy, water vapor and trace gases, in *Newcomer et al.* [2000].

Dickinson, R. E., Land surface processes and climate change-surface albedos and energy balance, in *Theory of Climate*, edited by B. Saltzman, vol. 25 of *Advances in Geophysics*, pp. 305–353, Academic Press, San Diego, Calif., 1983.

Dickinson, R. E., A. Henderson-Sellers, C. Rosenzweig, and P. J. Sellers, Evapotranspiration models with canopy resistance for use in climate models: A review, *Agric. For. Meteorol.*, *54*, 373–388, 1991.

Dixon, R. K., S. Brown, R. A. Houghton, A. M. Solomon, M. C. Trexler, and J. Wisniewski, Carbon pools and flux of global forest ecosystems, *Science*, *263*, 185–190, 1994.

Duan, Q., S. Sorooshian, and V. K. Gupta, Effective and efficient global optimization for conceptual rainfall-runoff models, *Water Resour. Res.*, *28*, 1015–1031, 1992.

Erbs, D. G., S. A. Klein, and J. A. Duffie, Estimation of the diffuse fraction for hourly, daily and monthly-average global radiation, *Sol. Energy*, *28*, 293–302, 1982.

Feddes, R. A., P. J. Kowalik, and H. Zaradny, *Simulation of field water use and crop yield*, John Wiley, New York, 1978.

Foley, J. A., J. E. Kutzbach, M. T. Coe, and S. Levis, Feedbacks between climate and boreal forests during the Holocene epoch, *Nature*, *371*, 52–54, 1994.

Frolking, S., et al., Modelling temporal variability in the carbon balance of a spruce/moss boreal forest, *Glob. Change Biol.*, *2*, 343–366, 1996.

Gates, W. L., et al., Climate models - evaluation, in *Climate change 1995: The science of climate change; contribution of Working Group I to the second assessment report of the Intergovernmental Panel on Climate Change*, edited by J. T. Houghton, L. G. Meira Filho, B. A. Callander,

N. Harris, A. Kattenberg, and K. Maskell, pp. 229–284, Cambridge University Press, Cambridge, 1996.

Goldammer, J. G., and V. V. Furyaev, Fire in ecosystems of boreal eurasia, ecological impacts and links to the global climate system, in *Fire in ecosystems of boreal Eurasia*, edited by J. G. Goldammer and V. V. Furyaev, pp. 1–20, Kluwer Academic Publishers, Dordrecht, 1996.

Goodison, B., Determination of snow cover variations in the boreal forest using passive microwave radiometry, in *Newcomer et al.* [2000].

Goudriaan, J., *Crop Meteorology: A Simulation Study*, Simulation monographs, Cent. for Agric. Publ. and Doc., Wageningen, Neth., 1977.

Goulden, M. L., B. Daube, S. Fan, D. Sutton, A. Bazzaz, J. W. Munger, and S. Wofsy, Physiological responses of a black spruce forest to weather, *J. Geophys. Res.*, *102*, 28,987–28,996, 1997.

Goutorbe, J. P., et al., An overview of HAPEX-SAHEL: A study in climate and desertification, *J. Hydrol.*, *189*, 4–17, 1997.

Grayson, R. B., I. D. Moore, and T. A. McMahon, Physically based hydrologic modeling, 2, Is the concept realistic?, *Water Resour. Res.*, *28*, 2659–2666, 1992.

Grelle, A., A. Lundberg, A. Lindroth, A.-S. Morén, and E. Cienciala, Evaporation components of a boreal forest: variations during the growing season, *J. Hydrol.*, *197*, 70–87, 1997.

Grelle, A., A. Lindroth, and M. Mölder, Seasonal variation of boreal forest surface conductance and evaporation, *Agric. For. Meteorol.*, *98-99*, 563–578, 1999.

Haddeland, I., and D. P. Lettenmaier, Hydrologic modeling of boreal forest ecosystems, *Water Resources Series, Technical Report 145*, University of Washington, 1995.

Haldinn, S., L. Gottschalk, A. A. van de Griend, S. E. Gryning, M. Heikinheimo, U. Högström,

A. Jochum, and L. C. Lundin, NOPEX – a northern hemisphere climate processes land surface experiment, *J. Hydrol.*, *212-213*, 172–187, 1998.

Hall, F. G., TE-18 regional scale carbon flux from modeling and remote sensing, in *Newcomer et al.* [2000].

Hall, F. G., D. E. Knapp, and K. F. Huemmrich, Physically based classification and satellite mapping of biophysical characteristics in the southern boreal forest, *J. Geophys. Res.*, *102*, 29,567–29,580, 1997.

Halldin, S., and S.-E. Gryning, Boreal forests and climate, *Agric. For. Meteorol.*, *98-99*, 1–4, 1999.

Harding, R. J., and J. W. Pomeroy, The energy balance of the winter boreal landscape, *J. Climate*, *9*, 2778–2787, 1996.

Hardy, J. P., R. E. Davis, R. Jordan, X. Li, C. E. Woodcock, W. Ni, and J. C. McKenzie, Snow ablation modeling at the stand scale in a boreal jack pine forest, *J. Geophys. Res.*, *102*, 29,397–29,405, 1997.

Hogg, E. H., and P. A. Hurdle, Sap flow in trembling aspen: implications for stomatal responses to vapor pressure deficit, *Tree Physiol.*, *17*, 501–509, 1997.

Jarvis, P., and J. Moncrieff, The $CO_2$ exchanges of boreal black spruce forest, in *Newcomer et al.* [2000].

Jarvis, P. G., The interpretation of the variations in leaf water potential and stomatal conductance found in canopies in the field, *Philosophical Transactions of the Royal Society, London B*, *273*, 593–610, 1976.

Jarvis, P. G., J. M. Massheder, S. E. Hale, J. B. Moncrieff, M. Rayment, and S. L. Scott, Seasonal variation of carbon dioxide, water vapour and energy exchanges of a boreal black spruce forest, *J. Geophys. Res.*, *102*, 28,953–28,966, 1997.

Jones, H. G., *Plants and Microclimate, a Quantitative Approach to Environmental Plant Physiology*, 2nd ed., Cambridge Univ. Press, New York, 1992.

Kattenberg, A., F. Giorgi, H. Grassl, G. A. Meehl, J. F. B. Mitchell, R. J. Stouffer, T. Tokioka, A. J. Weaver, and T. M. L. Wigley, Climate models - projections of future climate, in *Climate change 1995: The science of climate change; contribution of Working Group I to the second assessment report of the Intergovernmental Panel on Climate Change*, edited by J. T. Houghton, L. G. Meira Filho, B. A. Callander, N. Harris, A. Kattenberg, and K. Maskell, pp. 285–357, Cambridge University Press, Cambridge, 1996.

Kettunen, A., V. Kaitala, J. Alm, J. Silvola, H. Nyknen, and P. J. Martikainen, Cross-correlation analysis of the dynamics of methane emissions from a boreal peatland, *Global Biochem. Cy.*, *10*, 457–471, 1996.

Kirschbaum, M. U. F., J. R. Evans, K. Goulding, P. G. Jarvis, I. R. Noble, M. Rounsevell, and T. D. Sharkey, Ecophysiological, ecological, and soil processes in terrestrial ecosystems: A primer on general concepts and relationships, in *Climate change 1995: Impacts, adaptations and mitigation of climate change: Scientific-technical analyses; contribution of Working Group II to the second assessment report of the Intergovernmental Panel on Climate Change*, edited by R. T. Watson, M. C. Zinyowera, and R. H. Moss, Cambridge University Press, Cambridge, 1996a.

Kirschbaum, M. U. F., A. Fischlin, M. G. R. Cannell, R. V. O. Cruz, W. Galinski, and W. P. Cramer, Climate change impacts on forests, in *Climate Change 1995: Impacts, Adaptations and Mitigation of Climate Change, Scientific-Technical Analyses; Contribution of Working Group II to the Second Assessment Report of the Intergovernmental Panel on Climate Change*, edited by R. T. Watson, M. C. Zinyowera, and R. H. Moss, pp. 95–129, Cambridge Univ. Press, New York, 1996b.

Korovin, G. N., Analysis of the distribution of forest fires in Russia, in *Fire in ecosystems of*

*boreal Eurasia*, edited by J. G. Goldammer and V. V. Furyaev, pp. 112–128, Kluwer Academic Publishers, Dordrecht, 1996.

Kouwen, N., R. Soulis, and D. Knapp, From micro-scale to meso-scale: snowmelt, soil moisture and evapotranspiration from distributed hydrologic models, in *Newcomer et al.* [2000].

Lamb, H. H., *Climate: present, past and future; Volume 1: fundamentals and climate now*, Methuen & Co Ltd, London, 1972.

Larsen, D. R., and J. A. Kershaw, Jr., Influence of canopy structure assumptions on predictions from Beer's law, a comparison of deterministic and stochastic simulations, *Agric. For. Meteorol.*, *81*, 61–77, 1996.

Larsen, J. A., *The boreal ecosystem*, Physiological Ecology, Academic Press, Inc., New York, 1980.

LBA Science Planning Group, The Large Scale Biosphere-Atmosphere Experiment in Amazonia (LBA): Concise experiment plan, *Tech. rep.*, 1996.

Link, T. E., and D. Marks, Point simulation of seasonal snow cover dynamics beneath boreal forest canopies, *J. Geophys. Res.*, *104*, 27,841–27,857, 1999.

Linsley, R. K., M. A. Kohler, and J. L. H. Paulhus, *Hydrology for engineers*, 3rd ed., McGraw-Hill, Inc., New York, 1986.

Maidment, D. R., J. F. Olivera, A. Calver, A. Eatherall, and W. Fraczeck, A unit hydrograph derived from a spatially distributed velocity field, *Hydrol. Process.*, *10*, 831–844, 1996.

Melillo, J. M., I. C. Prentice, G. D. Farquhar, E.-D. Schulze, and O. E. Sala, Terrestrial biotic responses to environmental change and feedbacks to climate, in *Climate change 1995: The science of climate change; contribution of Working Group I to the second assessment report of the Intergovernmental Panel on Climate Change*, edited by J. T. Houghton, L. G. Meira Filho,

B. A. Callander, N. Harris, A. Kattenberg, and K. Maskell, pp. 445–481, Cambridge University Press, Cambridge, 1996.

Metcalfe, R. A., and J. M. Buttle, Semi-distributed water balance dynamics in a small boreal forest basin, *J. Hydrol.*, *226*, 66–87, 1999.

Middleton, E. M., and E. A. Walter-Shea, Optical properties of canopy elements in the boreal forest, in *International Geoscience and Remote Sensing Symposium*, vol. 1, pp. 789–793, Inst. of Electr. Eng., New York, 1995.

Monteith, J. L., and M. H. Unsworth, *Principles of Environmental Physics*, 2nd ed., Edward Arnold, London, 1990.

Moore, K. E., D. R. Fitzjarrald, R. K. Sakai, and J. M. Freedman, Growing season water balance at a boreal jack pine forest, *Water Resour. Res.*, *36*, 483–493, 2000.

Moosavi, S. C., P. M. Crill, E. R. Pullman, D. W. Funk, and K. M. Peterson, Controls on $CH_4$ flux from an Alaskan boreal wetland, *Global Biochem. Cy.*, *10*, 287–296, 1996.

Newcomer, J., D. Landis, S. Conrad, S. Curd, K. Huemmrich, D. Knapp, A. Morrell, J. Nickeson, A. Papagno, D. Rinker, R. Strub, T. Twine, F. Hall, and P. Sellers, eds., *Collected data of the Boreal Ecosystem-Atmosphere Study*, CD-ROM, NASA, 2000.

Ni, W., X. Li, C. E. Woodcock, J.-L. Roujean, and R. E. Davis, Transmission of solar radiation in boreal conifer forests: Measurements and models, *J. Geophys. Res.*, *102*, 29,555–29,566, 1997.

Nicholls, N., G. V. Gruza, J. Jouzel, T. R. Karl, L. A. Ogallo, and D. E. Parker, Observed climate variability and change, in *Climate change 1995: The science of climate change; contribution of Working Group I to the second assessment report of the Intergovernmental Panel on Climate Change*, edited by J. T. Houghton, L. G. Meira Filho, B. A. Callander, N. Harris, A. Kattenberg, and K. Maskell, pp. 133–192, Cambridge University Press, Cambridge, 1996.

Nijssen, B., and D. P. Lettenmaier, A simplified approach for predicting shortwave radiation transfer through boreal forest canopies, *J. Geophys. Res.*, *104*, 27,859–27,868, 1999.

Nijssen, B., D. P. Lettenmaier, M. S. Wigmosta, and W. A. Perkins, Testing an imposed channel network algorithm for hydrograph prediction with a distributed hydrological model, *Trans. Am. Geophys. Union (EOS)*, *77*, F232, Fall Meet. Suppl., 1996.

Nikolov, N., and H. Helmisaari, Silvics of the circumpolar boreal forest tree species, in *A systems analysis of the global boreal forest*, edited by H. H. Shugart, R. Leemans, and G. B. Bonan, pp. 13–84, Cambridge University Press, New York, 1992.

Omernik, J. M., and R. G. Bailey, Distinguishing between watersheds and ecoregions, *J. Amer. Water. Resour. Assoc.*, *33*, 935–949, 1997.

Pastor, J., and D. J. Mladenoff, The southern boreal-northern hardwood forest border, in *A systems analysis of the global boreal forest*, edited by H. H. Shugart, R. Leemans, and G. B. Bonan, pp. 216–240, Cambridge University Press, New York, 1992.

Pauwels, V. R. N., et al., A multiscale surface meteorological data set for boreas, *Water Resour. Res., in review*, 1999.

Peck, E. L., T. R. Carroll, R. Maxson, B. Goodison, and J. Metcalfe, Variability of soil moisture near flux towers in the BOREAS southern study area, *J. Geophys. Res.*, *102*, 29,379–29,388, 1997.

Pielke, R. A., and P. L. Vidale, The boreal forest and the polar front, *J. Geophys. Res.*, *100*, 25,755–25,758, 1995.

Pomeroy, J. W., and K. Dion, Winter radiation extinction and reflection in a boreal pine canopy: Measurements and modelling, *Hydrol. Process.*, *10*, 1591–1608, 1996.

Potter, C. S., J. C. Coughlan, and V. Brooks, Investigations of BOREAS spatial data in support of regional ecosystem modeling, *J. Geophys. Res.*, *104*, 27,771–27,788, 1999.

Price, A. G., K. Dunham, T. Carleton, and L. E. Band, Variability of water fluxes through the black spruce (*Picea mariana*) canopy and feather moss (*Pleurozium schreberi*) carpet in the boreal forest of Northern Manitoba, *J. Hydrol.*, *196*, 310–323, 1997.

Ross, J., Radiative transfer in plant communities, in *Vegetation and the Atmosphere, vol. I, Principles*, edited by J. L. Monteith, vol. 1 of *Vegetation and the atmosphere*, pp. 13–55, Academic Press, San Diego, Calif., 1975.

Roujean, J. L., A tractable physical model of shortwave radiation interception by vegetative canopies, *J. Geophys. Res.*, *101*, 9523–9532, 1996.

Roujean, J.-L., Measurements of PAR transmittance within boreal forest stands during BOREAS, *Agric. For. Meteorol.*, *93*, 1–6, 1999.

Saugier, B., A. Granier, J. Y. Pontailler, E. Dufrêne, and D. D. Baldocchi, Transpiration of a boreal pine forest measured by branch bag, sap flow and micrometeorological methods, *Tree Physiol.*, *17*, 511–519, 1997.

Schnur, R., T. W. Krauss, F. J. Eley, and D. P. Lettenmaier, Spatial and temporal analysis of radar-estimated precipitation during the BOREAS summer 1994 field campaigns, *J. Geophys. Res.*, *102*, 29,417–29,428, 1997.

Sellers, P., S. Los, C. Tucker, C. Justice, D. Dazlich, G. Collatz, and D. Randall, A global 1 by 1 degree NDVI data set for climate studies. part 2: The generation of global fields of terrestrial biophysical parameters from the NDVI., *Int. J. Remote Sens.*, *15*, 3519–3545, 1994.

Sellers, P., et al., The Boreal Ecosystem-Atmosphere Study (BOREAS): An overview and early results from the 1994 field year, *Bull. Amer. Meteor. Soc.*, *76*, 1549–1577, 1995.

Sellers, P. J., Canopy reflectance, photosynthesis and transpiration, *Int. J. Remote Sens.*, *6*, 1335–1372, 1985.

Sellers, P. J., F. G. Hall, G. Asrar, D. E. Strebel, and R. E. Murphy, An overview of the First International Satellite Land Surface Climatology Project (ISLSCP) Field Experiment (FIFE), *J. Geophys. Res.*, *97*, 18,345–18,371, 1992.

Sellers, P. J., D. A. Randall, G. J. Collatz, J. Berry, C. Field, D. A. Dazlich, C. Zhang, G. Collelo, and L. Bounoua, A revised land surface parameterization (SiB2) for atmospheric GCMs, 1, model formulation, *J. Climate*, *9*, 676–705, 1996.

Sellers, P. J., et al., BOREAS in 1997: Experiment overview, scientific results and future directions, *J. Geophys. Res.*, *102*, 28,731–28,769, 1997.

Shewchuk, S. R., Surface mesonet for BOREAS, *J. Geophys. Res.*, *102*, 29,077–29,082, 1997.

Shewchuk, S. R., Atmospheric sciences infrastructure core measurements for BOREAS (AFM-07), in *Newcomer et al.* [2000].

Shuttleworth, W. J., Evaporation, in *Handbook of hydrology*, edited by D. R. Maidment, pp. 4.1–4.53, McGraw-Hill, Inc., New York, 1993.

Sirois, L., The transition between boreal forest and tundra, in *A systems analysis of the global boreal forest*, edited by H. H. Shugart, R. Leemans, and G. B. Bonan, pp. 196–215, Cambridge University Press, New York, 1992.

Stathers, R. J., and D. L. Spittlehouse, Forest soil temperature manual, *Tech. rep.*, Canada/BC Economic and Regional Development Agreement, 1990.

Steyaert, L. T., F. G. Hall, and T. R. Loveland, Land cover mapping, fire regeneration, and scaling studies in the Canadian boreal forest with 1 km AVHRR and Landsat TM data, *J. Geophys. Res.*, *102*, 29,581–29,598, 1997.

Storck, P., D. P. Lettenmaier, B. A. Connelly, and T. W. Cundy, Implications of forest practices on downstream flooding, phase II final report, *Tech. rep.*, University of Washington, 1995.

Storck, P., L. C. Bowling, P. Wetherbee, and D. P. Lettenmaier, Application of a GIS-based distributed hydrology model for prediction of forest harvest effects on peak streamflow in the Pacific Northwest, *Hydrol. Process.*, *12*, 889–904, 1998.

Suyker, A. E., S. B. Verma, R. J. Clement, and D. P. Billesbach, Methane flux in a boreal fen: Season-long measurement by eddy-correlation, *J. Geophys. Res.*, *101*, 28,637–28,647, 1996.

Suyker, A. E., S. B. Verma, and T. J. Arkebauer, Season-long measurement of carbon dioxide exchange in a boreal fen, *J. Geophys. Res.*, *102*, 29,021–29,028, 1997.

Sveinbjörnsson, B., Arctic tree line in a changing climate, in *Arctic ecosystems in a changing climate, an ecophysiological perspective*, edited by F. S. Chapin III, R. L. Jefferies, J. F. Reynolds, G. R. Shaver, and J. Svoboda, Physiological Ecology, pp. 239–256, Academic Press, Inc., San Diego, 1992.

Verma, S. B., T. Arkebauer, and D. Valentine, Field micrometeorological measurements, process-level studies, and modeling of methane and carbon dioxide fluxes in a boreal wetland ecosystem, in *Newcomer et al.* [2000].

Wein, R. W., and W. J. De Groot, Fire - climate change hypotheses for the taiga, in *Fire in ecosystems of boreal Eurasia*, edited by J. G. Goldammer and V. V. Furyaev, pp. 505–512, Kluwer Academic Publishers, Dordrecht, 1996.

Wigmosta, M. S., L. W. Vail, and D. P. Lettenmaier, A distributed hydrology-vegetation model for complex terrain, *Water Resour. Res.*, *30*, 1665–1679, 1994.

Yamazaki, T., J. Kondo, and T. Watanabe, A heat-balance model with a canopy of one or two layers and its application to field experiments, *J. Appl. Meteor.*, *31*, 86–103, 1992.

# VITA

## Bart Nijssen

### Education:

**Ph.D. 2000**: Civil and Environmental Engineering, University of Washington, Seattle, Washington, USA. Dissertation title: *Aspects of Boreal Forest Hydrology: From Stand to Watershed.*

**M.Sc. 1991**: Tropical Land and Water Management, hydrological/meteorological orientation, Wageningen Agricultural University, Wageningen, The Netherlands. Thesis title: *Sampling and modeling of transport processes in the vadose zone.*

### Selected Publications:

Nijssen, B., G. M. O'Donnell, A. F. Hamlet, and D. P. Lettenmaier, 2000: Hydrologic vulnerability of global rivers to climate change. *Clim. Change*, **in revision**.

Nijssen, B., G. M. O'Donnell, D. P. Lettenmaier, D. Lohmann, and E. F. Wood, 2000: Predicting the discharge of global rivers. *J. Climate*, **in revision**.

Nijssen, B., R. Schnur, and D. P. Lettenmaier, 2000: Global retrospective estimation of soil moisture using the VIC land surface model, 1980–1993. *J. Climate*, **in press**.

Nijssen, B. and D. P. Lettenmaier, 1999: A simplified approach for predicting shortwave radiation transfer through boreal forest canopies. *J. Geophys. Res.*, **104**, 27,859–27,868.

Nijssen, B., I. Haddeland, and D. Lettenmaier, 1997: Point evaluation of a surface hydrology model for BOREAS. *J. Geophys. Res.*, **102**, 29,367–29,378.

Nijssen, B., D. P. Lettenmaier, X. Liang, S. W. Wetzel, and E. F. Wood, 1997: Streamflow simulation for continental-scale river basins. *Water Resour. Res.*, **33**, 711–724.

Comanor, K., B. Nijssen, and D. P. Lettenmaier, 2000: Comment on "Five-minute, 1/2$^o$ and 1$^o$ data sets of continental watersheds and river networks for use in regional and global hydrologic and climate modeling studies" by Graham et al. *Water Resour. Res.*, **in press**.

O'Donnell, G., B. Nijssen, and D. P. Lettenmaier, 1999: A simple algorithm for generating streamflow networks for grid-based, macroscale hydrological models. *Hydrol. Process.*, **13**, 1269–1275.

Lohmann, D., E. Raschke, B. Nijssen, and D. P. Lettenmaier, 1998: Regional scale hydrology: I. Formulation of the VIC-2L model coupled to a routing model. *Hydrological Sciences Journal*, **43**, 131–141.

Lohmann, D., E. Raschke, B. Nijssen, and D. P. Lettenmaier, 1998: Regional scale hydrology: II. Application of the VIC-2L model to the Weser River, Germany. *Hydrological Sciences Journal*, **43**, 143–158.

Wood, E. F., D. P. Lettenmaier, X. Liang, B. Nijssen, and S. W. Wetzel, 1997: Hydrological modeling of continental-scale basins. *Annual Review of Earth and Planetary Sciences*, **25**, 279–300, also appeared in *Hydrological processes, from catchment to continental scales*, W. E. Dietrich and G. Sposito, Eds., Annual Reviews, Palo Alto, Ca., 313–336, 1997.